MERCATOR
Quarterly Newsletter

Editorial – January 2010

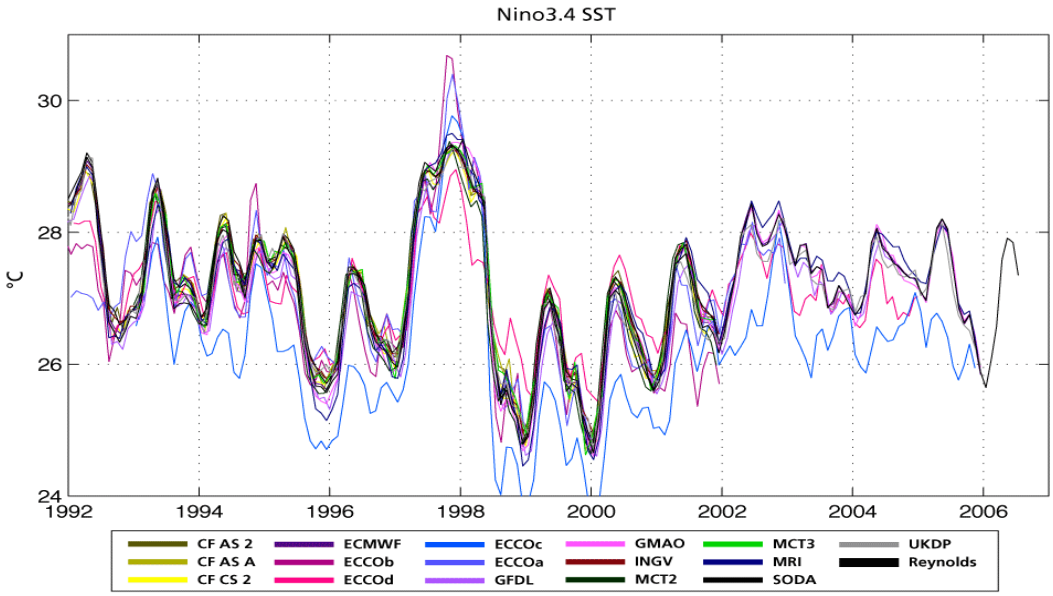

Figure: 1992-2007 Sea Surface Temperature (ºC) time series in the Nino3.4 Box in the Equatorial Pacific for various Ocean Reanalyses. MCT2 stands for Mercator Kalman filtering (PSY2G) system reanalysis. MCT3 stands for Mercator 3D-Var reanalysis (assimilation of altimetry and insitu profiles). SST comparison in all reanalyses shows a relatively robust interannual variability. SST uncertainty is stable with time. Credits: A. Fischer, CLIVAR/GODAE Ocean Reanalyses Intercomparison Meeting.

Greetings all,

This month's newsletter is devoted to data assimilation and its application to Ocean Reanalyses.

Brasseur is introducing this newsletter telling us about the history of Ocean Reanalyses, the need for such Reanalyses for MyOcean users in particular, and the perspective of Ocean Reanalyses coupled with biogeochemistry or regional systems for example.

Scientific articles about Ocean Reanalyses activities are then displayed as follows: First, Cabanes et al. are presenting CORA, a new comprehensive and qualified ocean in-situ dataset from 1990 to 2008, developped at the Coriolis Data Centre at IFREMER and used to build Ocean Reanalyses. A more comprehensive article will be devoted to the CORA dataset in our next April 2010 issue. Then, Remy at Mercator in Toulouse considers large scale decadal Ocean Reanalysis to assess the improvement due to the variational method data assimilation and show the sensitivity of the estimate to different parameters. She uses a light configuration system allowing running several long term reanalysis. Third, Ferry et al. present the French Global Ocean Reanalysis (GLORYS) project which aims at producing eddy resolving global Ocean Reanalyses with different streams spanning

different time periods and using different technical choices. This is a collaboration between Mercator and French research laboratories, and is a contribution to the European MyOcean project. Then, Masina et al. at CMCC in Italy are presenting the implementation of data assimilation techniques into global ocean circulation model in order to investigate the role of the ocean on climate variability and predictability. Fifth, Smith et al. are presenting the Ocean Reanalyses studies at ESSC in the U.K. which aim at reconstructing water masses variability and ocean transports. Finally, Langlais et al. are giving an example of the various uses of ocean reanalyses: they are using the Australian BlueLink Reanalysis in order to look into details at the various Southern Ocean fronts.

The next April 2010 newsletter will introduce a new editorial line with a common newsletter between the **Mercator Ocean** Forecasting Center in Toulouse and the **Coriolis** Data Center at Ifremer in Brest. Some papers will be dedicated to observations only, when others will display collaborations between the 2 aspects: Observations and Model. The idea is to wider and complete the subjects treated in our newsletter, as well as to trigger interactions between observations and modeling communities. This common **Mercator-Coriolis** Newsletter is a test for which we will take the opportunity to ask for your feedback.

We wish you a pleasant reading!

Contents

Ocean reanalyses: prospects for multi-scale ocean variability studies

***By** Pierre Brasseur*

MEOM-LEGI, Grenoble France

Over the past decade, the ocean weather prediction community has made terrific progress toward the establishment of an effective infrastructure for systematic acquisition and processing of *in situ* and space observations, assimilation of data into global, high-resolution ocean circulation models for real-time nowcast and short-range forecast, and delivery of synthetic products to users. This Operational Oceanography infrastructure represents a unique opportunity for applications that require time series describing the evolution of ocean state over sufficiently long periods of time (~ 20 to 50 years) to have value for climate research as well as for regional studies of the ocean variability. The vast majority of ocean weather prediction systems in operation indeed have the capacity to resolve the whole spectrum of interacting scales from mesoscale eddies to planetary waves, and this is believed to be a key asset for investigating climate-related modes of the ocean variability.

The application of an ocean weather prediction system to this purpose, however, is neither trivial nor immediate. Structural changes (e.g. in model resolution, data provision, or assimilation schemes) implemented intermittently in operational suites affect the accuracy of analyses and make the sequence of estimated ocean states inhomogeneous in quality. As a result, series of 3-D ocean analyses produced in real-time for nowcast purposes cannot be used for consistent exploration of ocean variability aspects such as trends and low-frequency signals. Instead, better products can be generated retrospectively by re-analysing past observations with a fixed ocean model and a fixed data assimilation scheme in which the best available parameterizations and assimilation options have been prescribed. A retrospective analysis, or reanalysis, offers the possibility of extracting additional information from data sets generated a posteriori with improved reprocessing algorithms. Reanalyses can therefore contribute to more confident attribution of the processes that are responsible for the observed variability as well as the expected geographical patterns and magnitudes of the responses. In return, reanalysis products could ultimately provide relevant information on how to design appropriate observing systems and optimized sampling strategies for the ocean, especially for the detection of climate variability signals. Dedicated Observation Sensitivity Experiments (OSEs) for instance, can provide information about the sensitivity of reanalyses to the density of the observation network.

In essence, the systems that are producing 4-D historical reconstructions should be different from those used in real-time. An obvious difference when operating an assimilation system in retrospective mode lies in the possibility of using both “past” and “future” observations. This motivates the development of new assimilation algorithms, such as Kalman-type smoothers that, in the future, should supersede the Kalman-type filters currently available in most operational centers.

Another fundamental difference between a reanalysis and a raw sequence of ocean state estimations produced at discrete time intervals lies in the “dynamical” dimension, which should be very carefully taken into account for the reconstruction of 4-D fields. The dynamical constraints imposed by physical laws are critical for inferring unobserved quantities such as currents, or to compute transport of tracers and integrated circulations through sections. To some extent however, the requirement for dynamical consistency over periods of time larger than the predictability time scales of the simulated flow remains an issue at conceptual level. This is especially true with eddy-resolving ocean models for which the so-called “weak-constraint” assimilation methods (i.e. assuming that the model equations are not strictly verified) represent the relevant framework to properly conciliate imperfect models with imperfect data.

Other key challenges will have to be addressed in the future, such as reanalyses with coupled components of the ocean-atmosphere-biosphere system and the need for consistent uncertainty estimates on the solutions. Ensemble methods are already being implemented for nowcast and short–term predictions, and provide an elegant and powerful statistical methodology to quantify uncertainty. However, running ensembles of statistical significance still represent a major computational issue with regard to the production of multi-decadal data sets. The same difficulty exists for variational assimilation methods, as in this case the error estimation process requires the computation of the inverse of the Hessian of the cost function.

The reanalysis concept has been proven first in the atmosphere in the eighties, and atmospheric reanalyses have become an essential by-product of major numerical weather prediction systems. In oceanography, reanalyses of the global ocean/sea-ice system have already been produced under the auspices of GODAE and CLIVAR, leading to intercomparison exercises coordinated at international level. Today, the production and delivery of ocean reanalyses is identified as a major task for the future Marine Core Services of GMES. In the framework of the EU-funded MyOcean project, several monitoring and forecasting centers (Mercator, INGV, MetNo …) are committed to provide qualified reanalyses to users from different applicative sectors (climate, seasonal and weather forecasting, management of marine resources, coastal environment monitoring and assessment). No doubt that users will be increasingly demanding in terms of quality and validation of products, and this will represent a very significant driver for the whole Operational Oceanography community in the next decade.

CORA -Coriolis Ocean database for Re-Analyses-, a new comprehensive and qualified ocean in-situ dataset from 1990 to 2008

By Cécile Cabanes [1], Clément de Boyer Montégut [1], Karina Von Schuckmann [1], Christine Coatanoan [2], Cécile Pertuisot [2], Loic Petit de la Villeon [2], Thierry Carval [2], Sylvie Pouliquen [1] and Pierre-Yves Le Traon [1]

[1] *Laboratory of Oceanography from Space (LOS), IFREMER/CNRS, Brest, France*
[2] *Coriolis Data Centre, IFREMER, Brest, France*

Introduction

An ideal set of oceanographic data would comprehends a global coverage, continuity in time, is subject to regular quality controls and calibration processes (i.e. durable in time), and encompasses several space/time scales. This goal is actually not easy to reach and reality is often different especially with in-situ oceanographic data, such as temperature and salinity profiles in our case. Those data have basically as many origins as there are scientific campaigns to collect them. Some efforts to make such an ideal dataset have been done for many years, especially since the initiative of Levitus (1982).

A program named Coriolis has been set up at Ifremer data centre the beginning of the 2000's in the wake of the development of operational oceanography in France. The project was launched in order to contribute to the ocean in situ measurements part of the French operational system (e.g. Mercator group). It has been especially involved in developing continuous, automatic, and permanent observation networks. The data centre is gathering ocean data in real time, which are then subject to its own quality procedures (Coatanoan and Petit de la Villéon, 2005). Our goal now is to distribute an extraction of this comprehensive and reprocessed set of ocean in-situ data, from 1990 to 2008. The aim is to publish this qualified dataset for operational as well as for research purposes. In doing this work, we can also evaluate the difference between our dataset and state of the art databases like the World Ocean Database 2009 (Boyer et al, 2009) for example. This is also a way to improve the quality of this “living” real time database. We first present a description of the dataset and of the quality controls applied, then we give examples of the main uses for which those data are meant for.

Description of the Dataset

Overview

The CORA dataset basically contains global, sub-surface ocean profiles of in-situ temperature and salinity at observed levels. Those data were extracted from the real-time CORIOLIS database at the beginning of 2008 (and early 2009 for 2008 data). From those raw data, we construct and make available profiles data at standardized levels, and gridded fields of T/S obtained through objective analysis.

Data type

CORA contains data from different types of instruments: mainly Argo floats, XBT, CTD and XCTD, and Mooring Data (see figure 1). The Coriolis centre receives data from Argo program, French research ships, GTS data, GTSPP, GOSUD, MEDS, voluntary observing and merchants ships, moorings, and the World Ocean Database (not in real time for the last one).

Quality controls

To produce this dataset, several tests have been developed in order to improve the quality flags of the raw database and to fit the level required by the physical ocean re-analysis activities. These tests include some simple systematic tests, a test against climatology and a more elaborate statistical test involving an objective analysis method (see Gaillard et al., 2009 for further details). Visual quality control (QC) is performed on all the suspicious temperature (T) and salinity (S) profiles. The statistical test is based on an objective analysis run with a three weeks window in order to capture the most doubtful profiles. They are then visually checked by an operator who decides whether or not they are bad data or real oceanic phenomena. Then a second run which takes into account only the good data is operated on a one week window in order to produce the gridded fields. Each release provides T and S gridded fields and individual profiles both on their original levels and interpolated levels.

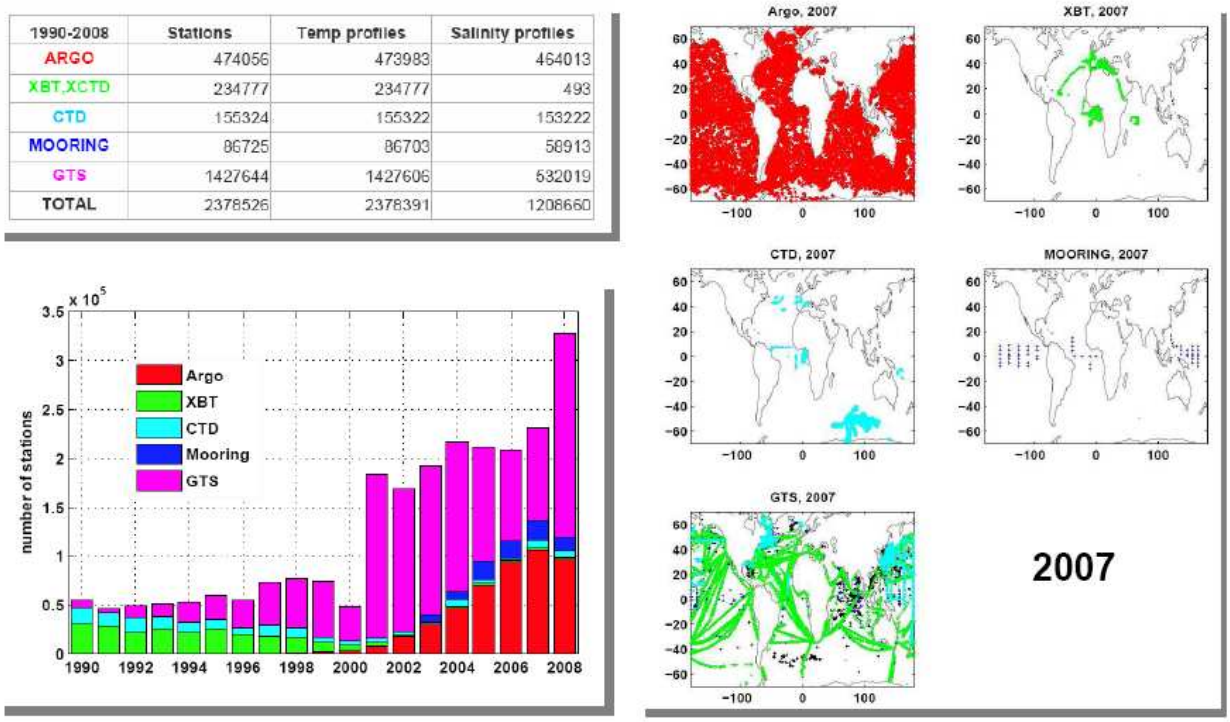

1990-2008	Stations	Temp profiles	Salinity profiles
ARGO	474056	473983	464013
XBT,XCTD	234777	234777	493
CTD	155324	155322	153222
MOORING	86725	86703	58913
GTS	1427644	1427606	532019
TOTAL	2378526	2378391	1208660

Figure 1

Temporal (left) and spatial distribution in 2007 (right) for the different type of data used in CORA.

Goals and uses of the Dataset

Research

CORA database is meant to investigate specific scientific questions. Achieving this goal will lead to the improvement of the quality of the dataset, by detecting abnormal data especially. That will benefit subsequently to the data centre real-time database and the operational results. It is also a way to monitor ocean variability as it is done on the framework of the MyOcean European project (http://www.myocean.eu.org/).

This dataset can be used to estimate the change in global ocean temperature and heat content during the 2003-2008 time period. As shown in previous results, the world ocean is warming (e.g. Levitus et al., 2005). The work of von Schukmann et al. (2009) shows that the signal propagates to increasing depth in time, especially in the northern hemisphere. The average warming rate is 0.77 ± 0.11 W/m2 for the 0-2000m depth layer during 2003-2008.

Ocean model validations

CORA can be used to construct elaborated products such as climatologies of heat content, depth of the thermocline or 20℃ isotherms, or indexes (niño3.4, MOC, PDO…). Such products are especially useful for validating ocean model outputs and improve their quality or assess their results. For example, de Boyer Montégut et al. (2007) validates their OGCM mixed layer depth outputs against in-situ observations in the northern Indian Ocean. After assessing the realism of their experience, they use the model to investigate surface heat budget variability.

Assimilation in ocean models

An important application of such a database is also for ocean model assimilation projects. In France, the goal of GLORYS (GLobal Ocean ReanalYsis and Simulations) project is to produce a series of realistic eddy resolving global ocean reanalyses. Several reanalyses are planned, with different streams. Each stream can be produced several times with different technical and scientific choices. Version 1 of Stream 1 (GLORYS1V1) is produced using the previous version of the CORA data set (see Ferry et al, this issue) and is available on request from products@mercator-ocean.fr. The ocean general circulation model used is based on ORCA025 NEMO OGCM configuration (Barnier et al., 2006).

Références

Barnier B., G. Madec, T. Penduff, J.-M. Molines, A.-M. Treguier, J. Le Sommer, A. Beckmann, A. Biastoch, C. Böning, J. Dengg, C. Derval, E. Durand, S. Gulev, E. Remy, C. Talandier, S. Theetten, M. Maltrud, J. McClean and B. De Cuevas et al., 2006: Impact of partial steps and momentum advection schemes in a global ocean circulation model at eddy permitting resolution. Ocean Dynamics, DOI: 10.1007/s10236-006-0082-1.

Boyer T.P., J. I. Antonov, O. K. Baranova, H. E. Garcia, D. R. Johnson, R. A. Locarnini, A. V. Mishonov, D. Seidov, I. V. Smolyar, and M. M. Zweng, 2009: World Ocean Database 2009, Chapter 1: Introduction, NOAA Atlas NESDIS 66, Ed. S. Levitus, U.S. Gov. Printing Office, Wash., D.C. , 216 pp., DVD.

de Boyer Montégut, C., J. Vialard, S. S. C. Shenoi, D. Shankar, F. Durand, C. Ethé, and G. Madec, 2007,:Simulated seasonal and interannual variability of mixed layer heat budget in the northern Indian Ocean, J. Climate, 20, 3249-3268

Coatanoan C., and L. Petit de la Villéon, 2005: Coriolis Data Centre, In-situ data quality control procedures, Ifremer report, 17 pp. (http://www.coriolis.eu.org/cdc/quality_control.htm)

Gaillard F., E. Autret, V. Thierry, P. Galaup, C. Coatanoan, and T. Loubrieu, 2009: Quality controls of largeArgo datasets, J. Atmos. Ocean. Tech., 26, 337-351

Levitus, S., 1982: Climatological Atlas of the World Ocean, NOAA Professional Paper 13, U.S. Government Printing Office, Rockville, M.D., 190 pp.

Levitus, S., J. Antonov, and T. Boyer, 2005: Warming of the world ocean, 1955-2003, Geophys. Res. Lett., 32.

von Schukmann, K., F. Gaillard and P.Y. Le Traon, 2009: Global hydrographic variability patterns during 2003-2008, J. Geophys. Res.

Large Scale Ocean Variability Estimated from a 3D-Var Reanalysis at Mercator: Sensitivity Experiments

By Elisabeth Remy [1,2]
[1] *CERFACS, Toulouse, France*
[2] *MERCATOR-OCEAN, Toulouse, France*

Introduction

Ocean reanalysis aims at combining available observations with a general circulation model (GCM) to provide a more accurate description of the historical ocean state than can be obtained by model or observations alone. In this context, the model can be interpreted as a space-time dynamical interpolator of the observations. Here we consider a large scale decadal ocean reanalysis that has been produced by combining in situ and altimeter observations with a global ocean GCM using a three-dimensional variational (3D-Var) approach. Our objective is to assess the improvement brought by data assimilation and to illustrate the sensitivity of the ocean state estimates to different assimilation configurations. We focus on the large scale interannual variability.

Model configuration

The ocean model is the LOCEAN primitive equation model OPA8.2 (Madec et al., 1998) in its low resolution configuration ORCA2°. The version of the model used here is a fre e-surface constant volume configuration. Atmospheric forcing fields are applied as “forced flux”. They are derived from the ECMWF atmospheric reanalysis ERA40. After year 2001 when ERA40 is not available, they are taken from ECMWF operational analyses. A strong restoring term to the weekly Reynolds SST is applied, with a coefficient of 200W/m2. The ERA precipitation field has been bias corrected using GPCP precipitation data (Troccoli and Källberg, 2004).

As the global water mass budget is not closed due to large errors in the fresh water fluxes, an additional constraint is applied to close the budget. As a consequence, the model is unable to represent that part of the eustatic trend due to atmospheric mass input observed in altimeter observations.

Variational assimilation method / code

The assimilation system is based on the OPAVAR system developed at CERFACS. The model configuration and assimilation parameters are very close to the setup of the ENSEMBLE experiments. A detailed description of the assimilation system and reanalysis procedure can be found in Daget et al. (2009). The major difference with our system is that we assimilate along track Sea Level Anomalies.

Here we quickly recall the basis of the variational approach. The 4dvar method is based on minimization of a cost function which contains the square root of the observation misfits and a priori information on the solution. The minimum, x*, is a model trajectory close to the observations in agreement with the prescribed model and observation errors. The problem to solve can be expressed as follows:

$$x^* \text{ as } J(x^*)=\min(J(x)), \qquad \text{(eq. 1)}$$

$$x \text{ verifying the model equation : } x_{i+1}=M(x_i)$$

$$\text{where : } \quad J(x) = \tfrac{1}{2} [x_0-x_0^b]^T B^{-1} [x_0-xb_0^b] + \tfrac{1}{2} \Sigma[H(x_i) - y^o]^T R^{-1} [H(x_i) - y^o] \qquad \text{(eq. 2)}$$

Here we search the optimal initial conditions, x_0.

- x_0 is the control vector we want to estimate: it contains the uncorrelated model state variable, x_0^b is the background estimate, usually taken as the final state of the previous assimilation cycle,

- B is the background model error covariance matrix,

- y^o observation vector,

- R is the observation error covariance matrix

This minimization of the cost function is done iteratively using a descent algorithm: at each iteration the gradient is used to compute a new correction in the direction of the minimum. This allows taking into account the non linearity of the model equations.

The 3dvar FGAT (First Guess at Appropriate Time) is derived from the incremental formulation of the 4Dvar. In the 3dVar FGAT approximation, the cost function is linearized and the gradient to compute the descent direction is approximated. The innovation, yo-H(xib), is computed at the observation time. The method is described in Weaver et al. (2003,2005).

The assimilation window for the experiment presented here is 10 days.

The background error covariance matrix, B, contains the variance of the model error on the diagonal, covariance terms and spatial correlation specification off diagonal. The standard deviation prescribed for each control variable depends on the current state of the ocean. The multivariate relations link the model variables using dynamical or physical relationships between the variables. For example, the “salinity balance operator” (Ricci et al, 2005) preserves the water mass properties, insuring that salinity varies according to temperature changes, even without any salinity data assimilated. First order physical equilibrium are also prescribed between the other variables, as the geostrophic equilibrium for velocity, steric component for the sea level.

Observations

Before assimilating observations, it is important to understand their information content, the data processing, and possible filtering, subsampling, in order to precisely compute their equivalent with the model variables and the error estimate.

In situ profiles : observation data sets

For the experiments described here we used the quality-controlled ENSEMBLES (EN3 v1a) in situ dataset produced at the Met Office. Details on the databases used to construct it and the quality control checks that were applied can be found on the dedicated webpage (http://hadobs.metoffice.com/en3/) and in the article by Ingleby and Huddleston (2007).

Sea level anomaly data

The dynamic topography reflects the elevation of sea level due to ocean currents, the steric expansion of the water, and mass forcing from land and atmosphere. It can be defined as the sum of a time mean, the so called Mean Dynamic Topography (MDT) and time variations about this mean: Sea Level Anomalies (SLA). Satellite altimeters estimate the distance to the sea surface, providing accurately the variations of the sea surface. Important pre-treatment of the data are done in order to correct this distance from propagation error in the atmosphere, tides, etc... Along track SLA are assimilated. A delayed time product from AVISO is chosen due to a higher quality of the post processing and its homogeneity over the time period.

The observation error covariance matrix, R, is diagonal. It represents the confidence interval given to the observation compared to its model equivalent. It takes into account not only the measurement error but also the representativity error. The measurement error can contain an instrument error and treatment error, as the representivity error contains signals viewed by observations but not represented by the model. This part of the error can be dominant especially with low spatial resolution model like ORCA2. The model is not able to represent explicitly the mesoscale activity, sharp fronts, etc…

The estimation of the representativity error is based on the statistical approach (Fu et al, 1993) under the hypothesis of uncorrelated observation error. The underlying assumption is that the representativity error can be computed using the variance of the observations compared to the variance of the model. Figure 1 shows the representativity error estimated for the in situ temperature observations and along track sea level anomalies.

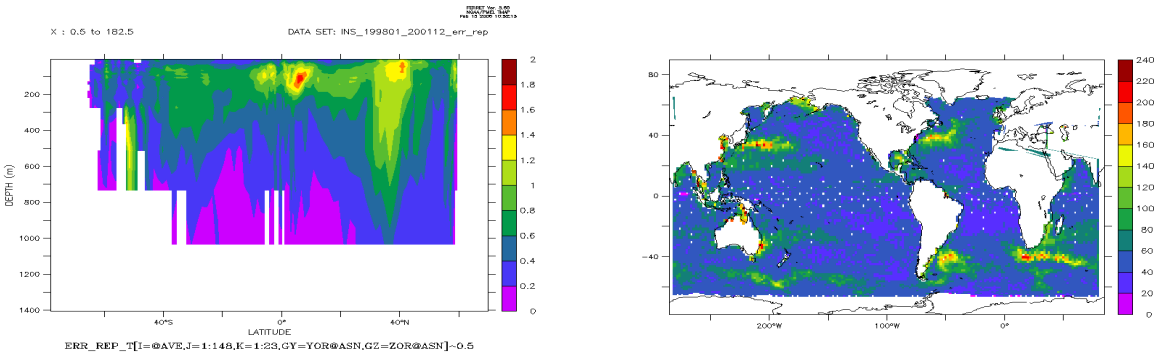

Figure 1

Representativity error maps for temperature observations (longitudinal mean for the global ocean) in °C and along track sea level anomalies in mm.

Experiment setup

We define a default experiment covering the period 1960-2005 using the available observations, in situ and SLA referenced to the model MDT. The model counter part of the observations is computed at the nearest time step. For moored buoy data (e.g., TAO), the model equivalent is a daily mean model temperature field. In space, the model counterpart is computed with an interpolation from the model grid to the observation point.

Different experiments were also done to test the sensitivity of the estimated ocean circulation to the MDT and the type of assimilated observations. The table 1 summarizes the setup of those experiments.

	Time frame	In situ observations	SLA observations
Control	1960-2005	No	No
b090	1960-1992	Yes	No
b09a	1993-2005	Yes	No
b09b	1993-2005	Yes	Yes + Model MDT
b09c	1993-2005	Yes	Yes + Rio MDT

Table 1

Experiments setup

To follow the global sea level rise observed from altimetry measurements, we let the global mean sea level in the model adjust freely. Note that theoretically, the correct approach would be to remove from the SLA observations this signal that the model is not able to properly represent: the global mass budget is forced to zero in the model and the model is built with a volume conservation hypothesis.

Sensitivity experiments

The sensitivity of the linear trend of different diagnosed quantities is presented here. We focus on the period 1993-2001 where we compare the trends estimated from the model with the trend estimated from observations. In experiment b09a only in situ observations are assimilated, while in b09b and b09c, SLA observations are assimilated in addition. The MDT used in the b09b experiment is the model MDT computed from the control model simulation whereas in b09c it is the Rio MDT (Rio and Hernandez, 2004) (Table 1). Estimates of the 0-300 meter mean temperature, salinity and sea level linear trends are presented in Figure 2. We compare the temperature estimation to monthly objectively analyzed subsurface temperature by Ishii et al.(2003) The analysis is based on different datasets including the World Ocean Database/Atlas.

Globally, one can see very similar estimates of the mean temperature trend over the first 300 meters in the different assimilation experiments, comparable to the observed trend. This robustness can be attributed to the data density which allows controlling this variable. In the Southern ocean were data are very sparse, solutions slightly differ. The observations analysis, done by Ishii et al. (2003), does not show significant trend in this region.

The salinity trend appears to be extremely sensitive and strongly differs between experiments. Unrealistically strong trends appear in the southern hemisphere when altimeter data are assimilated. The trend is even stronger when the Rio MDT is used.

The sea level trend is already well constrained by the in situ observations. The assimilation of altimeter data improves the amplitude. The trend is then very close to the observed one for whichever MDT is chosen.

To understand these results, we note that both in situ and SLA observations contain information on the temperature and salinity field. The in situ data provide direct information through T and S profiles, whereas the sea level data (MDT+SLA) reflect the heat and haline content over the whole water column due to the sea water expansion. A hypothesis is that the salinity tends to compensate the inconsistency between the dynamic height deduced from the MDT+SLA and from the in situ observations due to the use of different MDTs compared to the real one. The northern hemisphere is less sensitive probably due to a larger amount of salinity data in this region.

For all these diagnostics, the simulation without assimilation shows the right large scale patterns but with unrealistically small amplitudes: the impact of the assimilation is clearly positive in this respect.

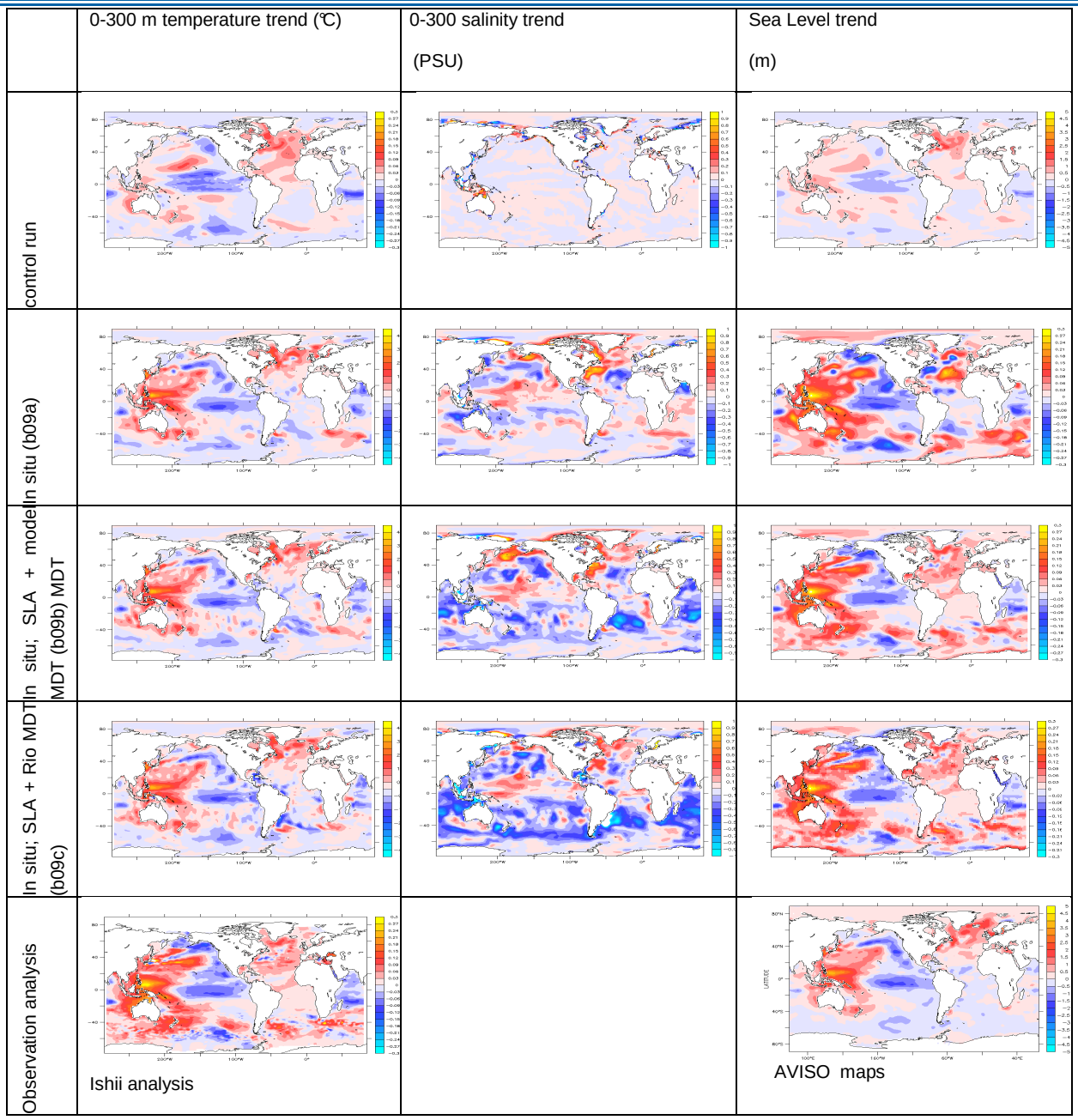

Figure 2

1993-2001 0-300 m temperature (°C), salinity (PSU) and sea level (m) linear trend from assimilation experiments and from analysis of observations

Analysis of the reference simulation 1960-2005

We illustrate the reanalysis results with a few diagnostics focusing on the subsurface representation of the ocean interannual variability estimated from the experiments b090 and b09b over the period 1960-2005 (Table 1). The large increase of the number of in situ observations at the beginning of the ARGO era improves the control of the ocean model variables: the mean misfit to the in situ observations is significantly reduced from 1960 to 2005, especially between 300 and 700 meters depth (not shown here).

Temperature, salinity and SSH trend

The temperature linear trend from 1960 to 2005 is clearly non uniform (Figure 3, left panel). The North Atlantic is warming, as the Pacific is cooling in the subtropical gyre and warming in the southern part. The vertical mean profile temperature evolution for the North East Atlantic (box shown on the temperature trend map) is presented on the right. Mode water formation occurs in this

region of subduction. Successive warm and cold signals propagate from the surface to deeper layers. This clearly shows the importance of the long term variability in the ocean. The situation is very different depending on the region we look at.

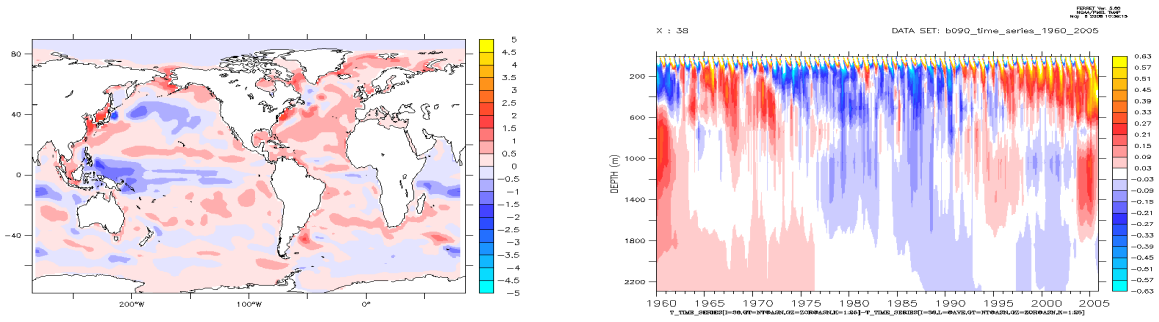

Figure 3

Mean 0-300 m temperature trend 1960-2005 on the left and mean temperature vertical profile evolution in the north east Atlantic (box on the left map) on the right, in °C.

Figure 4 represents the estimated linear trend of the sea level rise on the left and the dynamic height on the right. The Atlantic Ocean shows a rising sea level in the middle of the subtropical gyres, whereas the Pacific Ocean shows different tendencies depending on the latitude. The dynamical height reflects the steric part of the sea level. The differences with the sea level are due to mass changes: advection or input from land, including ice cap or atmosphere. They appear mainly in the southern Pacific Ocean and the Indian Ocean. The partition of the SLA into an eustatic and a steric contribution (dynamic height) is sensitive to the specification of the background error covariance between the different model variables in B (eq. 2). The full model description of the ocean state allows us to decompose the dynamic height into its thermosteric and halosteric part. Those components (not shown here) have opposite contributions: the halosteric tends to moderate the thermosteric part which has an even higher trend than the total dynamical height.

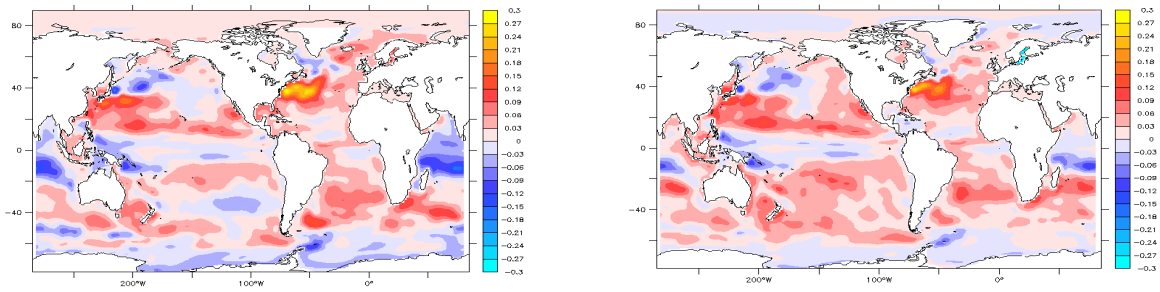

Figure 4

Sea level (left) and dynamical height (right) linear trend from 1960 to 2005 in meters.

Interannual variability

Up to now we have looked at the linear trend, while here we illustrate the use of the reanalysis to examine the interannual variability. A projection on Empirical Orthogonal Functions (EOF) gives an interesting way to analyse the variability of the ocean circulation. The modest size of the model state vector in ORCA2 allows us to perform this computation easily on the 45 years of the simulation.

Figure 5 shows the different spatial patterns associated with the first 3 EOFs of the mean temperature over 0-300m. The EOF coefficient time series is also presented. The seasonal signal has been removed. The ENSO pattern is largely dominant and corresponds to the 1st EOF which explains 26% of the variance. The balance between the eastern and western part represents the change of the slope of the thermocline. The link with the Indian Ocean also clearly appears. The signal in the Atlantic is too small to be significant. The second EOF is also mainly related to tropical Pacific dynamics, while in the Atlantic Ocean a quasi-uniform pattern exists. The third EOF looks like the warming trend, especially in the Atlantic Ocean. The fourth panel of Figure 5

shows the time evolution of the coefficients of the 1st three EOFs. The red curve corresponds to the first EOF, the green one to the second EOF, and the blue one to the third EOF.

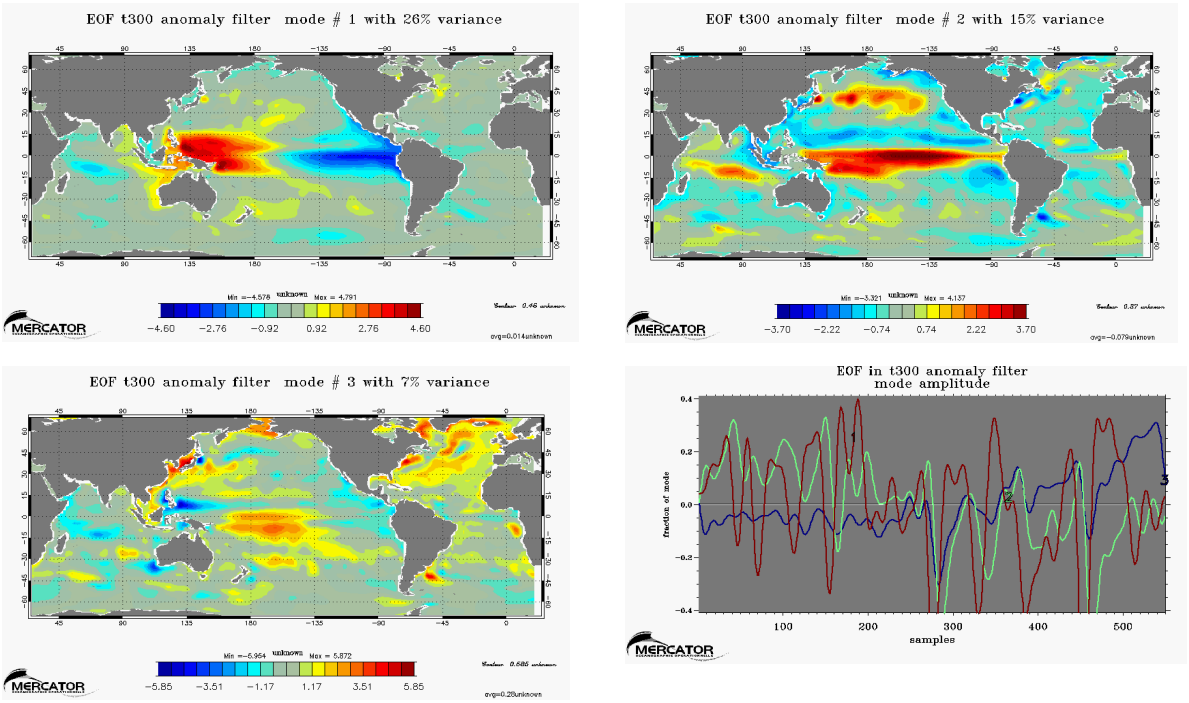

Figure 5

First three EOFS of the decomposition of the mean 0-300m temperature and the time series of the coefficients from 1960 to 2005 (1st eof in red, second in green, third in blue).

Conclusion

This study shows that even with a low resolution ocean model, the large scale variability of the upper ocean can be effectively constrained by assimilating in situ profiles and sea level observations. Some estimates are robust and close to the observed one; others appear to be more sensitive, like salinity. The low resolution configuration provides a useful tool for sensitivity experiments which are too expensive with high resolution models. The comparison of the reanalysis results with the forced run without assimilation shows a significant improvement in the amplitude of the variability of the upper ocean temperature field. The MERCATOR Glorys reanalysis is based on the ORCA ¼° global configuration and the SAM2 assimilation scheme using local inversions. It will be interesting to test the control of the large scale with this 3D-Var complementary to the local analysis method.

Acknowledgements

I would like to thank Anthony Weaver for his comments on this article.

References

Fu L.L., I. Fukumori, and R.N. Miller, 1993: Fitting dynamic models to the geosat sea level observations in the tropical Pacific Ocean. part ii : A linear, wind-driven model. Journal of Physical Oceanography, 23, p. 2162-2181.

Ingleby, B., and M. Huddleston, 2007: Quality control of ocean temperature and salinity profiles - historical and real-time data. Journal of Marine Systems, 65, 158-175.

Ishii, M., M. Kimoto, M. Kachi, 2003: Historical Ocean Subsurface Temperature Analysis with Error Estimates, Monthly Weather Review, Vol. 131, Issue 1, p. 51-73.

Madec, G., P. Delecluse, M. Imbard and C. Levy, 1998: OPA 8.1 Ocean General Circulation Model reference manual. Tech. rep., Institut. Pierre-Simon Laplace (IPSL), France, No11, 91pp.

Ricci S., A. T. Weaver, J. Vialard, P. Rogel, 2005: Incorporating State-Dependent Temperature–Salinity Constraints in the Background Error Covariance of Variational Ocean Data Assimilation, Monthly Weather Review, Vol. 133, Issue 1, p. 317-338.

Rio, M.-H., and F. Hernandez, 2004: A mean dynamic topography computed over the world ocean from altimetry, in situ measurements, and a geoid model, J. Geophys. Res., 109, C12032.

Weaver A. T, J Vialard, and D. L. T Anderson, 2003: Three- and four-dimensional variational assimilation with a general circulation model of the tropical Pacific Ocean. Part I: Formulation, internal diagnostics, and consistency checks. Mon. Wea. Rev., 131, 1360–1378.

Mercator Global Eddy Permitting Ocean Reanalysis GLORYS1V1: Description and Results

By Nicolas Ferry[1], Laurent Parent[1], Gilles Garric[1], Bernard Barnier[2], Nicolas C. Jourdain[2] and the Mercator Ocean team.

[1]*Mercator Océan, Ramonville St Agne, France*
[2]*MEOM-LEGI, CNRS, Université de Grenoble, Grenoble, France*

Abstract

We present here preliminary results from the French Global Ocean Reanalysis and Simulations (GLORYS) project which aims at producing a series of global ocean reanalyses. This project is a collaboration between Mercator-Ocean and French research laboratories, and is a contribution to the project of the European Union MyOcean. The overall objective is to produce state of the art eddy resolving global ocean simulations constrained by oceanic observations by means of data assimilation. GLORYS plans to produce different streams, spanning different time periods and using different technical choices. Here, we present GLORYS1V1 (the first version of the stream 1 reanalysis) covering the "Argo" era (2002-2008), a period characterized by its unique high density of remotely sensed and in situ observations. Assimilation diagnostics as well as the evaluation of the representation of some circulation features are presented.

Introduction

In the last decade, real-time high-resolution ocean analysis and forecasting have become routine tasks done by several operational centers throughout the world (Dombrowsky et al. 2009). Downstream applications of these near real-time operational analyses and forecasts have been demonstrated in many areas such as marine pollution monitoring (Hackett et al. 2009) and marine safety (Davidson et al. 2009), coastal modelling (De Mey et al. 2009), ocean initialization for seasonal forecasting (Balmaseda et al. 2009), support to the navies (Jacobs et al. 2009), biochemistry modeling (Brasseur et al. 2009) etc. Some specific applications of ocean state estimation however require long time series of the three dimensional ocean state called ocean reanalyses. Several groups have produced in the last years ocean reanalyses spanning, for the longest one, the 1960-present time period (Lee et al. 2009). This kind of product is used mostly for climate research, (Lee at al. 2009), for long coupled ocean-atmosphere hindcasts for seasonal forecasts (Balmaseda et al. 2009), and helps to the building of new climate indicators for coastal upwelling, precipitation and extreme weather events such as tropical storms and cyclones (Xue et al. 2009).

Most of the ocean reanalyses are available at coarse resolution (Rienecker et al. 2009) with a horizontal resolution of ~1° and do not include explicitly the mesoscale effects in the estimation of the ocean state. This means that during the altimetric years (1992-present) the observed eddy variability and its subsequent effects (e.g. eddy induced transports) may not be properly taken into account. Another reason why higher resolution reanalyses should be carried out is that fronts (associated to western boundary currents for example) are better resolved and regional biases (like the Gulf Stream overshoot) are reduced. Lastly, high resolution reanalyses should also be beneficial for downstream applications of like biogeochemical modelling or regional / coastal modelling.

With its experience in the field of ocean analysis and forecasting, Mercator has developed a global ocean eddy permitting resolution (1/4°) reanalysis system. This work is done in the framework of the French GLobal Ocean ReanalYsis and Simulations (GLORYS) and the EU funded MyOcean projects. The objective is to produce a series of realistic (i.e. close to the existing observations and consistent with the physical ocean) eddy resolving global ocean reanalyses. Here we present the stream 1 reanalysis (called GLORYS1V1) spanning the 2002-2008 time period (the "Argo" era). The reanalysis system is similar in many aspects to the Mercator operational ¼° global ocean analysis/prediction system (Dombrowsky et al. 2009). However, GLORYS1V1 benefits from significant improvements that are presented here. This paper describes the way Mercator operational ¼° global ocean analysis / forecast system has been modified to produce a 7-year reanalysis. Then, the results of the reanalysis are presented and compared to the operational system in 2007-2008.

Description of GLORYS1V1 reanalysis system

The ocean reanalysis system used (called GLORYS1V1) is based on the operational system PSY3V2 used at Mercator1. GLORYS1V1 benefits from several improvements that we present in the following section. We describe the different components, namely the ocean/sea-ice model, the data assimilation method, the ocean initialization and the observations assimilated. We also

[1] (http://bulletin.mercator-ocean.fr/html/produits/psy3v2/psy3v2_courant_en.jsp)

carefully review the improvements with respect to the operational system. Table 1 summarizes the main differences between the operational system PSY3V2 and GLORYS1V1. The starting date of GLORYS1V1 simulation is 3 October 2001.

Ocean-sea ice model

The model configuration is the same as the one used in the operational global ocean system operated in near real time at Mercator since November 2005 (Drevillon et al. 2008a, Drevillon et al. 2008b). It is a global implementation of the ocean/sea-ice NEMO numerical framework (version 1.09, Madec, 2008) and has many common features with the ORCA025 configuration developed by the European DRAKKAR collaboration (Drakkar group, 2007), the numerical details of which are given in Barnier et al. (2006). The ocean model component is the free surface, primitive equation ocean general circulation model developed at LOCEAN (Madec, 2008). The sea-ice component is the LIM2 sea-ice model (Goosse and Fichefet, 1999). The geographical domain extends from -77°S to the North Pole. The vertical discretisation uses partial steps with 50 vertical levels with an increased resolution near the surface (~1 m near the surface, 11 levels over the top 15m, 500 m at depth). Compared to the operational system PSY3V2, the sea-ice model used for GLORYS1V1 benefits from the following improvements: (i) an Elastic Viscous Plastic (EVP) dynamics of the ice and (ii) a computation at each time step of the ocean-ice stress. These two new parameterizations improve clearly the results of the ice model, in particular the ice extent during summer in the Arctic Ocean (Garric et al., 2008). This improved ice model version is referred to as LIM2_EVP. The CLIO bulk formula (Goose et al., 2001) are used in both GLORYS1V1 and the operational system to calculate the atmospheric forcing function. They are fed with surface variables from ECMWF operational analyses (1-day averages). The ECMWF precipitation field is corrected using GPCP monthly data (Garric, 2006) in a way similar to that proposed by Troccoli and Källberg (2004). This correction is however not sufficient to constrain the global average water budget (evaporation, precipitation and runoff) to a realistic value. That is why the global water budget is set to zero at each time step. Initial conditions used for the ocean are derived from the ARIVO climatology (Gaillard et al. 2008, Gaillard and Charraudeau, 2008) for the month of October. The sea ice initial condition is the sea ice state in October 2001 from a multi decadal model integration performed by the DRAKKAR group (namely G70, Drakkar Group 2007) with the same ocean-sea-ice model.

Data assimilation method

The data assimilation method developed at Mercator (Tranchant et al. 2008) is used in GLORYS1V1. The assimilation scheme is an extended Kalman filter based on the SEEK approach developed at LEGI (e.g. Testut et al. 2003). This approach is used since several years at Mercator and has been implemented in different ocean model configurations like the PSY3V2 1/4° global ocean operational analysis forecasting system.

The SEEK formulation requires knowledge of the forecast error covariance of the control vector. In GLORYS1V1, this vector is composed of the barotropic height field and the 3-dimensional temperature, salinity, zonal and meridional velocity fields. The forecast error covariance is based on the statistics of a collection of ocean state anomalies (typically ~300) and is seasonally dependent. This approach comes from the concept of statistical ensembles where an ensemble of anomalies is representative of the error covariances (ergodic theory). This approach is similar to the Ensemble Optimal Interpolation (EnOI) developed by Oke et al. (2008) which is an approximation to the EnKF (Ensemble Kalman Filter) that uses a stationary ensemble to define background error covariances. In our case, the anomalies are high pass filtered ocean states available over the 1992-2001 time period. It should be noted that the analysis increment is a linear combination of these error modes and depends on the model innovation (observation-model misfit) and on the observation errors.

The length of the assimilation cycle is 7 days and the data assimilation produces,, after each analysis, global increments for the ocean barotropic height, temperature, salinity, zonal and meridional velocity. An Incremental Analysis Update (IAU) method (Bloom et al. 1996) is used to apply the increment to reduce the spin up effects after the analysis time. We implemented the IAU variant described in Benkiran and Greiner (2008) where each analysis increment is applied during two assimilation cycles: the one before and the one after the analysis time.

Observations

The assimilated observations consist in Sea Surface Temperature (SST) maps, along track sea level anomaly (SLA) data, and in situ temperature and salinity profiles. The SST comes from the daily NCEP RTG 1/2° product (Thiébaux, 2003) and is assimilated once per week at the analysis time. The delayed-time along-track SLA data are provided by AVISO (SSALTO/DUACS Handbook, 2009) and benefit from improved SLA corrections. The various altimetric satellite data assimilated in GLORYS1V1 come from Topex/Poseidon, ERS-2, GFO, Envisat and Jason-1. The assimilation of SLA observations requires the knowledge of a Mean Dynamic Topography (MDT): The mean surface reference used is the RIOv5 product (Rio and Hernandez, 2004) combined with a model mean sea surface height near the coasts. In situ temperature and salinity profiles come from the CORA-02 in situ data base provided by CORIOLIS data centre (http://www.coriolis.eu.org/cdc/global_dataset_release_2008.htm). This in situ data base includes profiles originating from the NODC data base, from the GTS, from national and international oceanographic cruises (e.g. WOCE), from ICES data base, TAO/TRITON and PIRATA mooring arrays, and Argo array. The temperature and salinity profiles

have been checked through objective quality controls (Ingleby and Huddleston, 2007) but also visual quality check. Following the first quality check done by CORIOLIS data centre, additional quality check and data thinning is performed.

For each data set, an observation error including both the instrumental error and the model representativeness error (these two errors being supposed to be uncorrelated) are specified. The SST error is spatially variable with a minimum error equal to (0.9° C)2. In the regions of large eddy variability the error is larger and can reach (1.5 °C)2. The SLA obs ervation error is specified according to the knowledge of the satellite accuracy and to the model representativeness error. So, we use a (2 cm)2 instrumental error variance for JASON-1 and TOPEX-Poseidon and a (3.5 cm)2 error for ERS-2, GFO and ENVISAT. For in situ temperature and salinity profiles, the error is diagonal and depends on the geographical location and depth. For temperature, this error is dominated by the inaccuracy of the thermocline position given by the model and the data whereas for salinity, largest errors are located near the surface (Figure 1).

Features	Operational PSY3V2	GLORYS1V1
Model		
Net global water budget	No constrain	Net global water budget =0 at each time step
Sea Ice model	LIM2 (Goosse and Fichefet, 1999)	LIM2_EVP: Elastic Viscous Plastic dynamics of the ice and computation at each time step of the ocean-ice stress
Data assimilation		
Velocity increments	Based on physical balance operators	Based on background covariance
Initialisation	Sequential	Double backward IAU on T, S, U, V, SLA
Observations		
In situ	Operational from Coriolis	CORA-02 until end 2007
SST		Improved observation operator
SLA	Near real-time	Delayed mode

Table 1

Summary of the differences between the operational system PSY3V2 and GLORYS1V1 reanalysis system.

Results of the reanalysis over the Argo period (2002-2008)

Here we present the results of the 2002-2008 reanalysis. Assimilation diagnostics are first shown to check that the system is well constrained by the assimilated observations. Then we look at particular circulation features in order to assess the degree of realism of the reanalysis.

Assimilation diagnostics

Data assimilation is a way to optimally merge information from a model forecast and observations of the real ocean. Several hypotheses are made a priori and the model analyses and forecasts have to verify a posteriori statistics. In this study, we focus on innovation statistics (observation minus model forecast) for the different assimilated observations. A good way to evaluate globally the behaviour of the reanalysis with respect to its water masses is to check the temperature and salinity innovation root mean square as a function of depth and time. Figure 1 shows these statistics for Temperature and Salinity for GLORYS1V1 (reanalysis) and PSY3V2 (operational).

For temperature, the reanalysis and operational systems exhibit a large innovation RMS in the thermocline between 50 and 200 m, around 1.2°C. Because of the large vertical temp erature gradients in the thermocline, small errors in isotherms depth produce large errors. Near the surface and in the mixed layer, the RMS of the innovation is weaker, less than 1°C. The weakly vertically stratified surface layers are well constrained by the assimilation of sea surface temperature, as will be explained thereafter. Below 200 m depth, the RMS decreases with depth. Near 2000 m, which is the deepest immersion where in situ data are available (Argo profiles), the innovation RMS is close to 0.2°C. An interesting point in GLORYS1V1 is that the innovation RMS is stable throughout the reanalysis, showing that the global ocean state is well controlled by data assimilation.

a) GLORYS1V1 TEMPERATURE

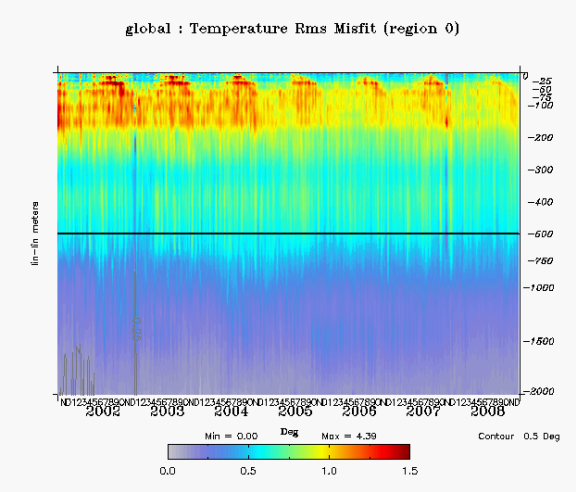

b) GLORYS1V1 SALINITY

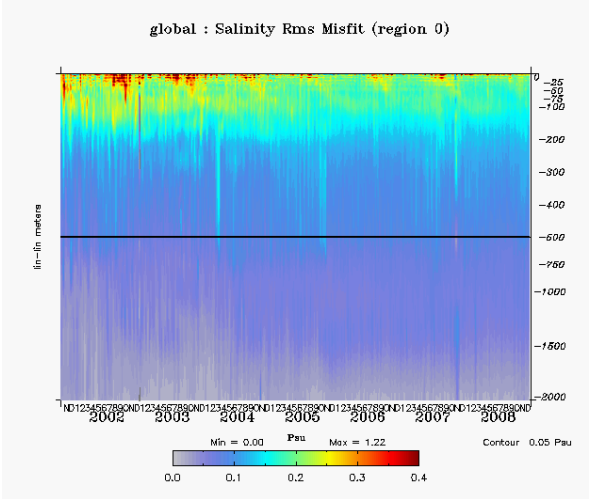

c) PSY3V2

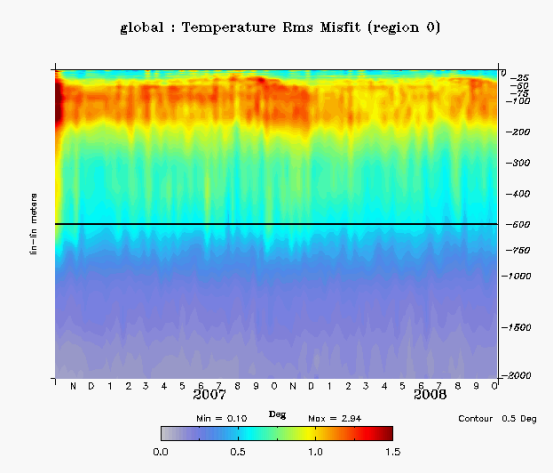

d) PSY3V2

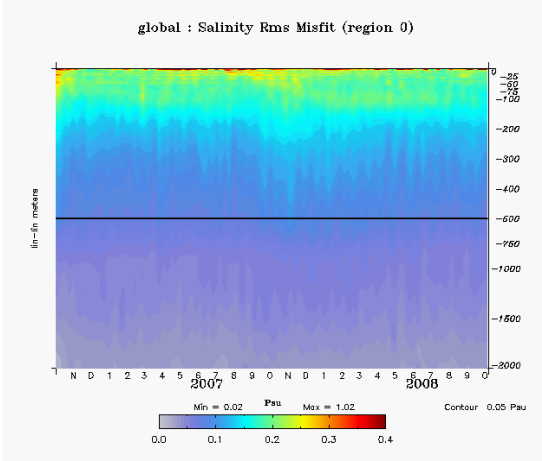

Figure 1

Global RMS of temperature (a, c) and salinity (b, d) innovations in GLORYS1V1 (a, b) and PSY3V2 (c, d) as a function of time and depth. Units are ℃ for temperature and PSU for sal inity.

Note that the temperature innovation RMS has a tendency to weaken with time (Figure 1a). This is related to the increase of the number of Argo profiles available from 2002 up to today (i.e. the observability of the ocean in 2008 is greater than in 2002). Also worth noting is that the RMS in GLORYS1V1 is weaker than in PSY3V2 in 2007 and 2008, improvement that we attribute to the use of IUA. The main difference between GLORYS1V1 and PSY3V2 is the use of an IAU procedure for the model initialization. The IAU procedure is known to remove spin--up effects such as spurious waves and to improve the forecast skill (Benkiran and Greiner, 2008, see their Figure 8).). For that reason, we suspect that the use of IAU is a major contributor to the reduction of the temperature innovation RMS in GLORYS1V1 with respect to PSY3V2.

The RMS of the salinity innovation (Figure 1b) is similar in many aspects to the one in temperature. The largest variability can be found near the surface and within the halocline. Because the halocline is less pronounced than the thermocline, the highest RMS values are found near the surface and not deeper as for the temperature. The high RMS values near the surface are mostly related to errors in the surface forcing (precipitation). The innovation RMS is fairly large in the early years of the reanalysis. As the Argo array becomes denser, the ocean is sampled more frequently and the analysis of the ocean surface salinity improves. Below 100m depth, the RMS is stable throughout the reanalysis except during the first 3 years where the innovation RMS increases slightly between 1000-2000m. During these years the observations are scarce at these depths and the ocean model is drifting away from its initial condition. After 2005, the model is much more constrained by the observations from the Argo array. The GLORYS1V1 innovation RMS reaches a level similar to the operational system.

One of the main assets of an eddy permitting ocean (re-) analysis system is to be able to describe the mesoscale activity of the ocean. During 2002-2008, the eddy variability is well observed thanks to altimetric satellites which provide a quasi-synoptic view of the ocean surface topography. The latter contains the scale information related to quasigeostrophic turbulence as well as climate or secular trends signals. Therefore, the assimilation of sea level anomaly data is a way to constrain efficiently the ocean thermodynamics with scales ranging from the Rossby radius of deformation to basin size. Figure 2 represents some statistics for the SLA innovation over 2007-2008 for GLORYS1V1 and PSY3V2. The RMS of the innovation (Figure 2a) is almost constant during the two years, both for the reanalysis and the operational system. In GLORYS1V1, the misfit RMS is around 8 cm, whereas in PSY3V2 it is slightly greater (8.5~9 cm). The improved performance of the reanalysis is likely to be attributed to the IAU procedure which reduces initialization shocks and produces a solution smooth and continuous in time. Figure 2b exhibits the global average of the misfit. In GLORYS1V1 the average is very close to zero during the 2 years shown (but this is true for the whole reanalysis), whereas low frequency departures from zero exist in PSY3V2. This means that GLORYS1V1 reproduces very well the global sea level variations observed by altimetry, something which is not as well taken into account in the operational system. This improvement can be attributed to the way the global hydrological cycle is parameterized in GLORYS1V1, as will be shown thereafter. Lastly, the RMS misfit / RMS persistence ratio (Figure 2c) is a way to evaluate the forecast skill of GLORYS1V1. A ratio value less than one indicates that the forecast is doing a better job than persistence in term of RMS. In the operational system, the ratio RMS misfit / RMS persistence is close to one, meaning that the model forecast and persistence have basically the same prediction skill for SLA when evaluated globally. In GLORYS1V1, the ratio is fairly constant throughout the reanalysis (not shown) and about 0.9, showing that the reanalysis has a better prediction skill than persistence. This improvement in GLORYS1V1 is also a consequence of the IAU scheme used which produces a continuous temporal description of the ocean. In PSY3V2, shocks due to sequential initialisation contribute to degrade the prediction skill of the model SLA.

a)

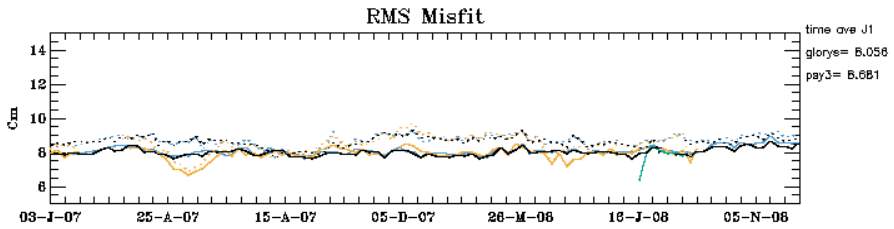

b)

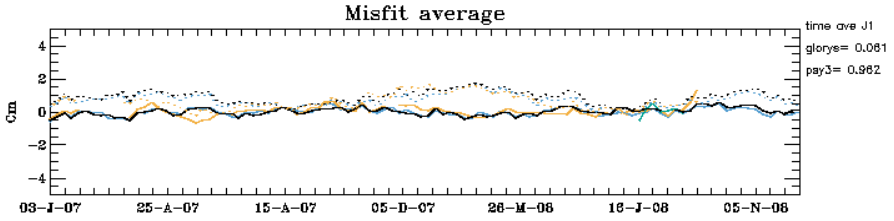

c)

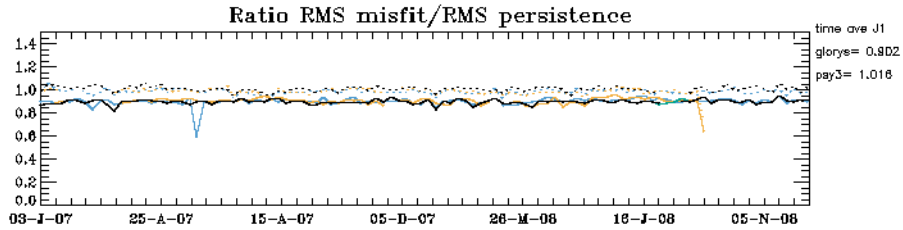

Figure 2

Innovation statistics for SLA computed over the whole ocean for GLORYS1V1 (solid line) and PSY3V2 (dotted line) in 2007-2008. RMS of the innovation (a), global mean innovation (b) and ratio of the RMS of the misfit over RMS of persistence (c). Each curve represents one satellite: Jason1 (black), Envisat (blue), GFO (orange) and Jason2 (green). Unit for (a) and (b) is cm, (c) has not unit.

The third type of observation assimilated is SST. It is a crucial quantity as it controls the coupling between the ocean and the atmosphere and their heat exchanges. The globally averaged misfit (Figure 3a) is close to zero all along the reanalysis. A weak seasonal cycle is present, with a minimum in December-January which does not exceed 0.1°C of amplitude. The misfit average in PSY3V2 reveals a small positive bias of the order of 0.1~0.2°C (SST is too cold). This positive bias is likely induced by the CLIO bulk formulation which is known to extract too much heat from the ocean, especially at mid latitudes. This bias is much less visible in the reanalysis because the IAU is able to project in the past and the future the analysis increment and hence reduces the bias (Benkiran and Greiner, 2008). The RMS of the innovation in GLORYS1V1 (Figure 3b) is around 0.4~0.5°C which is about 0.2°C less than the operational system. This is due to the use of an improved observation operator (see Table 2) in GLORYS1V1. In PSY3V2, the observation operator used is the Identity (i.e. the model forecast is linearly interpolated on the observation point). Because the 1/4° model SST contains much smaller scales than the assimilated SST product (NCEP RTG 1/4°), this leads to aliasing and unrealistic high innovation, as revealed by the large RMS in PSY3V2 in Figure 3b. In GLORYS1V1, an appropriate observation operator is used, removing the fine scales (typically less than 1°) contained in the forecast SST.

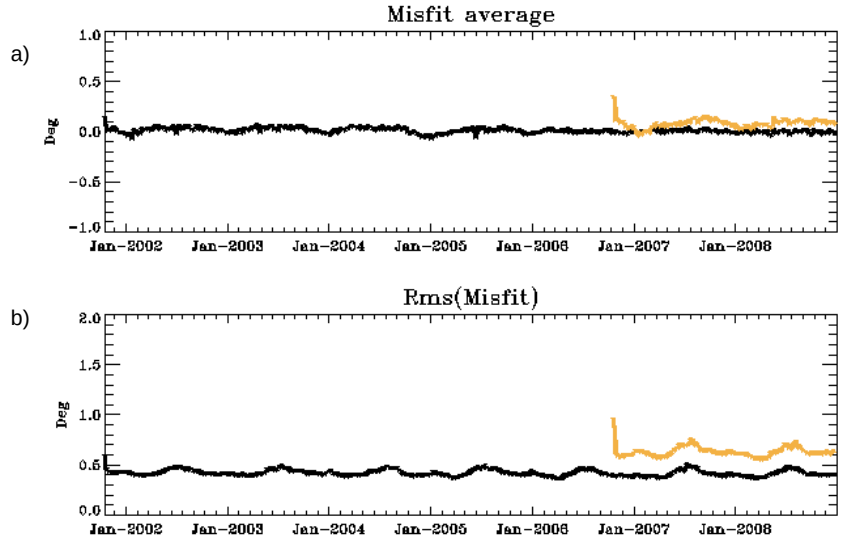

Figure 3

SST innovations statistics for GLORYS1 (black) and PSY3V2R2 (orange) with respect to the assimilated NCEP RTG ½° product. Global average of the misfit (a) and RMS of the misfit (b), in degree Celsius.

Water masses and sea ice extent

An extensive check of the ocean-sea ice model state is an enormous task; however a first measure of the reanalysis skill may be given by analyzing the system capability to conserve water masses. Figure 4a shows the probability density distribution of the temperature misfit in GLORYS1V1 with respect to the Ensembles EN3 in situ data set (Ingleby and Huddleston, 2007) as a function of depth in the North Atlantic over 2002-2006. We also show the results obtained in a free model run, namely G70 (Figure 4b), which has been performed with a similar ocean model configuration used by Drakkar consortium (Drakkar group, 2007). Simulation G70 does not include data assimilation, shares the same surface atmospheric forcing but does not have the same initial condition. We clearly see that the main effect of data assimilation is to reduce the PDF dispersion between the surface and 1200 m depth. The bias present in the free run between 400 and 1000m has been successfully corrected in GLORYS1V1. However, below 1200m depth, large negative temperature misfit (|misfit|>1.5°C) are diagnosed in the reanalysis, a feature which is not present in G70. This means that data assimilation tends to degrade slightly some water masses at depth. This is currently under investigation. Similar diagnostics have been done for the salinity (not shown), showing that the main effect of data assimilation is to reduce the dispersion of the PDF, avoiding the creation of flaws in water masses.

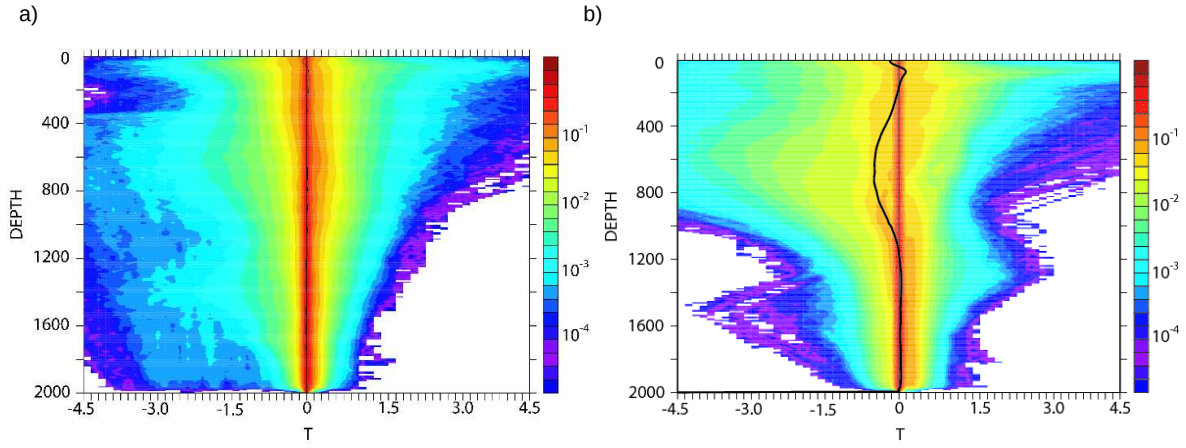

Figure 4

Probability density function (PDF) of the temperature misfit (model-obs.) with respect to EN3 in situ temperature as a function of depth over 2002-2006 in the North Atlantic Ocean. PDF for (a) GLORYS1V1 and (b) G70. The median for each depth is indicated by the black line. Misfit is computed with model monthly values. The colour scale represents the log of the PDF.

The analysis of the sea ice model reveals that the EVP ice dynamics (see Table 1) improve the model skill in the Arctic region (Figure 5a). The sea ice extent correlates significantly (correlation is 0.8) with the observations provided by CERSAT. The negative trend observed during the period is well captured, as well as the two major interannual events that occurred mid 2004 and especially in September 2007. This good skill is attributed mainly to the new physics implemented in the EVP sea-ice model as no assimilation of any sea ice quantities is present in GLORYS1V1, and to a lesser extent to the data assimilation performed in the ocean model. The sea ice extent in the Antarctic is not as well simulated as it is in the northern hemisphere. First of all, the large misfit observed at the beginning of the period (end of 2001) is the consequence of using initial conditions which are not in equilibrium with the LIM2-EVP physics. Also small errors during the sea ice extent minimum are amplified. As no sea ice data assimilation is implemented, the adjustment towards the balanced state lasts one to two years. Afterwards, we can see that the ice model fails to have a realistic seasonal cycle. A systematic overestimation of the summertime extent is observed, a flaw that we have related to the weakness, in terms of variability and amplitude, of the strong southerly winds coming from the Antarctic Continent (the katabatic winds). Stronger winds help to export more efficiently the sea ice off shore and, thus tend to reduce the sea ice cover along the coastlines during summer. The absence of high frequency variance (3 hours) in the daily surface wind stress used is likely qt the origin of the problem. High frequencies in the wind help to export more ice northward and to have a more realistic seasonal cycle.

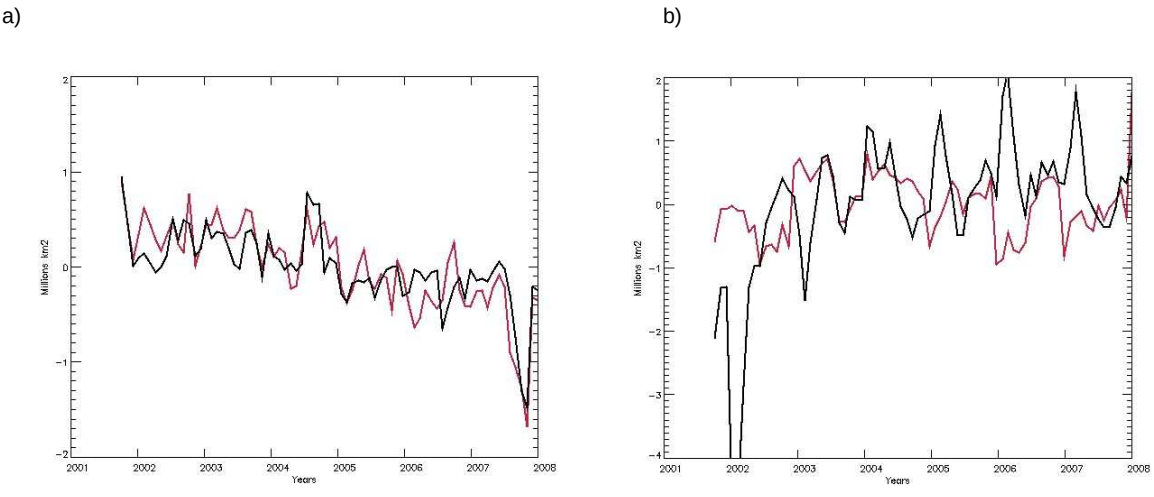

Figure 5

Sea ice extent monthly anomaly in (a) the Arctic and (b) the Antarctic. GLORYS1V1 is in black and sea ice extent provided by CERSAT is in red. Unit is 10^6 km^2.

Global mean sea level and water budget

The global mean sea level variability is an important issue in the context of climate monitoring and forecasting (IPCC, 2007). Ocean reanalyses are appropriate tools to synthesize the information of various kinds of observations in order to build a coherent picture of the past climate. Here we check the ability of GLORYS1V1 to describe realistically the global Mean Sea Level (MSL) and we discuss the main modelling issues related to this aspect. Figure 6 represents the global MSL in GLORYS1V1 and in the altimetric observations provided by AVISO SSALTO/DUACS during 2002-2008. The agreement between the two estimates of the MSL is remarkably good, consistent with the unbiased global average innovation of SLA (see Figure 2b). Small differences (like in November 2006, not shown) are due to the partial global sampling of the altimeters which does not measure ocean sea level under sea ice and at high latitude (beyond 66° for Topex/Poseidon and Jason1). It is interesting to note that these differences can reach as much as 5 mm during several months. GLORYS1V1 reproduces nicely the observed MSL drift (around 2.5 mm/year) as well as the ~1.5 cm peak to peak seasonal cycle.

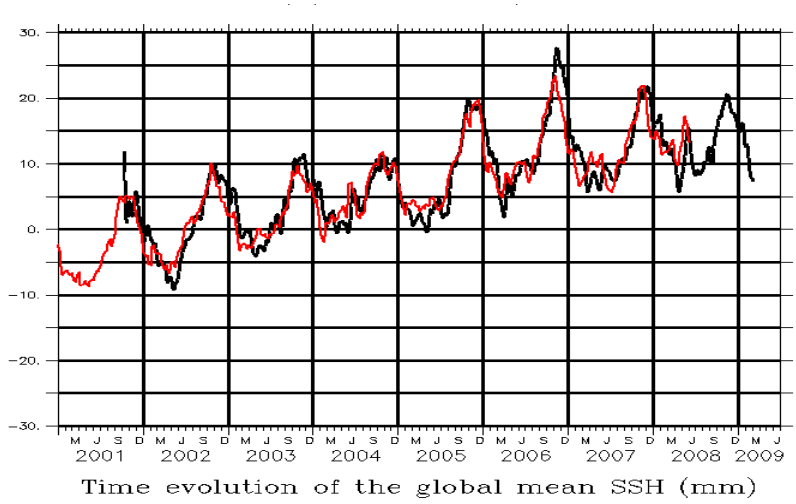

Figure 6

Global mean sea level anomaly in GLORYS1V1 (black) and altimetric AVISO data set (red). Unit is mm.

Simulation	Evaporation	Precipitation	Ice melting	River runoff	SSS damping under sea ice	Net water budget
PSY3V2 (2007)	1347	1150	51	113	0.4	135
GLORYS1V1 (2007)	1372	1106	77	113	19	95 (*)
Difference PSY3V2-GLORYS1V1	-25 (1.8%)	-44 (3.8%)	26 (40%)	0	-19	40 (36%)

Table 2

Global ocean water budget in GLORYS1V1 and PSY3V2 (in mm/year). (*) The net water budget is set to zero at each time step in GLORYS1V1.

The global ocean freshwater budget is an important issue as it contributes to the MSL budget closure (e.g. Cazenave et al. 2008). It directly impacts the sea level rise, but also the ocean freshwater content and thermohaline circulation through density changes (e.g. Latif et al. 2006, Smith and Gregory, 2009). However, the different contributions from precipitation, evaporation, runoff and glaciers have large uncertainties especially at inter annual time scales. Table 2 summarizes for the year 2007 the different contributions to that budget in the both the reanalysis and operational global ocean systems. The net water budget is largely unbalanced in the two simulations, leading to an unrealistic contribution to sea level rise. In PSY3V2, the 135 mm/year average water input would lead to an equivalent sea level rise. In GLORYS1V1, this value is weaker (95 mm/year) but still remains unrealistic when compared to the estimate of ~2 mm/year revealed by recent studies (e.g. Cazenave et al. 2008). Table 2 clearly

shows that the large uncertainty in the net water budget is related to the large errors in each one of the contributions. The relative difference between the two experiments is quite small for the evaporation and precipitation fields. However, as those are huge contributions, the absolute uncertainty is large. The ocean / sea ice exchange has a large relative error which is attributed to the change in the ice model thermodynamics (see Table 1). This shows that the choice of the sea ice model can be a significant source of uncertainty in the global net water budget. Considering these elements, it was decided in GLORYS1V1 to close artificially the water budget by removing the spatial average of the net water flux at every grid point. To our knowledge this is the best strategy to avoid unrealistic drifts in the model MSL (Balmaseda et al. 2007). This means that the net water budget, which is now perfectly balanced, will not be able to change the MSL, this quantity being then changed by the mean sea level increment provided by the data assimilation. This increment could be interpreted as a correction to the net water budget. Figure 2b shows that this way to control the MSL by data assimilation is quite efficient in GLORYS1V1. The choice made in PSY3V2 (no constrain on the net water budget) leads to a global bias, and differences can reach as much as 1.5 cm for MSL. This is due to the unbalanced net water budget which in average tends to increase (by an amount of 135 mm/year) the MSL. Data assimilation tends to compensate this large model error but this is only partly achieved in PSY3V2.

Meridional overturning circulation at 26.5°N

The meridional overturning circulation (MOC) in the Atlantic is an important feature of the climate system as it transports surface warm water to the North and deep cold water to the South. It is a natural mechanism of climate to redistribute heat from low to high latitudes and hence to reduce the meridional temperature gradient of the Earth. The climate change predictions over the next century, as revealed by coupled ocean atmosphere scenarii (IPCC, 2007) suggest that the strength of the Atlantic MOC could be reduced, limiting the global warming over Europe. Since 2004, the RAPID-MOCHA array (Cunningham et al. 2007) deployment permits to monitor the daily to interannual variability of the Atlantic MOC. In spite of the availability of these observations, the evidence of a slowdown of the MOC on a climate scale is still a widely open issue: such a slowdown could only be monitored with enough confidence after several decades of MOC observations (Baehr et al. 2007). Nevertheless RAPID-MOCHA array provides an unprecedented observational data set of the MOC and its different components (Kanzow et al. 2008). Here we use RAPID-MOCHA data to evaluate the capability of the reanalysis to simulate the Atlantic MOC from April 2004 until October 2007. It should be kept in mind that the RAPID-MOCHA data are not assimilated in GLORYS1V1 or PSY3V2 and hence are independent observations. Table 3 summarizes the features of the MOC in the RAPID-MOCHA observations, GLORYS1V1 and PSY3V2. Both ocean analyses compare well with the observations in term of mean and standard deviation. The depth of the maximum MOC at 26.5°N is stable throughout the reanalysis period with no trend (not shown), at about 977 m depth, a value close to the estimation provided by the observations.

Daily MOC at 26.5°N during April 2004-Oct. 2007	RAP ID	GLORYS1V1	PSY3V2
Mean (Sv)	18.5	17.4	19.6
Standard deviation (Sv)	5.1	5.1	5.7
Average depth of the max. MOC (m)	1018±143	977±177	1045±353
Correlation with RAPID MOC at 1000m	-	0.71 / 0.71*/ (0.57)	- / 0.18 / (-)
Correlation with RAPID Ekman transport	-	0.99 / 0.99* / (0.99)	-/ 0.99* / (-)
Correlation with Gulf Stream transport (cable data)	-	0.49 / 0.43* / (0.47)	- / 0.25 / (-)
Correlation with RAPID Southward density transport between Bahamas and Africa	-	0.60 / 0.61*/(0.55)	- / 0.63 / (-)

Table 3

Daily Atlantic MOC volume transport (Sv) at 26.5°N estimated in RAPID data set, GLORYS1V1 and PSY3V2. Correlation is calculated over April 2004-October 2007 time period. For PSY3V2 and values with (*), the time period is November 2006 / October 2007. Values in parentheses are correlations for the interannual part of the signal. Significant correlation with 95% confidence interval is in grey.

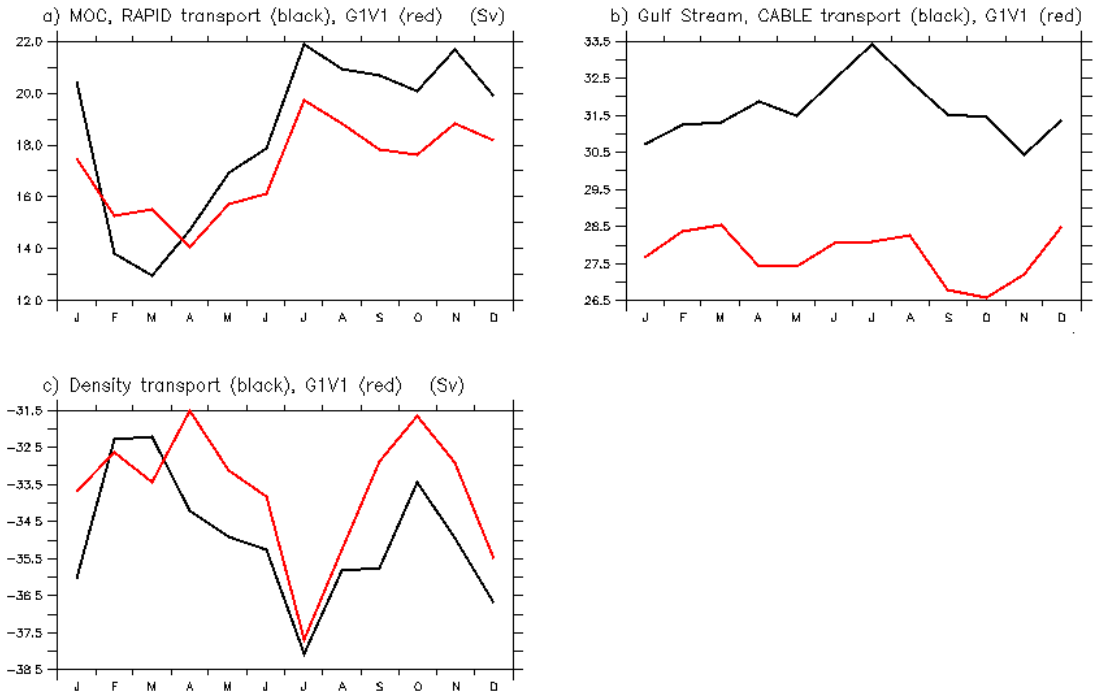

Figure 7

Volume Transport Climatological cycle of (a) MOC, (b) Gulf Stream and (c) between Bahamas and Africa at 26.5°N per density classes. Volume transport is computed from April 2004 until October 2007, and climatologically averaged. GLORYS1V1 is in red and RAPID-MOCHA is in black. Unit is Sv (10^6 m^3/s).

As revealed by Kanzow et al. (2009), the seasonal cycle of the observed MOC estimate at 26.5°N is marked, with peak to peak amplitude of about 7 Sv and maximum in October. This feature is well reproduced by GLORYS1V1 although the amplitude is slightly reduced (~5 Sv, see Figure 7a). Because the MOC is the result of different contributions to the meridional circulation we split here the seasonal signal of the MOC in three parts: the Ekman transport (northward), the Gulf Stream transport between Bahamas and Florida (northward) and the southward density transport between Bahamas and Africa (see Kanzow et al. 2008 for further details). The seasonal cycle is well reproduced in the density transport (Figure 7c), with a strong semi-annual signal. In GLORYS1V1 the Gulf Stream transport (Figure 7b) is weaker (~3 Sv) than the "cable" data and exhibits a well marked semi annual signal whereas the observations indicate rather an annual signal. The Ekman transport (not shown) is nearly identical in GLORYS1V1 and RAPID estimate because ECMWF operational analyses assimilate Quickscat wind stress. Due to the short overlap period of PSY3V2 and RAPID (November 2006 / October 2007), it is not possible to calculate a seasonal cycle with enough confidence. In order to have a comparison between RAPID, GLORYS1V1 and PSY3V2, the correlation between the observations and both (re)analyses was calculated (Table 3). The correlation is also computed for the interannual part of the signal in the case of GLORYS1V1. In the reanalysis, the correlation with RAPID is significant whatever the period, the component of the MOC or the kind of signal considered (total, interannual). In the operational system, correlation is lower and significant only for the density transport between Bahamas and Africa. As GLORYS1V1 and PSY3V2 share the same surface forcing and ocean model configuration, this difference arises from the assimilation and subsequent changes in the ocean states. This also points out that the data assimilation technical choices implemented in GLORYS1V1 are more appropriate to describe the physical processes involved in the MOC.

Conclusion

The GLORYS project has developed an eddy resolving global ocean reanalysis system. The core of the reanalysis system is based on the operational model, and includes some additional innovation like the IAU initialization procedure or the LIM2_EVP ice model. GLORYS has produced the first version of a reanalysis covering the Argo era (2002-2008). The results show that the ocean state is well constrained by data assimilation, and that the ocean physics appears well represented in many aspects. GLORYS plans to extend the reanalyses over a longer period (1992-2009) and to include new developments. The ocean model will benefit from an increased vertical resolution and improved surface forcing based on ECMWF Interim reanalysis. New data

assimilation developments are being tested and include bias correction, the use of a new mean dynamic topography and the assimilation of sea ice concentration data.

Acknowledgements

The authors acknowledge support from Météo France, CNRS, Mercator Ocean, CLS and CERFACS. Computations were performed with the support of Météo-France HPC Centre. The realisation of global ocean reanalyses had the benefit of the grants that Groupe Mission Mercator Coriolis, Mercator-Ocean, and INSU-CNRS attributed to the GLORYS project, and of the support of the European Union FP7 via the MYOCEAN project. The Florida Current cable and section data are made freely available on the Atlantic Oceanographic and Meteorological Laboratory (www.aoml.noaa.gov/phod/floridacurrent/) and are funded by the NOAA Office of Climate Observations. Data from the RAPID-WATCH MOC monitoring project are funded by the Natural Environment Research Council and are freely available from www.noc.soton.ac.uk/rapidmoc.

References

Baehr J., Haak H., Alderson S., Cunningham S.A., Jungclaus J.H., Marotzke J., 2007: Timely detection of changes in the meridional overturning circulation at 26ºN. J. of C limate, 20, 5827-5841.

Balmaseda, M., A. Vidard and D. Anderson, 2007: The ECMWF System 3 ocean analysis system. ECMWF Tech. Mem. 509, pp47.

Balmaseda M, O.J. Alves, A. Arribas, T. Awaji, D.W. Behringer, N. Ferry, Y. Fujii, T. Lee, M. Rienecker, T. Rosati, and D. Stammer, 2009. Ocean initialisation for seasonal forecasts. Oceanography. 22:154-159.

Barnier, B., G. Madec, T. Penduff, J.M. Molines, A.M. Treguier, J. Le Sommer, A. Beckmann, A. Biastoch, C. Böning, J. Dengg, C. Derval, E. Durand, S. Gulev, E. Remy, C. Talandier, S. Theetten, M. Maltrud, J. McClean, B. De Cuevas 2006: Impact of partial steps and momentum advection schemes in a global ocean circulation model at eddy permitting resolution. Ocean Dynamics, DOI: 10.1007/s10236-006-0082-1.

Benkiran M. and Greiner E., 2008: Impact of the Incremental Analysis Updates on a Real-Time System of the North Atlantic Ocean. Journal of Atmospheric and Oceanic Technology 25(11): 2055.

Bloom, S.C., Takas, L.L., Da Silva, A.M., Ledvina, D. 1996: Data assimilation using incremental analysis updates. Monthly Weather Review, 124, 1256–1271.

Brasseur P., Gruber N., Barciela R., Brander K., Doron M., El Moussaoui A., Hobday A., Huret M., Kremeur A.-S., Lehodey P., Matear R., Moulin C., Murtugudde R., Senina I. and Svendsen E., 2009: Integrating Biogeochemistry and Ecology Into Ocean Data Assimilation Systems. Oceanography. 22:206-215.

Cazenave A., K. Dominh, S. Guinehut, E. Berthier, W. Llovel, G. Ramillien, M. Ablain and G. Larnicol: Sea level budget over 2003–2008: A reevaluation from GRACE space gravimetry, satellite altimetry and Argo. Global and Planetary Change, Volume 65, Issues 1-2, January 2009, 83-88.

Cunningham S.A., Kanzow T., Rayner D., Baringer M.O., Johns W.E., Marotzke J., Longworth H.R. Grant E.M., Hirschi J.J.-M., Beal L.M., Meinen C.S., Bryden H.L, 2007: Temporal variability of the Atlantic Meridional Overturning Circulation at 26ºN, Science, 317 , 935-938, doi:10.1126/science.1141304

Davidson F, A. Allen, G.B. Brassington, Ø. Breivik, P. Daniel, M. Kamachi, S. Sato, B. King, F. Lefevre, M. Sutton, and H. Kaneko, 2009: Safety and effectiveness of operations at sea. Oceanography 22:176-181.

De Mey P P. Craig, F. Davidson, C.A. Edwards, Y. Ishikawa, J.C. Kindle, R. Proctor, K.R. Thompson, J. Zhu, and the GODAE Coastal and Shelf Seas Working Group (CSSWG) Community, 2009. Coastal modelling and applications. Oceanography 22:198-205.

Dombrowsky E., L. Bertino, G.B. Brassington, E.P. Chassignet, F. Davidson, H.E. Hurlburt, M. Kamachi, T. Lee, M.J. Martin, S. Mei, and M. Tonani, 2009: GODAE systems in operations. Oceanography. 22:80-95.

Drakkar group 2007. Eddy-permitting Ocean Circulation Hindcasts of past decades. CLIVAR Exchanges, No 42, 12(3), 8-10.

Drévillon, M.; Bourdallé-Badie, R.; Derval, C.; Drillet, Y.; Lellouche, J-M.; Rémy, E.; Tranchant, B.; Benkiran, M.; Greiner, E.; Guinehut, S.; Verbrugge, N.; Garric, G.; Testut, C-E.; Laborie, M.; Nouel, L.; Bahurel, P.; Bricaud, C.; Crosnier, L.; Dombrowsky, E.; Durand, E.; Ferry, N.; Hernandez, F.; Galloudec, O Le; Messal, F.; Parent, L. 2008a. The GODAE/Mercator Ocean global ocean forecasting system: results, applications and prospects. J. of Operational Oceanogr.,1:51-57.

Drévillon M., J-M. Lellouche, E. Greiner, E. Rémy, N. Verbrugge, L. Crosnier, 2008b : Ocean circulation and water properties in 2007 described by the MERSEA/Mercator Ocean V2 global ocean analysis and forecasting system. Mercator Newsletter, 29:9-22.

Gaillard, F., E. Autret, V. Thierry, P. Galaup, 2008: Quality control of large Argo datasets, J. Atmos. Ocean. Tech., 26, 337-351.

Gaillard, F. and R. Charraudeau, 2008: New climatology and statistics over the global ocean. MERSEA del. 5.4.7. June 2008.

Goosse, H., and T. Fichefet, 1999: Importance of ice-ocean interactions for the global ocean circulation: A model study. J. Geophys. Res.,104 :23,337-23,355.

Goosse H, Campin J-M, Deleersnijder E, Fichefet T, Mathieu P-P, 2001: Description of the CLIO model version 3.0. Institut d'Astronomie et de Géophysique Georges Lemaitre, Catholic University of Louvain, Belgium.

Hackett B, Comerma E, Daniel P, Ichikawa H. 2009. Marine pollution monitoring and prediction. Oceanography, 22:168-175.

Ingleby and Huddleston, 2007: Quality control of ocean temperature and salinity profiles – historical and real-time data. J. Mar. Sys., 65:158-175.

Intergovernmental Panel on Climate Change, 2007: Climate Change 2007: Synthesis Report : Contribution of Working Groups I, II and III to the Fourth Assessment Report of the IPCC. Core Writing Team, Pachauri, R.K. and Reisinger, A. (Eds.) IPCC, Geneva, Switzerland. pp 104.

Jacobs G et al. 2009. Applications from GODAE to Navies throughout the world. Oceanography. 22:182-189.

Kanzow, T., J. J.-M. Hirschi, C. S. Meinen, D. Rayner, S. A. Cunningham, J. Marotzke, W. E. Johns, H. L. Bryden, L. M. Beal, and M. O. Baringer, 2008: A prototype system of observing the Atlantic Meridional Overturning Circulation - scientific basis, measurement and risk mitigation strategies, and first results, J. of Operational Oceanography, 1, 19-28.

Kanzow T., S.A. Cunningham, W.E. Johns, J.J.-M. Hirschi, J. Marotzke, M.O. Baringer, C.S. Meinen, M.P. Chidichimo, C. Atkinson, L.M. Beal, H.L. Bryden, J. Collins, 2009: Seasonal variability of the Atlantic meridonal overturning circulation at 26.5N, Journal of Climate [submitted].

Latif,M., C. Böning, J. Willebrand, A. Biastoch, J. Dengg, N. Keenlyside, G. Madec and U. Schweckendiek, 2006: Is the thermohaline circulation changing? J. Clim. 19:4631–4637.

Lee T T. Awaji, M.A. Balmaseda, E. Greiner, and D. Stammer, 2009. Ocean State Estimation for Climate Research. Oceanography 22: 160-167

Madec G. 2008. NEMO ocean engine. Note du Pole de modélisation, Institut Pierre-Simon Laplace (IPSL), France, No 27. pp205. ISSN No 1288-1619.

Oke, P.R., Brassington, G.B., Griffin, D.A. and Schiller, A. 2008: The Bluelink Ocean Data Assimilation System (BODAS), Ocean Modelling, 21, 46-70, doi:10.1016/j.ocemod.2007. 11.002.

Rienecker M., T. Awaji, M. Balmaseda, B. Barnier, D. Behringer, M. Bell, M. Bourassa, P. Brasseur, L.-A. Breivik, J. Carton, J. Cummings, E. Dombrowsky, C. Fairall, N. Ferry, G. Forget, H. Freeland, W. Gregg, S. M. Griffies, K. Haines, D. E. Harrison, P. Heimbach, M. Kamachi, E. Kent, T. Lee, P.-Y. Le Traon, M. McPhaden, M. J. Martin , P. Oke, M. D. Palmer, E. Remy, A. Rosati, A. Schiller, D. M. Smith, D. Stammer, N. Sugiura, K. E. Trenberth, Y. Xue, 2009; Synthesis and assimilation systems: essential adjuncts to the Global Ocean Observing System, Oceanobs'09 plenary talk, available at http://www.oceanobs09.net/blog/?p=803

Rio, M.-H., and F. Hernandez (2004), A mean dynamic topography computed over the world ocean from altimetry, in situ measurements, and a geoid model, J. Geophys. Res., 109, C12032, doi:10.1029/2003JC002226.

Roullet, G., and G. Madec, 2000: Salt conservation, free surface, and varying levels: a new formulation for ocean general circulation models, J. Geophys. Res., 105(C10):23,927–23,942.

Smith, R. S., and J. M. Gregory, 2009: A study of the sensitivity of ocean overturning circulation and climate to freshwater input in different regions of the North Atlantic, Geophys. Res. Lett., 36, L15701, doi:10.1029/2009GL038607.

Ssalto/Duacs User Handbook, 2009: (M)SLA and (M)ADT near-real time and delayed time products. SALP-MU-P-EA-21065-CLS, Edition 1.9). Reference: CLS-DOS-NT-06.034

Nomenclature: SALP-MU-P-EA-21065-CLS .Issue: 1 rev 10. Date: 4 March 2009.

Testut, C-E., P. Brasseur, J-M Brankart and J. Verron , 2003 : Assimilation of sea-surface temperature and altimetric observations during 1992–1993 into an eddy permitting primitive equation model of the North Atlantic Ocean. J. Mar. Sys., 40-41:291-316.

J. Thiébaux, E. Rogers, W. Wang, B. Katz, 2003: A New High-Resolution Blended Real-Time Global Sea Surface Temperature Analysis. Bull. Am. Met. Soc., 84: 645-656 doi: 10.1175/BAMS-84-5-645.

Tranchant B., C-E Testut, L.Renault, N. Ferry, F. Birol and P. Brasseur, 2008: Expected impact of the future SMOS and Aquarius Ocean surface salinity missions in the Mercator Ocean operational systems: New perspectives to monitor ocean circulation. Remote Sensing of Environment, 112:1476-1487.

Troccoli A. and Källberg P., 2004. Precipitation correction in the ERA-40 reanalysis. ERA-40 Project Report Series, 13.

Y. Xue, O. Alves, M. A. Balmaseda, N. Ferry, S. Good, I. Ishikawa, T. Lee, M. J. McPhaden, A. Peterson, M. Rienecker, 2009: Ocean State Estimation for Global Ocean Monitoring: ENSO and Beyond ENSO. Oceanobs'09 Community White Paper.

Re-analyses in the Global Ocean at CMCC-INGV: Examples and Applications

By Simona Masina[1,2], Pierluigi Di Pietro[2], Andrea Storto[1], Srdjan Dobricic[1], Andrea Alessandri[1], Annalisa Cherchi[1,2]
[1]*Centro Euro-Mediterraneo per i Cambiamenti Climatici,Bologna,Italy*
[2]*Istituto Nazionale di Geofisica e Vulcanologia, Bologna, Italy*

Abstract

Global ocean modelling activities at Centro Euro-Mediterraneo per i Cambiamenti Climatici (CMCC) include the development and implementation of data assimilation techniques applied to a global ocean general circulation model to investigate the role of the ocean on climate variability and predictability. The main objective is the production of global ocean re-analyses over multidecadal periods to reconstruct the state of the ocean and the large scale circulation over the recent past for climate applications and for the assessment of the benefits of assimilating ocean observations on seasonal and longer climate predictability.

Here we present the main characteristics of the assimilation system and a set of global ocean re-analyses produced with this system. Applications of these data assimilation products to the study of climate variability and to the assessment of subsurface ocean initialization contribution to seasonal climate predictability will also be reported.

Introduction

Estimating the state of the ocean is a primary target in the context of both climate variability assessments and predictability purposes such as the production of ocean initial conditions for seasonal and longer time-scale climate forecasts. Several efforts aimed at extending the available observational dataset of the global ocean have been made in the past two decades. However, observations provide a patchy description of the ocean state, and a reliable state estimate can only be achieved by combining in an optimal way the existing observations with our theoretical knowledge of the dynamics embodied in ocean general circulation models (OGCMs). Considerable advancements have been made in the development of ocean data assimilation techniques, partly fed by the long used expertise developed within the Numerical Weather Prediction (NWP) community.

Over the course of the past two decades, a number of global ocean data assimilation (ODA) systems have been developed to estimate the time-evolving, three-dimensional state of ocean circulation. Results are especially useful for analyzing unobserved quantities, as the meridional overturning circulation and the oceanic heat transport, important elements for monitoring climate variations.

Today, several global ocean data assimilation products are available and can be used for several purposes as climate applications and initialization problems. The number of studies that utilize the products from these systems to investigate various aspects of ocean circulation and climate variability is increasing (for a review see Lee et al. 2010, and Stammer et al., 2010). For instance, ODA products have been applied to studies over a wide range of topics in physical oceanography and climate research, like the nature of sea level variability (e.g., Carton et al. 2005, Köhl and Stammer 2008), and mixed-layer heat balance (e.g., Drbohlav et al., 2007 and Halkides and Lee, 2009). Moreover, the relationship between atmospheric variability and a local or a remote response of the deep ocean was investigated by Masina et al. (2004), and feedback processes acting during ENSO were summarized by Capotondi et al. (2006). Pierce et al. (2000) and Pohlmann et al. (2009) show applications of ODA products for initializing coupled climate models and many examples exist about their beneficial impact on climate forecasts at the seasonal time scale (among the most recent Balmaseda et al., 2007, Zheng et al., 2007, Hackert et al., 2007).

This paper describes the development of a global ODA system at CMCC, some recent developments aimed at producing multi-decadal re-analyses of the three-dimensional ocean state used for climate research, and initial conditions for a seasonal climate prediction system (Alessandri et al., 2009). Finally, we describe the most recent and on-going activities.

The Global Ocean Data Assimilation System

The CMCC-INGV Global Ocean Data Assimilation System (CIGODAS) is composed of the OGCM OPA 8.2 (Madec et al., 1999) in the ORCA2 global configuration 2° longitude x 2° cos(φ) latitude of resolution, and an Optimal Interpolation (OI) scheme based on the System for Ocean Forecasting and Analysis (SOFA) assimilation software (De Mey and Benkiran, 2002). The original SOFA code has been modified in order to implement data assimilation of temperature and salinity into the global ocean code (Bellucci et al., 2007).

Ocean model and the CONTROL experiment

In all the re-analyses that we produce, the ocean model OPA 8.2 (Madec et al., 1999) is spun up with ERA-40 (Uppala et al. 2005) derived climatological fluxes of momentum, heat, and freshwater, for five years, starting from a motionless ocean, and Levitus hydrographical initial conditions (Levitus et al., 1998).

A spin up that covers the period from 1953 to 1957 is followed by a simulation forced with daily ERA-40 fluxes from January 1958 to December 1961. Sea surface temperatures are restored to an ERA-40 climatological year (1971-2000) with a Newtonian damping heat flux of 200 W/°C/m^2, corresponding to a restoring time scale of about 12 days (assuming a mixed layer thickness of 50 m). A weaker relaxation to Levitus et al. (1998) temperature and salinity climatology along the whole water column is also applied, with a 3-yr damping time scale.

The ocean state at the end of 1961 provides the initial conditions for the interannually forced run (Control, see Table 1), starting on 1st January 1962. The integrations are performed using the same forcings and restoring parameters adopted to generate the 1958-61 non-climatological spin up. This is not true for sea surface temperatures that are relaxed to monthly HadISST data (Rayner et al., 2003) up to Dec 1981, then Reynolds temperatures (Reynolds, 1988) from Jan 1982 to Aug 2002, linearly interpolated to daily values. Operational ECMWF SST fields are then used, starting from September 2002 onwards.

During the model integration, a daily adjustment is applied to the global sea surface height, aimed at removing a drift associated with the nonzero residual of the globally averaged freshwater fluxes. An improved version of ERA-40 freshwater fluxes, correcting a bias in the precipitation (Troccoli and Källberg, 2004) is used. From Jan 2002 onwards operational ECMWF fields are used as forcing fields (wind stress, heat and freshwater fluxes).

In order to prevent the onset of a numerical instability in the Southern Ocean, off the Antarctic coast, a full-depth relaxation to Levitus temperature and salinity climatology is applied poleward of 60°N/60°S, with a gradual reductio n of the restoring time scale from 3 year to 50 days occurring in the 60°-70° N/S latitude belt. The restoring time scale is 50 days at the top level, gradually increasing to 1 year at the bottom.

Experiment	Period	Forcing	Assim Data	EOF Set
Control	1962-2006	ERA40, OP	--	--
OI1	1962-2001	ERA40	EN1	V1
OI2	1962-2001	ERA40	EN2	V2
OI3	1962-2006	ERA40, OP	EN3	V2
OI4	1962-2006	ERA40, OP	EN3	V3

Table 1

Experiment set-up summary table.

Assimilation scheme

The assimilation of observed temperature and salinity profiles is done through a Reduced Order Optimal Interpolation (ROOI) scheme. This scheme is implemented using the SOFA 3.0 software (De Mey and Benkiran, 2002) after ad-hoc changes in both the numerical and assimilation aspects which transform the original code into a more computationally efficient and suitable code to be used for global assimilation. More technical information about the assimilation system can be found in the CIGODAS technical report (Di Pietro and Masina, 2009).

An important feature of this ROOI scheme lies in the multivariate structure of the background error covariance matrix, which spreads the corrections over different parameters. In the present implementation the state vector is defined as the temperature and salinity vector. Bivariate background-error vertical covariances are represented by EOFs of temperature and salinity. This implies that when, for example, only vertical temperature profiles are assimilated, corrections are applied to salinity as well by the vertical EOFs (Belluci et al., 2007).

The multivariate EOFs used for assimilating in situ data have been diagnosed from the synthetic dataset of vertical temperature and salinity profiles provided by the ocean model simulation where no data assimilation was applied, i.e., the Control experiment. In order to reduce the problem size and filter out noisy vertical correlations, only the first ten dominant modes are retained.The re-analyses are composed of a sequence of assimilation tasks and ocean model integrations. The frequency of the re-analyses is 15 days, although ocean variables are computed as daily averages by the ocean model. The daily outputs are then processed to produce monthly means of the same variables, which are then stored.

Within our experiments, we have used three different sets of static EOFs (see Table 1):

in version V1 of multivariate EOFs, they are calculated for different sub regions, defined according to homogeneous dynamical regimes;

in version V2 of multivariate EOFs, they are calculated for each grid point, and are seasonally dependent . The EOFs are evaluated from horizontally smoothed temperature and salinity fields, using a three point radial mean filter;

in version V3 of multivariate EOFs, they are calculated for each grid point, and are seasonally dependent. The EOFs are evaluated from temperature and salinity fields without horizontal smoothing.

Observed temperature and salinity profiles

The observed temperature and salinity used in our re-analyses are taken from the ENSEMBLES dataset. The profiles are obtained primarily from the WORLD OCEAN DATABASE 2005, supplemented using data from other sources: GTSPP from 1990 onwards and the USGODAE Argo Global Data Assembly Centre (GDAC) for Argo data from 1999 onwards. The processing was performed for the EU supported project ENSEMBLES. Earlier quality control development and processing was performed for the EU ENACT project (Ingleby and Huddleston, 2007).

Three different releases have been used (see Table 1):

EN1: this dataset covers the period from 1956 to 2001. A bug over the XBTs (erroneous double drop rate-correction) affects this dataset.

EN2: this dataset covers the period from 1956 to 2001. The bug affecting the XBTs has been removed in this release

EN3: this dataset covers the period from 1956 to 2006. The quality check adopted in this release has been further refined, mainly adopting a new reference background obtained from objectively analyzed temperature and salinity fields derived from the EN2 dataset.

Data assimilation from 2007 onwards is performed using quality checked vertical profiles delivered by the Coriolis dissemination centre (http://www.coriolis.eu.org).

An ensemble of global ocean re-analyses

A set of the re-analyses produced with the CIGODAS (see Table 1) have been compared with the aim to estimate their differences and the associated uncertainties. Some of these re-analyses can be downloaded at www.bo.ingv.it/contents/Scientific-Research/Projects/oceans/enact1.html.

Several methods can be used to evaluate the skill of an analysis, the most common being comparison with independent observed data or objectively analyzed fields. We use here the TOGA-TAO moorings monthly temperature and salinity, from 1987 to 2001 (Hayes et al., 1991) to evaluate the system skill in representing the equatorial thermal and salinity structure and variability. Even if the TOGA-TAO observations are not independent since they have been assimilated into the system, the comparison is a proof of the efficiency and of the limitations of the assimilation system. From 1962 to 2001 the Bermuda Station (32°N, 64°W) observed monthly salinity time-depth series is used as well, being the longest available salinity record.

Temperature in the Pacific Ocean

In the Pacific Ocean, sample time-depth sections of temperature differences between model and TAO (not shown) indicate that the assimilation of observed temperature brings a more realistic thermal structure in the Pacific Equatorial region and in particular it improves the vertical gradient at the thermocline level. In order to give a quantitative evaluation of the impact of the different EOFs and assimilated observations in the Equatorial Pacific, temperature and salinity Root Mean Squared Differences (RMSD) between TAO, Control simulation and ocean re-analyses have been calculated at every TAO location.

For instance at 235°E (Figure 1), temperature shows a clear RMSD reduction when Control Run is compared with OI1. A further slight RMSD reduction is also obtained in OI2 and an overall improvement is achieved with OI3. The greater improvement obtained by OI3 can be explained by the better quality of observed data (EN3 vs EN2) used, considering that the same EOFs of OI2 are used. On the other hand, a further little improvement in RMSD derived from OI4 can be attributed to the new EOFs adopted (V3 vs V2).

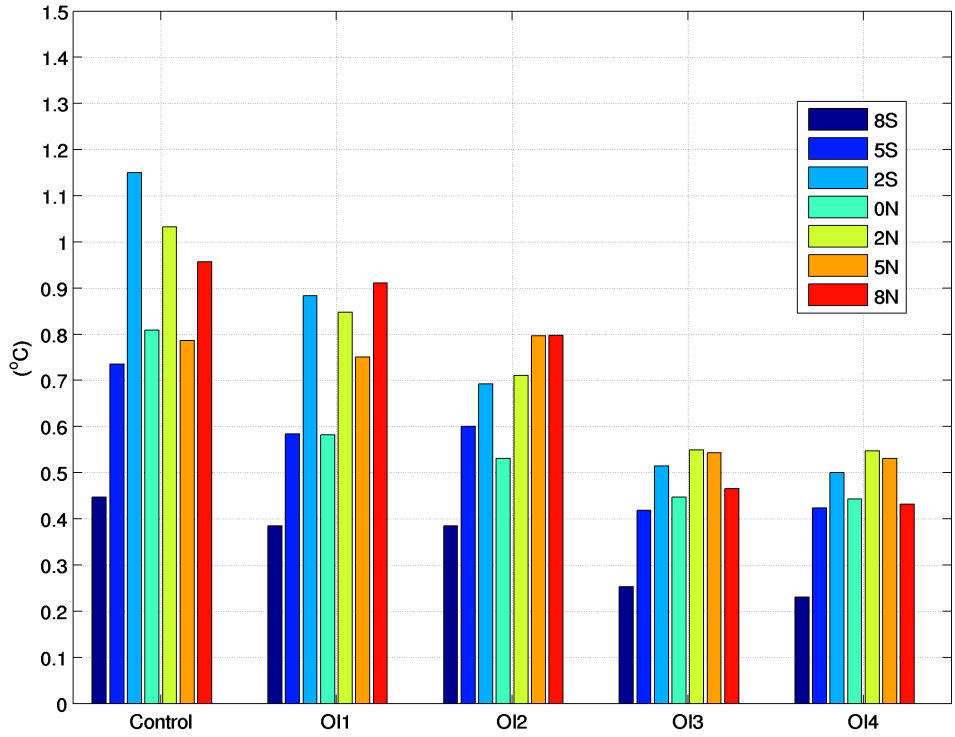

Figure 1

RMS differences (°C) between temperature TAO observ ations and temperature from the re-analyses in Table 1 at 235°E and various latitudes.

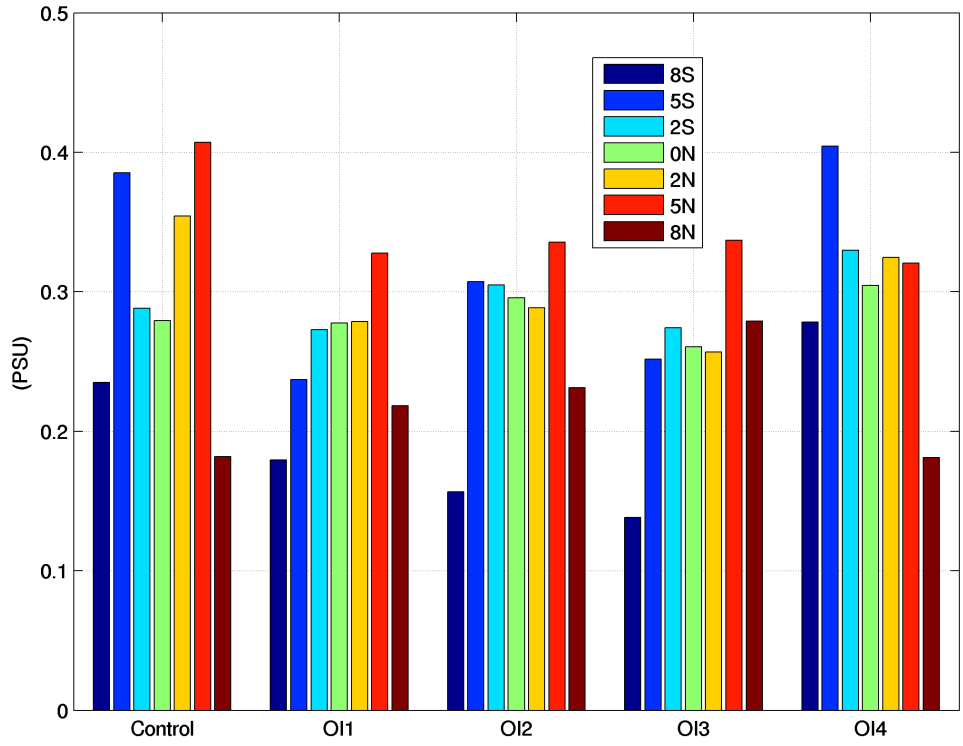

Figure 2

RMS differences (psu) between salinity TAO observations and salinity from the re-analyses in Table 1 at 165°E and various latitudes.

Salinity in the Pacific and North Atlantic Ocean

In the Pacific at the TAO location, RMSD evaluation using the TAO salinity data does not always show a positive impact of the assimilation with respect to the control run. In the OI the salinity RMSD of the buoys located along the 165°E longitude (Figure 2) decreases with respect to the RMSD of the Control at all the latitudes but at 8°N. Nevertheless, in the Eastern part of the Equatorial Pacific, some local RMSD reduce and others increase (not shown). OI2 shows that the introduction of EN2 dataset is of little effect, producing slight improvements in the eastern part of the Equatorial Pacific (not shown) and slight worsening in the western part, with respect to the OI1 (Figure 2). The introduction of V2 and V3 EOFs does not have a general improving effect either. Being the EOFs derived by the model itself, a probable conclusion is that the statistic embedded into them is not able to translate temperature corrections (that constitutes the large bulk of observations) into realistic salinity corrections, using its locally defined statistic.

In the North Atlantic at the Bermuda buoy location, the assimilation system skill has been evaluated using the Bermuda Station time series (Figure 3). We will focus here on the salinity, being more critical than temperature. The time-depth series (not shown) show that the Control run is unable to correctly represent the salinity evolution in the upper layers (0-300 m.); though broadly preserving a realistic vertical structure in the lower levels (300-500m). The ocean re-analyses, on the other hand, are able to better reproduce the salinity time variability in the upper levels, but the side effect (mostly for OI2 and OI3) is an increase of salinity in the lower levels. OI1 is apparently less affected by this problem, but it shows a large freshening beginning from 1994 onwards (not shown). To quantify the individual skill at Bermuda, the average RMSD over the entire period has been evaluated (Figure 3). The figure confirms that the best performing analysis in reproducing Bermuda Salinity is OI4.

In general, it is evident that at least at the TOGA-TAO and Bermuda stations the effect of assimilating salinity in a direct or indirect way (when observations are not available) with the ROOI system is not always positive and the reconstruction of the haline state and variability remains a critical problem.

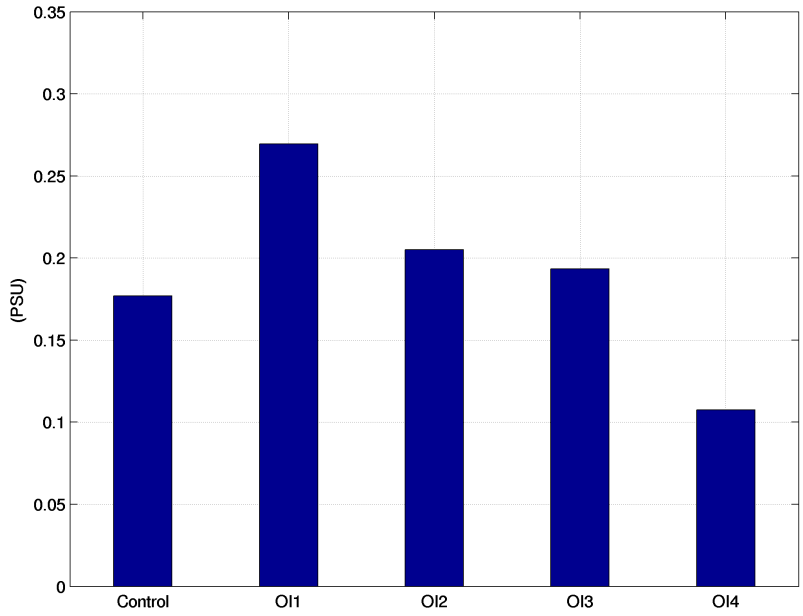

Figure 3

RMS differences (psu) between salinity observations and salinity from the re-analyses in Table 1 at Bermuda station.

Temperature and Salinity Data Assimilation effect

The effect of temperature and salinity assimilation at the global scale has been assessed comparing horizontal fields of temperature and salinity differences between climatologies from the re-analyses and observations (Antonov et al., 2006). In terms of temperature in the upper ocean there is a large bias reduction in the northern hemisphere, while in the southern hemisphere the improvement is not so evident. The latter feature is clearly related to the data scarcity that affects all releases of the EN datasets in this region until the introduction of the ARGO floats in the early 2000. On the other hand, in the northern hemisphere the Kuroshio Current, the Labrador Current and the Gulf Stream thermal front are better represented, due to the large number of data available (not shown).

The same differences have been analysed for the salinity in the upper ocean. The Control Run and OI1 show that in the North Pacific there is a general reduction of the salinity bias when assimilation is introduced (not shown). On the other hand, a large negative bias in the North Atlantic and a positive bias in the Gulf of Mexico are introduced by the assimilation (Figure 4, panels a and b). In the rest of the globe the assimilation impact on salinity is small and overall difficult to be quantified. Comparison with the OI2 shows that introduction of EN2 dataset and V2 EOFs does not reflect into a reduction of salinity differences with regard to the OI1 experiment (not shown). The OI3 on the other hand, shows a better overall result than OI1 in the Pacific and Indian Ocean, but again in the Northern Atlantic and in the Gulf of Mexico there are unexpected large biases that are absent from the Control Run (Figure 4, panel c). The skill improves with the introduction of V3 EOFs in the OI4 analysis. While maintaining the good results obtained with the OI3 analysis in the Pacific and Indian basins, in the North Atlantic the differences with Levitus are now minimal (Figure 4, panel d).

This feature shows that the smoothing applied to the Control Run temperature and salinity fields used to produce the V2 EOFs, and the averaging over large areas adopted to produce the V1 EOFs are introducing in the assimilation of salinity in the Northern Atlantic a large error due to the mixing of different water masses.

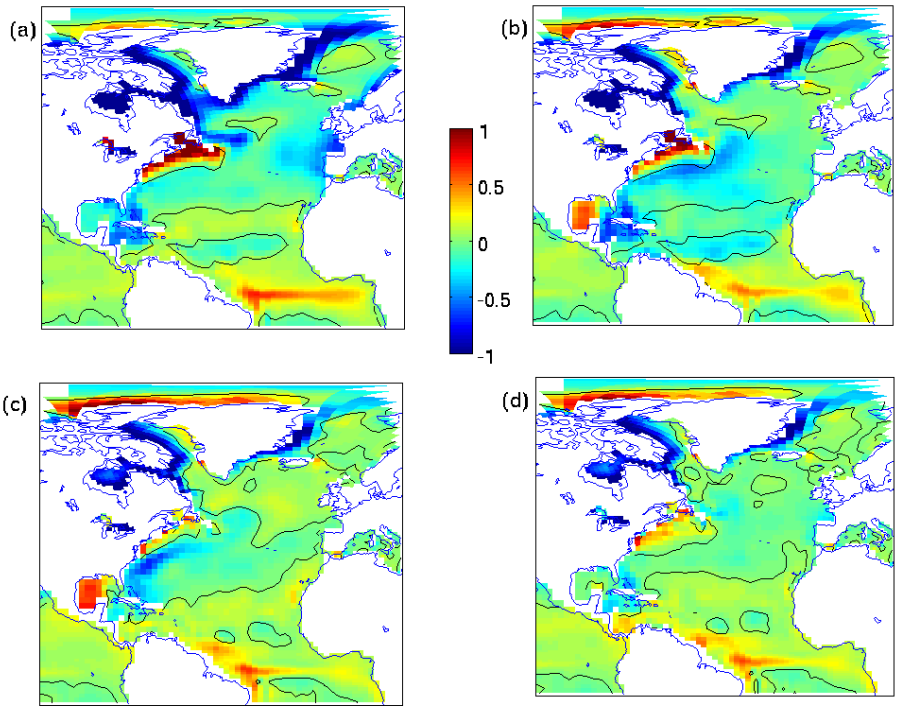

Figure 4

Climatological salinity differences (psu) at 95 m depth between CONTROL (a), OI1 (b), OI3 (c), OI4 (d) and Levitus, respectively.

Heat and Freshwater content

We now consider the time evolution of the global averaged heat and freshwater content anomalies integrated over the uppermost 700m. We use also the objectively analyzed temperature and salinity fields derived from the EN3 dataset (figure 5).

The heat content change time series (Figure 5) show that all the re-analyses have similar trends, with the exception of OI1 and OI2 from 1994 onwards. In particular, the warming trend of OI1 from starting in 1994 is particularly overestimated but this anomalous behaviour is related to the XBT double correction bug affecting the EN1 dataset used in this analysis. The Control Run, though broadly following the general trend, has a much reduced decadal variability with respect to the re-analyses and EN3, giving a measure of the effect of the assimilation on the model. All the re-analyses show an increase in heat content in the 1970s followed by a decrease in the late 1980s. The “warm period” in the 1970s has been recently recognized as one with enhanced data errors. This notion is now supported by recent studies using corrected XBT observations (Domingues et al., 2008) although the issue concerning the quality of XBT as well as other instrumental data has not been completely resolved and will continue to affect the estimates derived from the re-analyses.

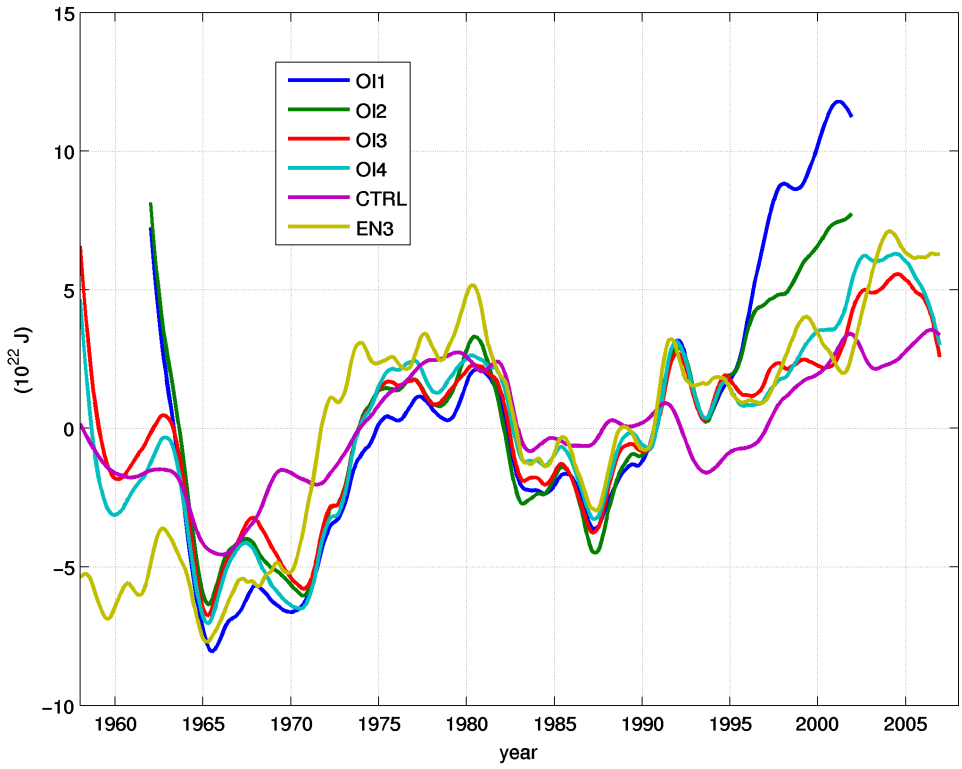

Figure 5

Global average of heat content [0-700m] anomaly with respect to climatology (10^{22} Joule) for the ocean re-analyses in Table 1 and EN3 (see text for definition).

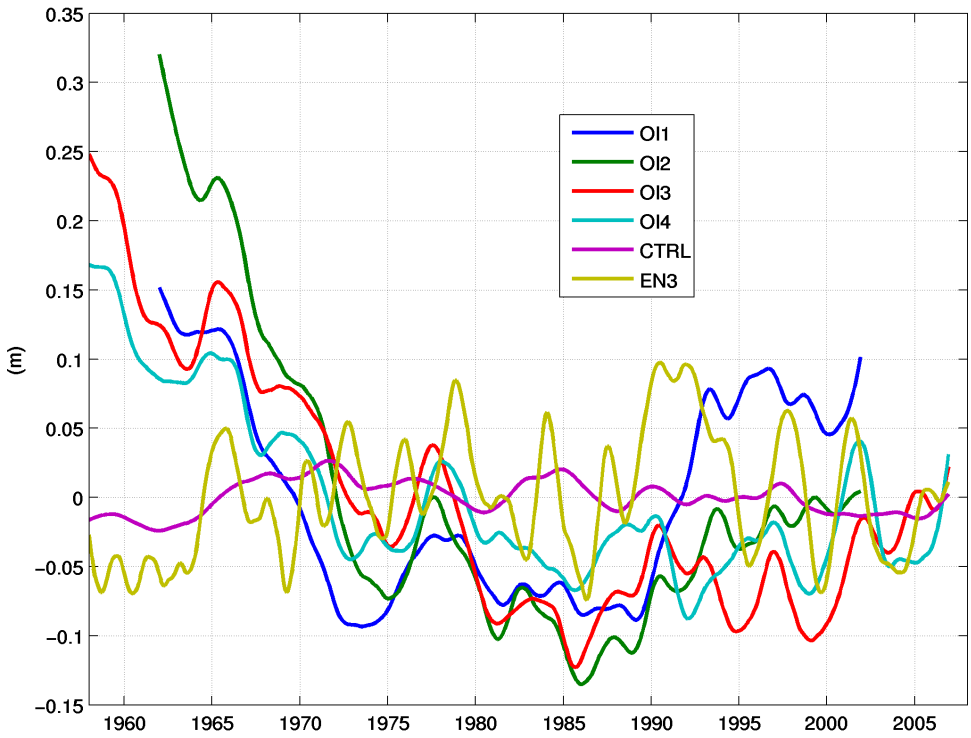

Figure 6

Global average of freshwater content [0-700m] anomaly with respect to climatology (m) for the ocean re-analyses in Table 1 and EN3 (see text for definition).

The freshwater content anomalies time series is shown in Figure 6. The main feature is that the Control Run and the EN3 are relatively stable over the entire period, while each analysis starts with a freshwater contents value higher than the mean. All the re-analyses show a negative trend in the 1960-1975 period, while in the following years the freshwater content difference tend to vary much slowlier, with the exception of OI1 which has a strong positive trend starting in 1990 and reflecting the large salinity bias introduced by the assimilation in the North Atlantic. This feature is mostly due to an indirect effect of the EN1 XBT bug which is generating biased salinity corrections evaluated from biased temperature corrections through the bi-variate EOFS used in the assimilation.

The main conclusion is that the uncertainties affecting the freshwater content derived by the re-analyses are larger than for the heat content. All the re-analyses tend to stabilize after about 20 years. However, it is not possible to detect any kind of correlations among the re-analyses at short time scales and the variability among them is quite large.

Applications for Climate Studies

Some of the global re-analyses that were produced in the past with a different assimilation system (Masina et al., 2001) have been used for climate studies to estimate the interannual-to-decadal variability of the upper-ocean.

Drbohlav et al., (2007) used the re-analyses to compute the mixed-layer heat budget for the Indian Ocean dipole mode during El Niño and non–El Niño years. The relationship between atmospheric variability and the subsurface ocean was investigated by Masina et al. (2004) where it was found evidence of subsurface temperature quasi-decadal variability in the North Atlantic correlated with the NAO index only when temperature observations were assimilated into an ocean model.

Similarly to the common practice with atmospheric re-analyses, the recent availability of global ocean re-analyses has allowed to use them as a reference for the evaluation of model performances. For example, two ocean re-analyses have been used to validate nine coupled general circulation models in terms of the spatial structure and frequency of ENSO (Capotondi et al., 2006). It was found that the feedback processes acting during ENSO are not correctly simulated by some coupled models primarily due to the weaker upwelling in the models with respect to the re-analyses.

Furthermore, ocean re-analyses have been used to estimate coupled model biases in simulating the thermal vertical structure in the Equatorial Pacific (Cherchi et al., 2008) and the ENSO dynamics (Navarra et al. 2008). In the latter study it has been shown that the increased atmospheric resolution of a coupled climate model has a beneficial impact on the ENSO frequency and that the model represents the delayed oscillator mechanism differently, depending on the atmospheric resolution. In the coarse experiment the delayed oscillator is confined close to the equator involving fast equatorial modes. In the higher resolution experiment it involves broader latitudinal regions and slower waves similarly to the processes shown by the re-analyses.

Some of the re-analyses described in this paper are currently utilized in the global ocean reanalysis inter-comparison effort coordinated by the Global Synthesis and Observations Panel (GSOP) of the Climate Variability and Predictability (CLIVAR) Program and by the Global Ocean Data Assimilation Experiment (GODAE) and provided in detail on the web page of CLIVAR's "Global Synthesis and Observations Panel (GSOP), (http://www.clivar.org/organization/gsop/synthesis/synthesis.php). Examples and applications of some of these re-analyses are provided by Lee et al. (2010) and Stammer et al. (2010). As part of this effort, a large suite of indices and diagnostic quantities obtained from various ODA products are intercompared and evaluated using observations when available. For example, Lee et al., (2009) provides an overview of the current skills of the global ODA products in their ability to reproduce one of the critical components of the global thermohaline circulation, the Indonesian Through Flow (ITF). The study shows that the consistency of ITF transport estimated by various ODA products is larger after 1980 reflecting the impact of the assimilated observations on the estimate of the ITF whatever the model and data assimilation method used. Carton and Santorelli (2008) examined the trend and variability of the upper ocean heat content using nine re-analyses and several other assessments are going on in parallel.

Impact of the ocean subsurface assimilation on seasonal climate predictability

The beneficial impact on the skill of seasonal climate forecasts stemming from the use of ocean re-analyses as initial conditions for Coupled General Circulation Models (CGCMs) has been assessed in a number of papers, mostly focusing on the El Niño–Southern Oscillation (ENSO) phenomenology (Ji and Leetmaa 1997; Balmaseda et al. 2007). Beneficial effects on predictability have been also reported increasing the space-time coverage of the observational network (Ji and Leetmaa 1997; Balmaseda et al. 2007). These studies have often showed reductions of the model errors and possibly increased skill in ENSO predictions. However, results are substantially depending on the model, the geographical region, the year and the season under consideration. The INGV-CMCC Seasonal Prediction System (SPS; Alessandri et al., 2009) includes the ocean initial conditions estimation provided by the method described in this work. Two sets of nine member ensemble hindcasts have been produced for the period 1991-2003 for two starting dates per year in order to assess the sensitivity of the seasonal predictions to the improvement of the oceanic initial conditions estimation through the assimilation of the in situ data. As described in Alessandri et

al. (2009), the comparison with the results of the control simulations shows that the improved ocean initialization leads to increased skill in the prediction of tropical Pacific SSTs in the CMCC SPS. In particular, the data assimilation in the ocean initial conditions leads to a considerable improvement in the representation of the onset and development of the El Niño 1997-1998. Considering the boreal winter forecasts, important significant effects coming from the subsurface initialization of the ocean model has been evidenced. Differently from boreal winter, the impact of the ocean data assimilation on the forecasts started in May is small and mostly negligible.

Large SST biases in the central tropical Pacific and quite a prominent initial ”coupling shock” has been documented for the CMCC SPS. With this regard, more efforts are needed on the problem of initialization of coupled models and on reducing SST biases as they are probably limiting the effect of subsurface assimilation in the CMCC SPS (Alessandri et al., 2009).

Conclusions and on-going developments

A global ocean data assimilation system such as the one developed at CMCC provides an important tool to synthesize all available observations into a complete dynamical description of the time-varying ocean and its interaction with the remaining climate system. However, the evaluation of the accuracy of the ocean re-analyses by comparison with observations is a preliminary requisite to assess the values of such products and use them to analyze climate variability especially through derived integrated quantities not observable and climate indices.

In conclusion, it can be observed that assimilation of in-situ temperature and salinity with the CMCC Global Ocean Data Assimilation System is beneficial for the ocean mean state estimation and its variability. Quality and coverage of assimilated observations is extremely important and ocean re-analyses can only be as good as the data provided. Ocean state estimation has a deep need for high-quality ocean data, especially data covering the decades before the 1990s and possibly going back to the beginning of the century. A careful choice of the statistic embedded into the EOFs used into the OI is also critical to obtain good results especially for salinity which is scarcely observed and indirectly corrected using statistical assumptions. At the same time, even if we do not show this aspect, the quality of the re-analyses is highly dependent on the model and the forcing used.

A major issue with all data assimilation products such as the one that we presented here is that no formal estimates of uncertainties of the estimated ocean states or derived information are provided. Such uncertainties depend on the observing system, the errors of the ocean model, of the atmospheric fluxes, and of the assimilation system, which are often not easy to estimate. To increase the value of ocean data assimilation products, much effort is needed to characterize the uncertainties in each re-analysis product and to improve them through more advanced assimilation approaches. For example, a clear disadvantage of the OI scheme currently used at CMCC and presented here is that the solution is always local and, furthermore, the computational cost of an OI scheme is approximately proportional to the number of observations that are assimilated. In the future this may become an important practical limit for the application of OI schemes, because there is a continuous growth of the number of satellite and in situ observations available for assimilation in oceanographic systems. As a consequence, at present the CMCC Ocean group is developing a global ocean 3D-Var variational assimilation system (Storto et al., in preparation, 2010) with the aim to assimilate also the along-track sea-level anomaly (SLA) observations, along with the in-situ observations. In addition to the possibility to provide global solutions for the analysis, an important advantage of a 3D-Var scheme is that its computational cost mainly depends on the size of the state vector and much less on the number of observations. The method is the global implementation of an assimilation system originally developed by Dobricic and Pinardi (2008) for operational analysis and forecast in the Mediterranean Sea. Along-track SLA observations are assimilated via a local hydrostatic adjustment scheme, which splits the sea-level increment, proportional to the water-column integrated density increment, into thermo- and halo- steric contributions, provided that the increment is spread into vertical profiles of temperature and salinity according to the local structure of the bivariate background-error vertical covariances.

The new 3D-Var data assimilation system includes also a more advanced observations preprocessing, which consists in particular of a background quality-check and an observation type-dependent spatial thinning. Further, observational errors for in-situ observations are re-tuned according to the assimilation output diagnostics (as in Desroziers et al. 2005). SLA observational error is decomposed in mean dynamic topography error, deducted from the model sea-level height anomaly variability, accuracy of the observation operator, instrumental precision and representation error, diagnosed from the differences between gridpoint-averaged values and the raw data.

This new scheme will be implemented on an eddy-permitting global ocean model in the framework of MyOcean project with the aim to provide multidecadal optimal reconstructions of the dynamical ocean using remote sensing and in situ measurements recorded during the past two decades. An eddy-permitting model will allow to more fully utilizing the existing observations that capture eddy variability (e.g., the multi-altimeter system).

Acknowledgements

The authors wish to thank the Centro Euro-Mediterraneo per i Cambiamenti Climatici for its financial and scientific support of some of the activities presented in this work. The implementation and the following improvements of the global ocean assimilation system were carried out in the framework of the ENACT (EVK2-CT2001-00117) and ENSEMBLES (GOCE-CT-2003-505539) projects. We wish to thank Dr. A. Bellucci for his effort in this activity during the ENACT project. We are grateful to the TAO Project Office for the TAO data, and James Carton and Gennady Chepurin for supplying salinity data from Bermuda station. The MyOcean (FP7-SPACE-2007-1) project is feeding some of the most recent developments.

References

Alessandri A., A. Borrelli, S. Masina, A.F. Carril, P. Di Pietro, A.F. Carril, A. Cherchi, S. Gualdi and A. Navarra, 2010: The INGV-CMCC Seasonal Prediction System: Improved Ocean Initial Conditions. Monthly Weather Review, Accepted.

Antonov, J.I., Locarnini, R.A., Boyer, T.P., Mishonov, A.V., Garcia, H.E., Levitus, S. ,2006: World Ocean Atlas 2005 Volume 2: Salinity. NOAA Atlas NESDIS, 62(2). NOAA. 182 pp.

Balmaseda, M., D. Anderson, and A. Vidard, 2007: Impact of argo on analyses of the global ocean. GRL, 34, L16 605, doi:10.1029/2007GL0304452.

Bellucci, A., Masina, S., Di Pietro, P., and Navarra, A. 2007: Using temperature-salinity relations in a global ocean implementation of a multivariate data assimilation scheme. Monthly Weather Review, vol. 135, pp. 3785-3807.

Capotondi, A., Wittenberg, A., Masina, S. 2006 **:** Spatial and temporal structure of ENSO in 20th century coupled simulations. Ocean Modelling Vol 15, (3-4), 274-298.

Carton, J.A., and Santorelli, A. 2008: Global decadal upper-ocean heat content as viewed in nine analyses. Journal of Climate, 21, pp.6015-6035.

Carton, J.A., B.S. Giese, and Grodsky, S.A., 2005: Sea level rise and the warming of the oceans in the Simple Ocean Data Assimilation (SODA) ocean reanalysis. J. Geophys. Res., 110, C09006, doi:10.1029/2004JC002817.

Cherchi, A., Masina, S., Navarra, A., 2008: Impact of extreme CO2 levels on tropical climate: A CGCM study. Climate Dynamics , vol 31, pp. 743-758.

De Mey, P., and M. Benkiran, 2002: A multivariate reduced-order optimal interpolation method and its application to the Mediterranean basin-scale circulation. Ocean Forecasting: Conceptual Basis and Applications, N. Pinardi and J. D. Woods, Eds.,Springer Verlag, 281-306.

Desroziers G., Berre L., Chapnik B., Poli P., 2005 : Diagnosis of observation, background and analysis-error statistics in observation space. Quarterly Journal of the Royal Meteorological Society. Vol. 131, Issue 613, Part C, pp. 3385-3396

Di Pietro, P., and Masina, S., 2009: The CMCC-INGV Global Ocean Data Assimilation System (CIGODAS). CMCC Research Papers, RP0071.

Dobricic, S., and Pinardi, N. 2008: An oceanographic three-dimensional assimilation scheme. Ocean Modelling, 22, pp. 89-105.

Domingues, C. M., Church J. A., White N. J., Gleckler P. J., Wijffels S. E., Barker P. M. and Dunn, J. R. 2008: Improved estimates of upper-ocean warming and multi-decadal sea-level rise. *Nature,* 453**,** pp. 1090–1093.

Drbohlav, H.K.L., Gualdi, S., Navarra, A., 2007: A diagnostic study of the Indian Ocean dipole mode in El Nino and non El-Nino years. Journal Of Climate, Vol. 20 Issue: 13 pp. 2961-2977.

Hackert, E., J. Ballabrera-Poy, A. J. Busalacchi, R.-H. Zhang, and R. Murtugudde, 2007: Comparison between 1997 and 2002 El Niño events: Role of initial state versus forcing, J. Geophys. Res., 112, C01005.

Halkides, D., and Lee, T., 2009: Mechanisms controlling seasonal-to-interannual mixed-layer temperature variability in the southeastern tropical Indian Ocean. J. Geophys. Res., 114, C02012, doi:10.1029/2008JC004949.

Hayes, S.P., Magnum, L.J., Picaut, J., Sumi, A., and Takeuchi, K. 1991: TOGA-TAO: A moored array for real-time measurements in the Tropical Pacific Ocean, Bulletin of the American Meteorological Society, Vol. 72, pp. 339-347.

Ingleby, B., and Huddleston, M., 2007: Quality control of ocean temperature and salinity profiles - historical and real-time data. Journal of Marine Systems, 65, 158-175

Ji, M. and Leetmaa, A., 1997: Impact of data assimilation on ocean initialization and El Niño prediction. MWR, 125, 742–753.

Köhl, A., and Stammer, D., 2008: Decadal sea level changes in the 50-year GECCO ocean synthesis. J. Clim., 21, 1866-1890.

Lee T, Awaji T., Balmaseda M., Ferry N., Fujii Y., Fukumori I., Giese B., Heimbach P., Köhl A., Masina S., Remy E., Rosati A., Schodlok M., Stammer D., Weaver A., 2009: Consistency and fidelity of Indonesian-throughflow total volume transport estimated by 14 ocean data assimilation products. Dynamics of Atmosphere and Ocean, Accepted.

Lee T., Stammer D., Awaji T.,Balmaseda M., Behringer D., Carton J., Ferry N., Fischer A., Fukumori I., Giese B., Haines K., Harrison E., Heimbach P., Kamachi M., Keppenne C., Köhl A., Masina S., Menemenlis D., Ponte R., Remy E., Rienecker M., Rosati A., Schroeter J., Smith D., Weaver A., Wunsch C., Xue Y,2010: Ocean State Estimation for Climate Research. In *Proceedings of OceanObs'09: Sustained Ocean Observations and Information for Society (Vol. 2)*, Venice, Italy, 21-25 September 2009, Hall, J., Harrison, D.E. & Stammer, D., Eds., ESA Publication WPP-306.

Levitus, S., Conkright M.E., Boyer T.P., O'Brien T., Antonov J., Stephens C., Stathoplos L., Johnson D., Gefeld R., 1998b: World Ocean Database 1998, Volume 1: Introduction. NOAA Atlas NESDIS 18, U.S. Government Printing Office, Wash., D.C., 346 pp.

Madec, G., Delecluse, P., Imbard, I. and Levy, C., 1999: OPA 8.1 Ocean General Circulation Model reference manual, Note du Pôle de modélisation, Inst. Pierre-Simon Laplace (IPSL), France, No. 11, 91 pp.

Masina, S., Pinardi, N., Navarra, A., 2001: A global ocean temperature and altimeter data assimilation system for studies of climate variability. Climate Dynamics, 17, 687-700.

Masina, S., Di Pietro, P., Navarra, A., 2004: Interannual-to-decadal variability of the North Atlantic from an ocean data assimilation system, Climate Dynamics, 23, pp. 531-546.

Navarra, A., Gualdi, S., Masina, S., Behera , S., Luo, J.-J, Masson, S., Guilyardi, E., Delecluse, P., Yamagata, T., 2008: Atmospheric horizontal resolution affects tropical climate variability in coupled models. Journal of Climate, 21, pp.730-750.

Pierce, D. W., Barnett, T. P., and Latif, M., 2000: Connections between the Pacific Ocean tropics and midlatitudes on decadal timescales, J. Clim., 13, 1173–1194.

Pohlmann, H., Jungclaus J., Marotzke J., Köhl A. & Stammer D., 2009: Improving Predictability through the Initialization of a Coupled Climate Model with Global Oceanic Reanalysis. J. Clim., 22, 10.1175/2009JCLI2535., p. 3926 — 3938.

Rayner, N. A., Parker, D. E., Horton, E. B., Folland, C. K., Alexander, L. V., Rowell, D. P., Kent, E. C., Kaplan, A., 2003: Global analyses of sea surface temperature, sea ice, and night marine air temperature since the late nineteenth century. Journal of Geophysical Research, Vol. 108, No. D14, 4407.

Reynolds R. W., 1988: A real-time global surface temperature analysis. J. Climate, 1, 75-86.

Stammer D., Köhl A., Awaji T., Balmaseda M., Behringer D., Carton J., Ferry N., Fischer A., Fukumori I., Giese B., Haines K., Harrison E., Heimbach P., Kamachi M., Keppenne C., Lee T., Masina S., Menemenlis D., Ponte R., Remy E., Rienecker M., Rosati T., Schröter J., Smith D., Weaver A., Wunsch C. and Xue Y. , 2010: Ocean Information Provided through Ensemble Ocean Syntheses**.** In *Proceedings of OceanObs'09: Sustained Ocean Observations and Information for Society (Vol. 2)*, Venice, Italy, 21-25 September 2009, Hall, J., Harrison, D.E. & Stammer, D., Eds., ESA Publication WPP-306.

Storto A., Dobricic S., Masina S., and Di Pietro P., 2010: Assimilating along-track altimetric observations through local hydrostatic adjustment in a global ocean variational assimilation syste. To be submitted.

Troccoli, A., and Kallberg, P., 2004: Precipitation correction in the ERA-40 reanalysis. ERA-40 Project Rep. Series 13, 6 pp.

Uppala, S., and Co-authors, 2005: The ERA-40 reanalysis. Quart.J. Roy. Meteor. Soc., 131, 2961-3012.

Zheng F., J. Zhu, and R.-H. Zhang, 2007: Impact of altimetry data on ENSO ensemble initializations and predictions, Geophys. Res. Lett., 34.

Ocean Reanalysis Studies in Reading: Reconstructing Water Mass Variability and Transports

By Gregory C. Smith[1,2], Dan Bretherton[1], Alastair Gemmell[1], Keith Haines[1], Ruth Mugford[1,3], Vladimir Stepanov[1], Maria Valdivieso[1] and Hao Zuo[1]
[1]ESSC, Univ. of Reading,Reading, UK
[2]Now at: Environment Canada, Dorval, Canada
[3]Now at: Cambridge Univ., Cambridge, UK

Abstract

This paper describes the ocean reanalyses carried out by the University of Reading group using water mass based observation operators for assimilation of historical and recent hydrographic data using the ORCA1 and ORCA025 NEMO configurations. The results of these early reanalyses demonstrate improvements in bias reduction, and a stronger constraint to in situ observations than other reanalyses and operational products. In particular we show improvements in high latitude properties and transports (Arctic Ocean and Denmark Strait dense overflow). Transports generally are in good agreement with observational estimates, with important improvements found through key ocean sections as compared to the model control run made without data assimilation.

Introduction

A major challenge in understanding ocean variability is the relative scarcity of ocean observations, together with errors in model simulations. In particular, model simulations suffer from errors in the physical parameterizations and surface forcing, leading to a trade-off between having a model with a spun-up circulation and the development of biases (model drift). In recent years, there have been a number of efforts aimed at reconstructing past ocean states by using data assimilation methods to constrain uncertainty in ocean models using in situ and satellite observations (e.g. ECCO, SODA, ECMWF, MERCATOR).

At the University of Reading, our focus is on using ocean reanalysis to reconstruct historical water mass variability and the resulting transports. For this purpose, we have designed a relatively simple data assimilation system that assimilates salinity directly as a function of temperature, S(T), as the observable property over most of the ocean in order to more accurately recover water mass properties (Haines et al 2006, Smith and Haines, 2009). This system has been used within the NEMO modeling framework to provide global ice-ocean reanalyses at 1° and 1/4° resolution in collaboration with the D RAKKAR group (Barnier et al. 2007). Herein, we describe results from the early reanalyses and discuss ongoing and future research directions.

Model Description

The numerical model used is the NEMO coupled ice-ocean model (Madec, 2008) version 2.3, based on the OPA9 ocean model (Madec et al., 1998) and the LIM2.0 sea ice model (Louvain sea Ice Model: Fichefet and Maqueda, 1997; Goosse and Fichefet, 1999). The ocean model is a primitive equation z-level model making use of the hydrostatic and Boussinesq approximations. The model employs a free surface (Roullet and Madec, 2000) with partial cell topography (Adcroft et al., 1997). The version used here has a tri-polar “ORCA” grid and 46 levels in the vertical, with thicknesses ranging from 6 *m* at the surface to 250 *m* at the ocean floor.

The first model configuration has a global 1° resol ution with a tropical refinement to 1/3° (ORCA1). T he second is a global eddy-permitting model at ¼° resolution (ORCA025). Both c onfigurations have been developed through the DRAKKAR Consortium (Barnier et al., 2007) and use model parameter settings as defined in Barnier et al. (2006) and Penduff et al. (2009). Both configurations employ an energy-enstrophy conserving momentum advection scheme (Barnier et al., 2006) and a Laplacian diffusion. Horizontal viscosity is parameterized with a biharmonic operator in ORCA025, and a Laplacian in ORCA1. Additionally, ORCA1 makes use of the Gent and McWilliams (1990) mixing parameterization. Vertical mixing is parameterized using a one-equation turbulent kinetic energy scheme (Blanke and Delecluse, 1993). A detailed evaluation and comparison of these model configurations with satellite sea surface height observations is given by Penduff et al. (2009).

Surface atmospheric forcing for these reanalyses is obtained from the DRAKKAR Forcing Set 3 (DFS3; Brodeau et al., 2010). DFS3 is a hybrid dataset making use of temperature, humidity and winds from the ERA40 atmospheric reanalysis (1958-2001) and the ECWMF operational analyses thereafter. Short and long wave radiative fluxes are obtained from the Common Ocean Reference Experiment (CORE) dataset (Large and Yeager, 2004), which are derived from the International Satellite Cloud Climatology Project. Precipitation and snow fields have also been taken from CORE and have been subsequently modified to provide a more balanced global freshwater budget. The DFS4 and ERAInterim forcing sets have also been used more recently.

S(T) Assimilation System

A new data assimilation method has been developed and implemented with NEMO in order to improve the accuracy of water mass variability, referred to as the *S(T)* assimilation scheme (Haines et al 2006, Smith and Haines, 2009) and this is also currently employed in the ECMWF System 3 reanalysis (Balmaseda et al. 2008). This is a sequential scheme for hydrographic data based on an Optimal Interpolation approach. Temperature profiles (*T*) are assimilated along with a salinity balancing increment as advocated by Troccoli and Haines (1999). Salinity profiles (*S*) are then assimilated along isotherms (i.e. *S(T)*) as advocated by Haines et al. (2006), up to latitudes of around 50°N/S. At higher latitudes salinity is assimilated in a univariate way on z levels. By evaluating model errors as $S(T)$ rather than on depth levels $S(z)$, the large dynamical variability present in $S(z)$ is removed (i.e. heaving of water up and down), allowing a more accurate assessment of water mass errors. With the $S(T)$ increments being spread along isotherms this means that corrections to a particular water mass do not influence adjacent water masses, which may have uncorrelated errors. The scheme envisages different, larger, covariances to take advantage of this feature but this has not been implemented here.

Model-data differences (innovations) are evaluated at the closest model time step, and assimilation increments are calculated every 5 days (73 cycles per year). Increments are then introduced into the model evenly over the following day (known as Incremental Analysis Updating, see Bloom et al., 1996). Smith and Haines (2009) give more details of the assimilation and report on experiments performed with the 1° resolution ORCA1 model, showing the impact of Argo data in a 3 year reanalysis of the period 2002-2004. The only change to the assimilation system here from that presented in Smith and Haines (2009) is the addition of balancing increments for sea surface height and geostrophic velocity to reduce variability induced by the model adjustments. This was found to be beneficial when studying circulation and transport variability, eg. Smith et al (2009) describes the behaviour of the Atlantic MOC in the reanalysis.

In situ temperature and salinity observations are obtained from the UK MetOffice quality controlled ENACT/ENSEMBLES (EN3_v1c) dataset (Ingleby and Huddleston, 2007). This dataset is largely composed of observations from the World Ocean Database 2005 (WOD05) (Boyer et al., 2006), supplemented by data from the GTSPP (Global Temperature and Salinity Profile Program) and Argo autonomous profiling floats (Gould, 2005), with SOLO/FSI floats omitted due to pressure errors. As such, the dataset includes all available hydrographic observations, including those from shipboard Expendable Bathythermographs (XBTs) and Conductivity-Temperature-Depth (CTD) measurements, as well as observations from mooring arrays (such as TAO and PIRATA). The operational quality control system used for the UK MetOffice FOAM assimilation products (Martin et al., 2007) is used to perform a number of consistency checks on the data, including buddy checks, track checking, testing for density inversions and thinning of the data, see Ingleby and Huddleston (2007).

Description of Reanalyses

The initial reanalyses build directly upon the DRAKKAR hierarchy of model-only hindcast simulations performed over 1958-2004 using NEMO resolutions of 2°, 1°, 1/2° and 1/4°. All configurations are forced by DFS3 fields (as described above) and initialized following a 10-year spin-up from climatological temperature and salinity using repeated forcing for 1959. These control simulations provide a baseline against which to evaluate changes due to the data assimilation.

Two initial reanalyses were performed: a 50-year reanalysis (1958-2007; UR1.1) using the 1° resolution configuration and a 22-year reanalysis (1987-2008; UR025.1) with the ¼° resolution configuration. The 1° resolution reanalysis was initialized from the 10-year spin-up as was done for the DRAKKAR hindcast (DRAK1). The 1/4° resolution reanalysis was initialized directly from the 1/4° DRAKKAR hindcast in 1987 (ORCA025-G70; hereafter DRAK025).

Assessing the accuracy of modeled water mass properties

The model-only hindcasts DRAK1 exhibit a number of drifts and biases in water mass properties. Figure 1 (left and center columns) shows a comparison of DRAK1 with the World Ocean Atlas 2001 Climatology (Conkright et al., 2002), where differences in excess of 2°C and 0.5psu are present. When the model is constrained by observations (UR1.1; Figure 1 right panels) these differences are mostly eliminated. The remaining differences between UR1.1 and the climatology are probably representative of real interannual and decadal variability. UR025.1 shows an equivalent improvement in model bias as compared to climatology.

A more accurate assessment of the water mass properties in the reanalyses can be evaluated by comparing the model background (i.e. model fields prior to assimilation) with in situ temperature and salinity profiles. As the assimilation system evaluates differences between the observations and the model at the closest model timestep (ie. First Guess at Appropriate Time, FGAT), and does not use observations in the future, these comparisons provide a nearly independent evaluation of the modeled water mass properties, excepting covariances between observations.

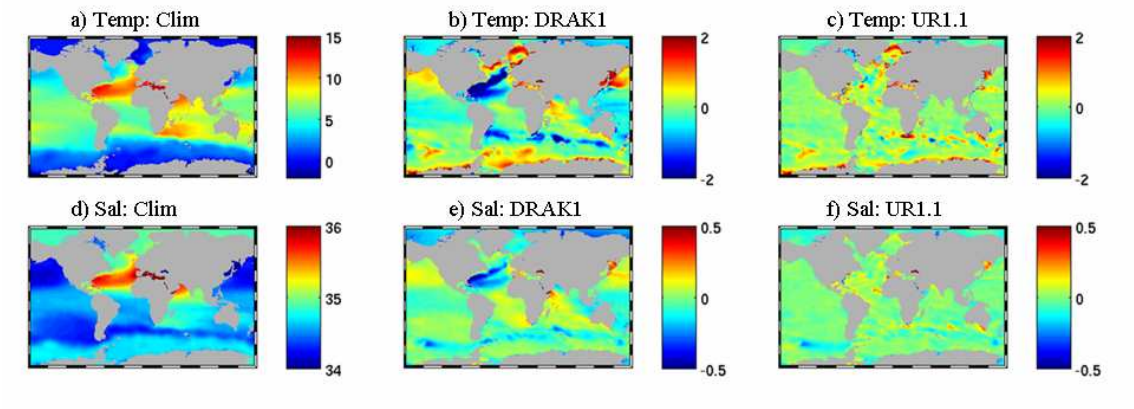

Figure 1

Global maps of annual-mean model anomalies for 2004 averaged over depths of 300-1000 m as compared to climatological fields of temperature (°C) (upper row) and salinity (psu) (lower row). The climatological fields are shown in the left column, followed by the difference between mean model temperature and climatology for the 1° resolution control run (DRAK1 ; centre column) and the 1° resolution reanalysis (UR1.1; right column).

Figures 2 and 3 show the root-mean-squared (RMS) temperature and salinity misfits between the UR1.1 and UR025.1 reanalyses and the EN3 observations over the full global domain, as well as for a selection of basins for the period 1988-2004. Both reanalyses give significant improvements over the model-only hindcast DRAK1, with a reduction in RMS misfits of rough half for both temperature and salinity. The two reanalyses provide nearly the same level of agreement with in situ observations, with the 1/4° reanalysis showing slightly lower RMS misfit v alues throughout the Pacific.

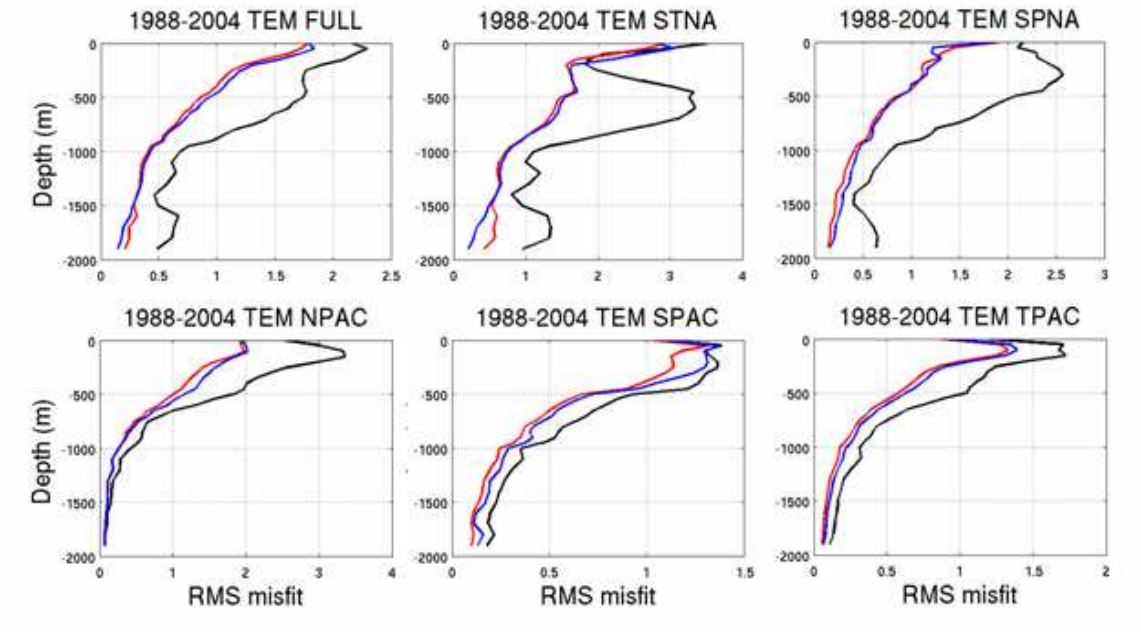

Figure 2

Root-mean-squared (RMS) misfit (in ℃) between mode l forecast for temperature and EN3 observations for the period 1988-2004. RMS misfits are shown for the 1° resolution control run (DRAK1; black), the 1° resolution reanalysis (UR1.1; blue) and ¼° resolution reanalysis (UR025.1; red). Statistics are shown for the full global domain (FULL), the Subtropical North Atlantic (STNA), the Subpolar North Atlantic (SPNA), the North Pacific (NPAC), the South Pacific (SPAC) and the tropical Pacific (TPAC).

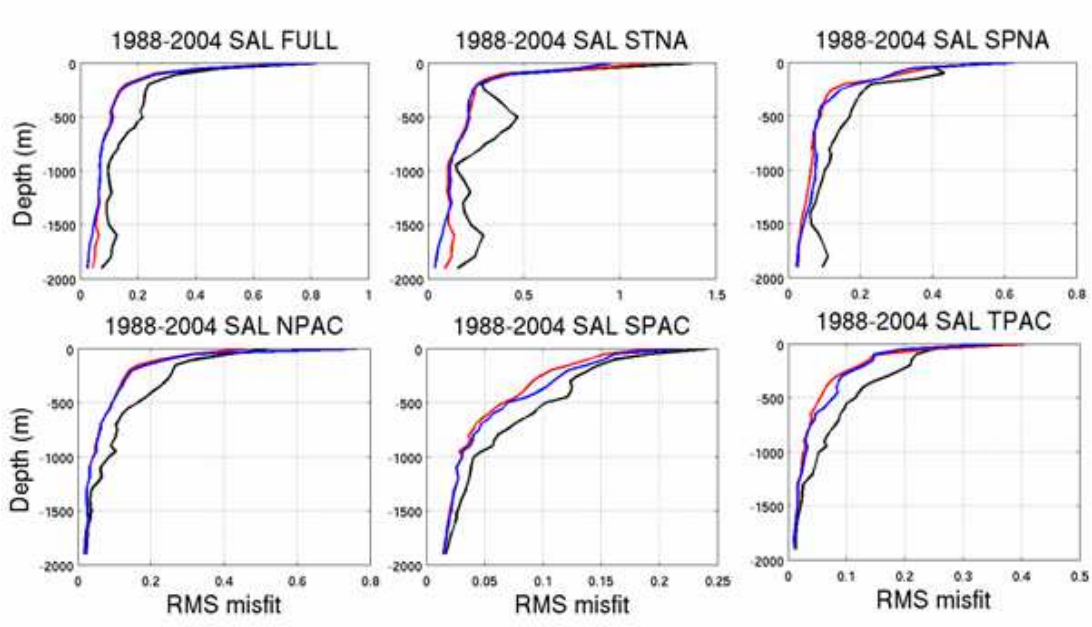

Figure 3

Root-mean-squared misfit (in psu) between model forecast for salinity and EN3 observations for the period 1988-2004. RMS misfits are shown for the 1° resolution control run (DRAK1; black), the 1° resolution reanalysis (UR1. 1; blue) and the ¼° resolution reanalysis (UR025.1; red). Statistics are shown for the full global domain (FULL), the Subtropical North Atlantic (STNA), the Subpolar North Atlantic (SPNA), the North Pacific (NPAC), the South Pacific (SPAC) and the tropical Pacific (TPAC).

Figure 4 shows another way of examining the temperature and salinity misfits to observations, for a number of different reanalysis products whose data are available through OpenDAP and FTP servers. A single month (September 2004) is chosen where a substantial set of Argo observations allow good resolution of water masses. The left panels show misfits in the depth of temperature surfaces, z(T), while the right hand panels show misfits in the salinity on isotherms, S(T), all for the North Pacific region. Details of the different reanalysis products used and a discussion of some of the discrepancies for the different products can be found in Gemmell et al. (2008, 2009), apart from the addition of the recent GLORYS1 reanalysis produced by MERCATOR (see Ferry et al. in this issue). Here we just note that the 2 reanalysis products UR1.1 and UR025.1 (labeled as Reading 1° and ¼° respectively) show some of the smallest misfits of any of the reanalysis products. The z(T) misfits for all reanalysis products show some enhanced error spread around the North Pacific subtropical mode water temperature of 17°C while the S(T) misfits are very small for all temperature classes, demonstrating the effectiveness of the S(T) assimilation approach.

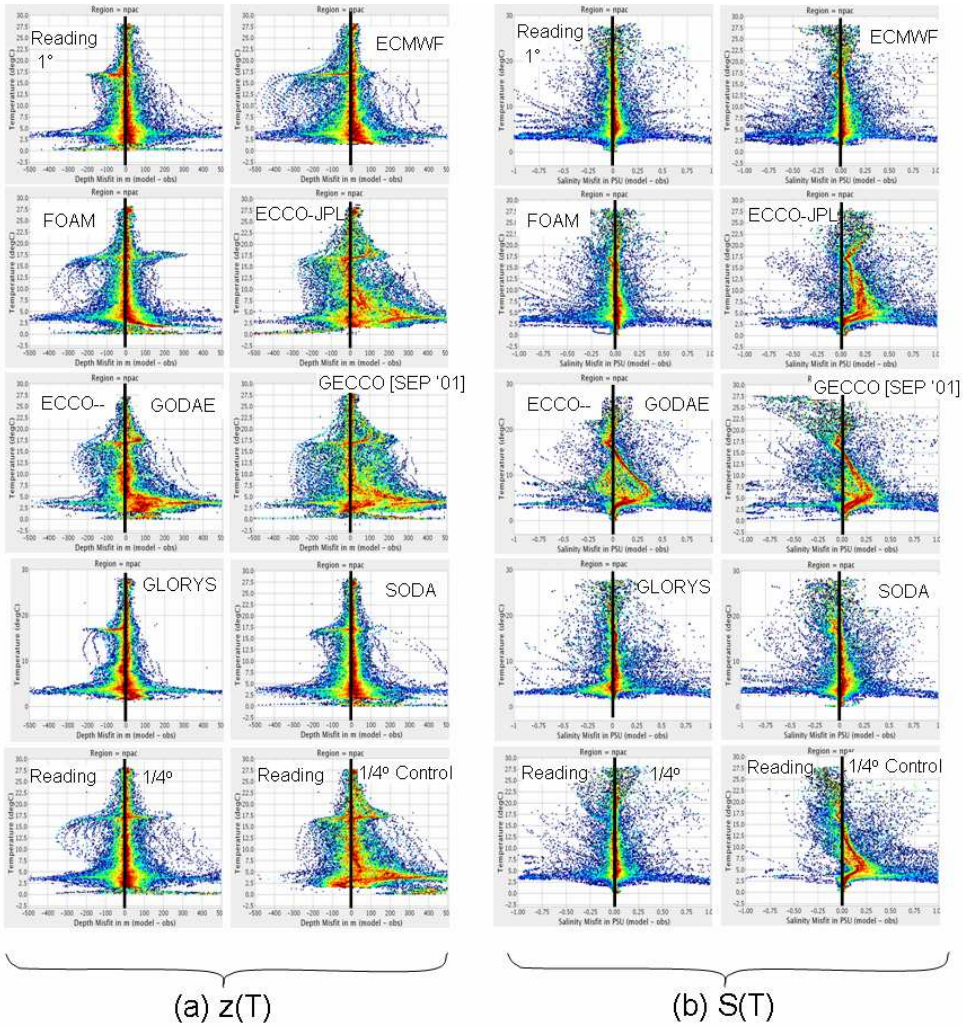

Figure 4

Probability density functions of misfits evaluated on temperature surfaces against September 2004 profile data for a number of different reanalysis products. Depth misfits, z(T), and salinity misfits, S(T), for the North Pacific are shown in panels a) and b) respectively. Saline (fresh) biases in the reanalyses are positive (negative). All model data are from September 2004, except GECCO from September 2001.

Recovery of high latitude water mass properties, transports and variability

Despite the relative paucity of in situ observations from WOD05, and hence EN3, in the Arctic, a significant improvement in modeled water mass properties can be seen in Figure 5. In DRAK025 (G70) there is a steady warming and freshening of waters in the Arctic over the first 15 years of the simulation, leading to the biases in Fig 5. In the ¼° reanalysis UR025.1 we see that this bias has been removed and much more realistic colder and more saline waters are now present at mid-depth in the Arctic. Given that there are so few observations being assimilated in the central Arctic this change may seem surprising. However, the

observational dataset is quite dense in the Greenland-Iceland-Norwegian (GIN) seas and there are also a reasonable set of observations north of Alaska in the Beaufort gyre. It is possible that by correcting the properties of waters that enter the Arctic, along with their transports, an important impact is seen on the properties in the interior Arctic basins (Mugford et al., in prep.). Further work is underway to evaluate the Arctic heat and freshwater budgets and their changes using a much denser set of Arctic observations gathered by the UK IPY project ASBO (Arctic Synoptic Basin-wide Oceanography).

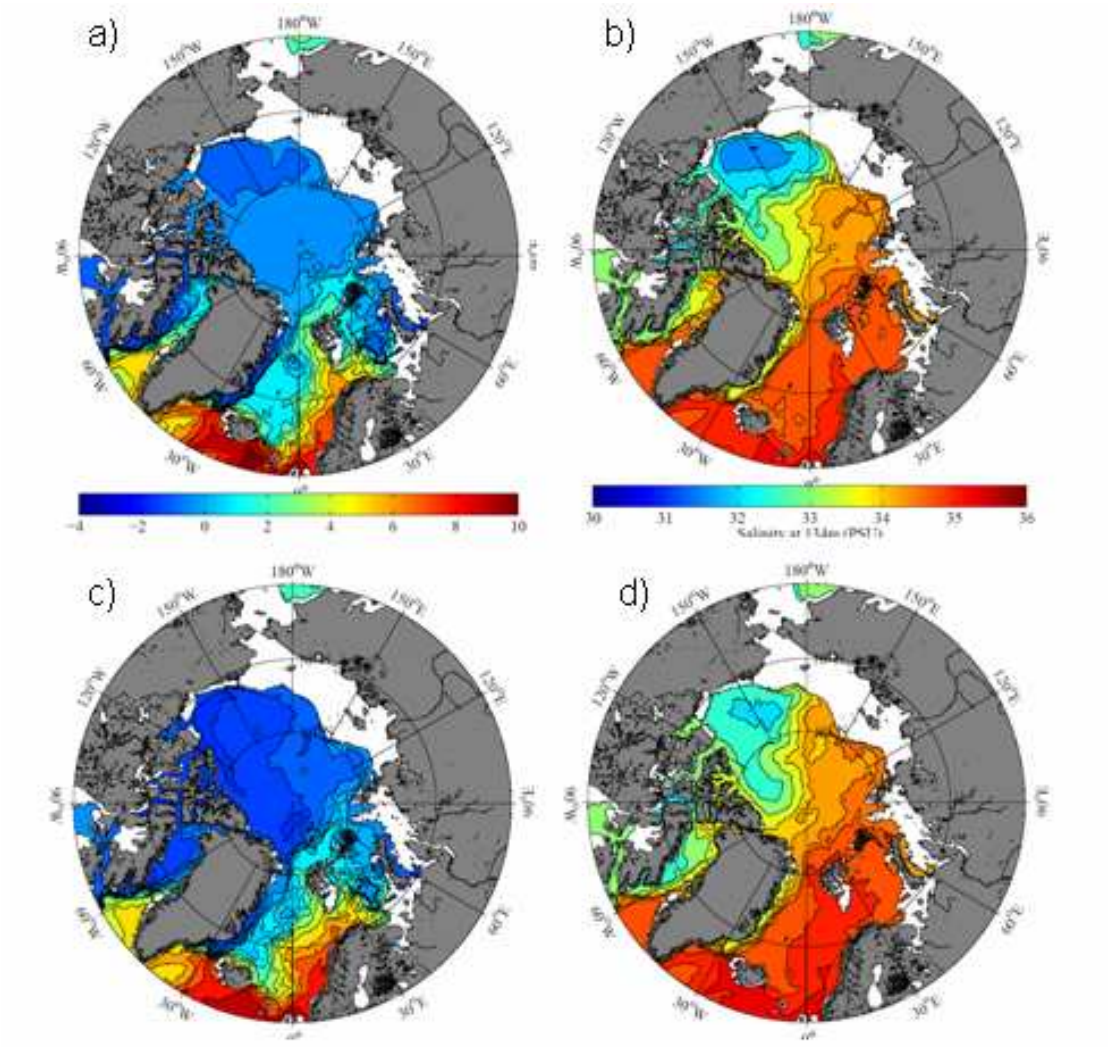

Figure 5

Annual mean 2004 temperature (℃) (a,c) and salinit y (psu) (b,d) for the 1/4° resolution control DRAK 025 (a,b) and reanalysis UR025.1 (c,d) over the north polar region.

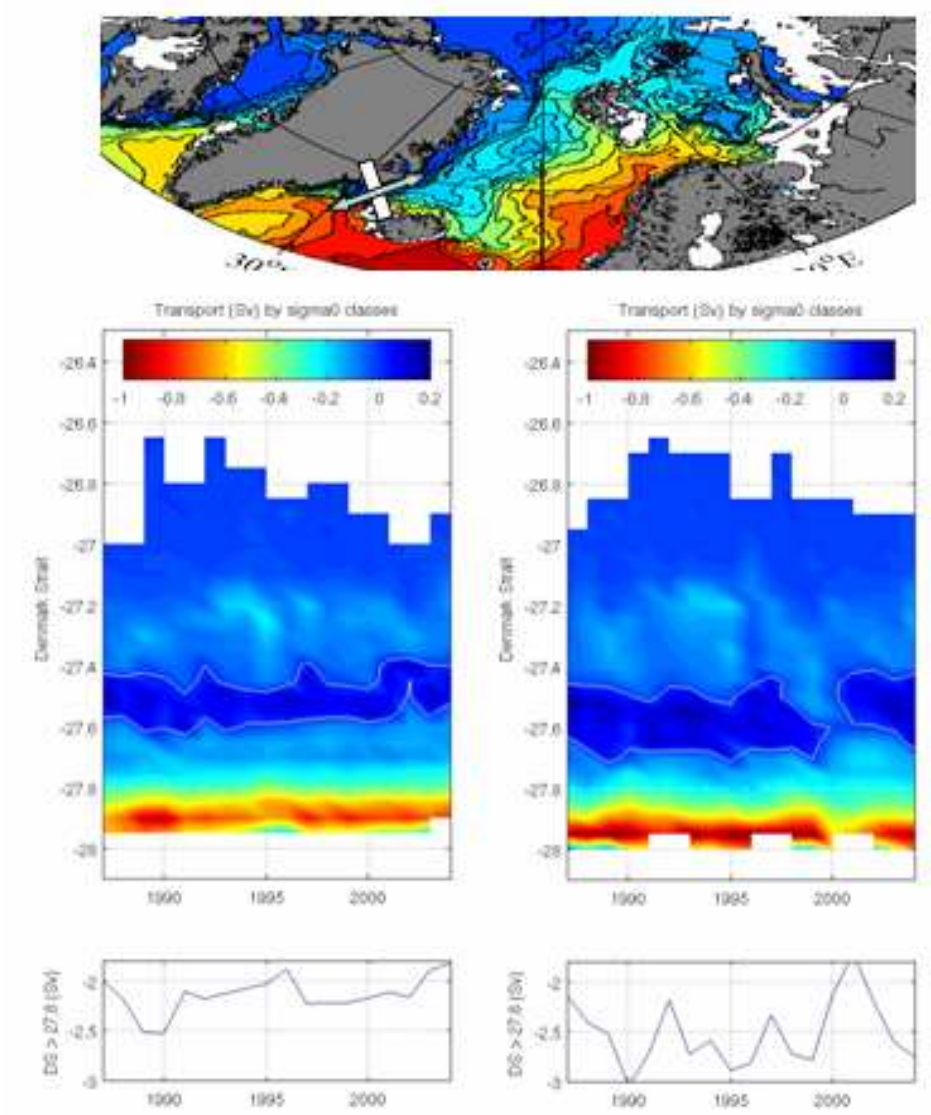

Figure 6

Modelled Volume transports (in Sv) through Denmark Strait as a function of density class. The upper panel shows the location of Denmark Strait. Transports are shown for the ¼° resolution control run (DRAK025; left column) and reanalysis (UR025.1; right column). Warm colours indicate a transport of dense waters from the GIN seas to the North Atlantic. The total transport for waters of density greater than 27.8 (in Sv) is shown in the bottom row.

Improvements in water mass properties in the GIN seas also lead to better Arctic exports to the Atlantic. Figure 6 shows the transports across Denmark Strait (location shown in upper panel) as a function of density class (middle panels). In the ¼° simulation DRAK025 (also known as ORCA025-G70) there is a steady upward drift in the density of the southward transport, while in the ¼° reanalysis UR025.1, this drift is not present and there is a substantially stronger southward flow of dense waters, along with more significant interannual variability. Thus, the assimilation corrects for the lower volume of dense water formation in the model, providing an increased dense water export to the Atlantic. Given that this export has been shown to play an important role in driving the intensity and variability of the MOC, improvements in the variability of dense water exports should have a positive impact on the reproduction of the modeled meridional overturning circulation. Further work is underway to examine the ability of data assimilation to recover the MOC, eg. Smith et al (2009), and the extent to which data assimilation can be used to initialize decadal forecasting of the MOC.

Constraining uncertainty in atmospheric forcing

Recent work has been looking at the potential role of assimilation increments in constraining model errors. A twin experiment was run with the 1° resolution model assimilating the E N3 dataset. Two assimilation runs each used ERA-Interim meteorological bulk formula forcing in all aspects except that one experiment used the Short Wave (SW) radiation from the DFS4 dataset, i.e. from

CORE. The experiments were run from 1989-2008 inclusive. Figure 7 (top panel) shows the mean difference in the SW radiation between these 2 runs while Fig 7 (bottom panel) shows the difference in the thermal increments integrated through the top 100m of the model. Apart from minor regional differences these 2 terms in the local heat budget compensate for each other very well demonstrating that information about the surface forcing differences can be extracted directly from the data assimilation increments. The latent heat term does also change because the SSTs are not very tightly constrained but this is a second order term compared to the assimilation. The assimilation of hydrographic data ensures that the model transports are tightly enough constrained to ensure that advection is fixed in this problem allowing the interpretation of increments in terms of surface flux changes. Further work is underway looking at how the assimilation increments can be used directly to infer potential errors in the surface flux forcing fields.

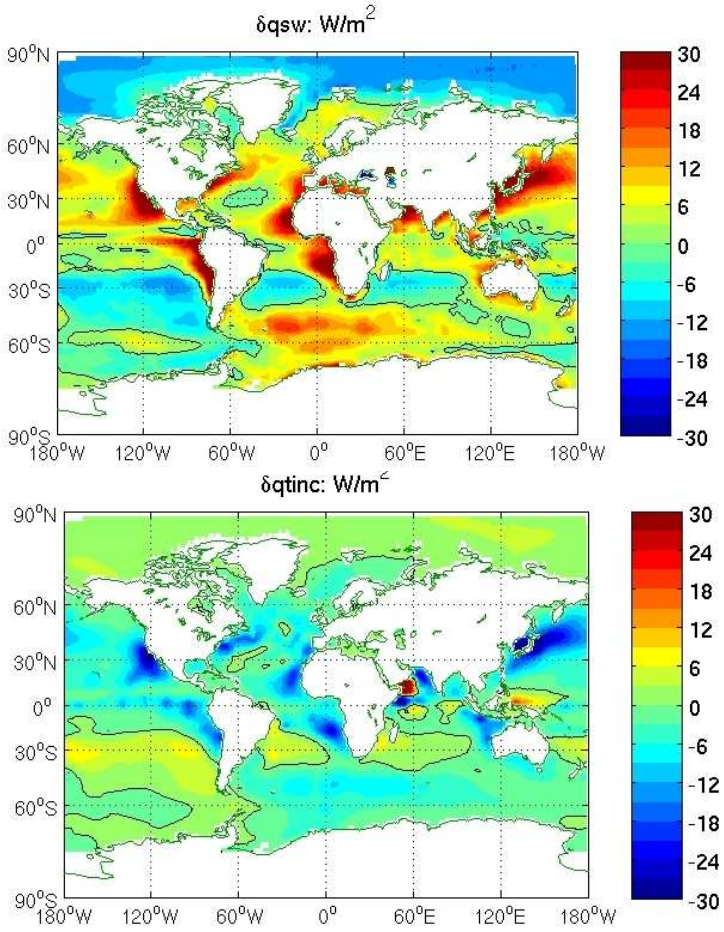

Figure 7

The upper panel shows the difference in Short Wave (SW) (in W/m^2) radiation between ERA-Interim and DFS4. A twin assimilation experiment was carried out whose only difference was the use of DFS4 SW forcing, with the rest of the forcing fields coming from ERA-Interim. The lower panel shows the difference in assimilation increments for temperature between the two experiments for the upper 100m interpreted as a heat flux (in W/m^2). The close correspondence of the two panels shows how the assimilation is able to account for errors in the atmospheric forcing.

Recovery of transports

Figure 8 shows how drifts in water mass properties will affect volume transports. In the DRAK025 simulation the transports through Drake Passage, the Australia-Antarctic section and the Mozambique Channel all show steady declines in the course of the long model integration (black lines). These transports all return to something close to their initial levels after a few years of assimilation (UR025.1 experiment starts from the simulation in 1987). The drifts around the Antarctic are likely related to insufficient dense water formation around Antarctica. Improvements in the subtropical North Atlantic also intensify the gyre circulation and lead to improved agreement with cable measurements of Florida Current, and ongoing work is comparing the Meridional Overturning Circulation (MOC) with the Rapid program measurements (Smith et al., 2009). Figure 9 shows the Atlantic MOC from 2004-2007 for ORCA1 control and assimilation runs, both with and without assimilating the Rapid Array T,S boundary profiles at 26.5N (see legend for details). The inclusion of profile data close to the western boundary, and particularly the deep array data below 2000m, seems to be critical to improving the MOC bias and variability against the Rapid Array calculated transports.

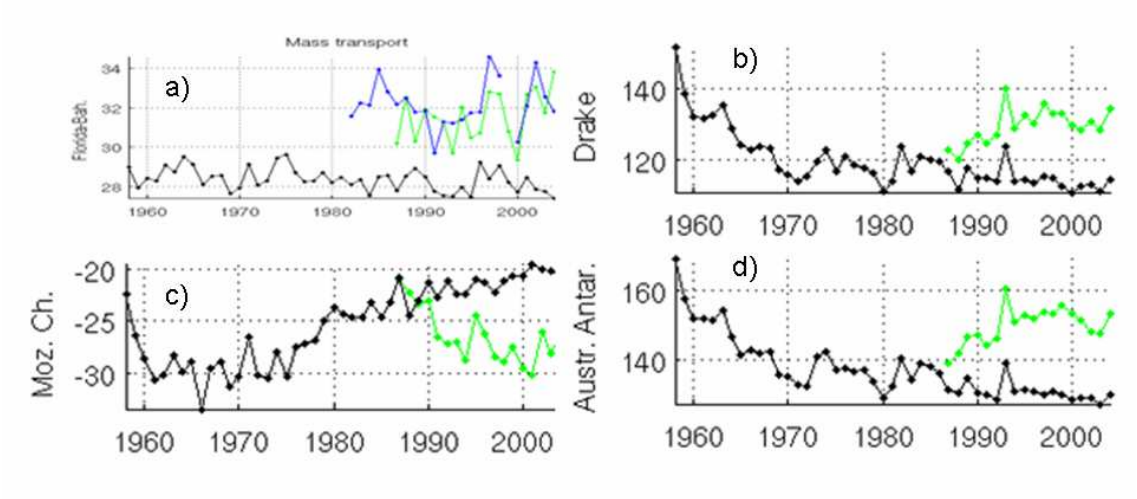

Figure 8

Volume transports (in Sv) across a selection of ocean sections. Transports are shown for the Florida Straits (a), Drake Passage (b), Mozambique Channel (c) and Australia-Antarctica (d). The ¼° resolution control run (DRAK025) is shown in black and the ¼° resolution reanalysis (UR025.1) in green. Cable measurements of the volume transport between the Bahamas and Florida is shown in blue in panel (a).

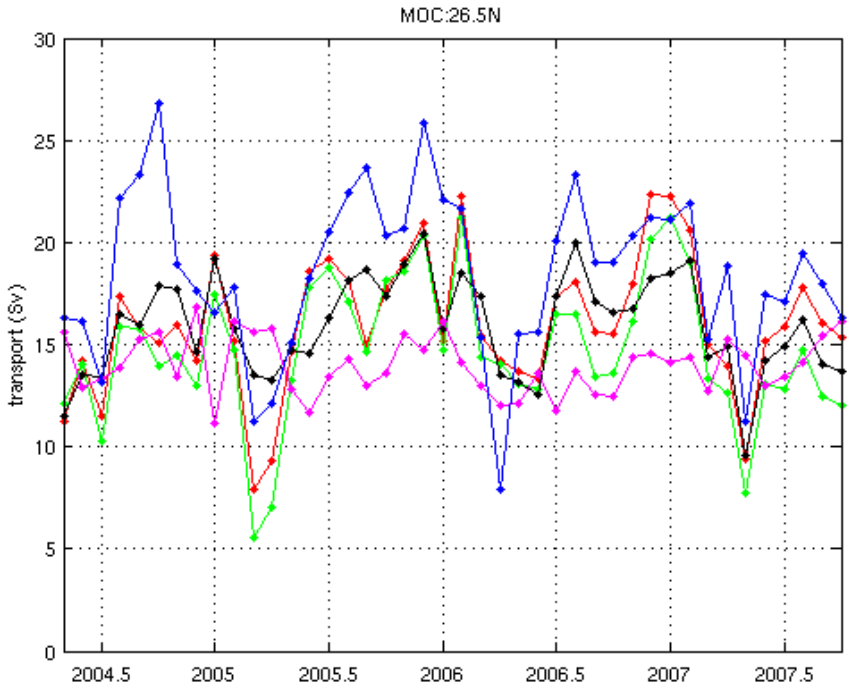

Figure 9

Atlantic MOC transports at 26.5N from April 2004 to September 2007. Transport estimates from the Rapid array are shown in blue (mean 18.5Sv, s.d. 4.0Sv). Transports are shown for a control run with no data assimilation (mauve, 13.3Sv, std 2.2Sv), a run with assimilation of EN3 data only excluding data within 200km of coasts (green, 14.7Sv, std 3.5Sv); a run with assimilation of Rapid Array boundary data only (black, 15.9Sv, std 2.4Sv); and finally a run with assimilation of EN3 and Rapid data (red, 16.0Sv, std 3.3Sv). The NEMO ORCA1 model was forced with ERA-Interim surface conditions (including radiation).

Conclusion

Work on ocean reanalysis being carried out at the University of Reading is intended to converge with research at the UK Met Office and ECMWF to help form the new NEMOVar assimilation system for operational use. This convergence will become easier with the implementation of the MOnSOON shared computer system between NERC and the Met Office that now allows joint model development work. An agreed modeling framework is being developed using NEMO 3.2 coupled with the CICE sea ice model and using 75 vertical levels in the ocean. The original treatment of water masses in the assimilation system has been implemented previously in the ECMWF HOPE model system and it is intended to investigate the incorporation of water mass focused cost functions within NEMOVar at some point in the future. Most assimilation development work will continue in the ORCA1 framework which will remain relevant for seasonal to interannual prediction into the near future, with a second strand of work focusing on altimeter and mean dynamic topography assimilation to be carried out in ORCA025. The University of Reading group remains committed to diagnostics of reanalyzed fields and will continue to perform comparisons between different reanalysis products such as those listed on the CLIVAR-GSOP web page (http://www.clivar.org/organization/gsop/gsop.php).

Acknowledgements

This work benefited greatly from technical and scientific assistance provided by the DRAKKAR Group. We also acknowledge the contribution of A. Coward and S. Alderson in setting up the ORCA1 configuration. Research was funded by the UK RAPID Climate Change Programme through a NERC Grant to KH (NE/C509058/01) and by partial funding from the EU DAMOCLES and NERC ASBO projects. Recent diagnostics work is continuing under the NCEO climate theme programme. Argo data were collected and made freely available by the International Argo Project and the national programs that contribute to it (http://www.argo.ucsd.edu, http://argo.jcommops.org). Argo is a pilot program of the Global Ocean Observing System. Computer time for the high resolution assimilation experiments was provided by ECMWF special project SPGBDAOC.

References

Adcroft A, Hill C, Marshall J. 1997. Representation of topography by shaved cells in a height coordinate ocean model. *Mon. Wea. Rev. 125*: 2293-2315.

Balmaseda MA, Vidard A, Anderson D. 2008. The ECMWF ORA-S3 ocean analysis system. *Mon. Wea. Rev.*, 136, 3018-3034.

Barnier B, Madec G, Penduff T, Molines JM, Treguier AM, Le Sommer J, Beckmann A, Biastoch A, Böning C, Dengg J, Derval J, Durand E, Gulev S, Remy E, Talandier C, Theetten S, Maltrud M, McClean J, De Cuevas B. 2006. Impact of partial steps and momentum advection schemes in a global ocean circulation model at eddy-permitting resolution. *Ocean Dynamics* 56: 6543-567. DOI 10.1007/s10236-006-0082-1.

Barnier, B. and the DRAKKAR Group. 2007. Eddy-permitting ocean circulation hindcasts of past decades. *Clivar Exchanges*, 12(3): 8–10.

Blanke B, Delecluse P. 1993. Variability of the Tropical Atlantic Ocean Simulated by a General Circulation Model with Two Different Mixed-Layer Physics. *J. Phys. Oc.* 23: 1363–1388.

Bloom SC, Tacks LL, daSilva AM, Ledvina D. 1996. Data assimilation using incremental analysis updates. *Mon. Wea. Rev.* 124: 1256−1271.

Boyer TP, Garcia HE, Johnson DR, Locarnini RA, Mishonov AV, Pitcher MT, Baranova OK, Smolyar IV. 2006. World Ocean Database 2005. NOAA Atlas NESDIS 60. S. Levitus, ed., 190 pp. U.S. Gov. Print. Off.: Washington D. C.

Brodeau L, Barnier B, Treguier AM, Penduff T, Gulev S. 2010. An ERA40 based atmospheric forcing for global ocean circulation models. *Ocean Modelling*, in press.

Conkright, M.E., R.A. Locarnini, H.E. Garcia, T.D. O'Brian, T.P. Boyer, C. Stephens, J.I. Antonov, 2002: *World Ocean Atlas 2001: Objective Analyses, Data Statistics, and Figures, CD-ROM Documentation*. National Oceanographic Data Center, Silver Spring, MD, 17 pp.

Fichefet T, Maqueda MAM. 1997. Sensitivity of a global sea ice model to the treatment of ice thermodynamics and dynamics. *J. Geophys. Res*. 102: 12609-12646.

Gemmell, A, Smith GC, Haines K, Blower J. 2008. Evaluation of water masses in ocean synthesis products. *CLIVAR Exchanges*, 13(4), 7-9.

Gemmell A, Smith GC, Haines K, Blower J. 2009. Validation of ocean model syntheses against hydrography using a new web application. *J. Operational Ocean.* 2: 29-41.

Gent, PR, McWilliams, JC. 1990. Isopycnal Mixing in Ocean Circulation Models. *J. Phys. Oc.* 20: 150-155.

Goose H, Fichefet T. 1999. Importance of ice-ocean interactions for the global ocean circulation: A model study. *J. Geophys. Res.* 104(23): 23337-23355.

Gould J. 2005. From swallow floats to Argo—The development of neutrally buoyant floats. *Deep Sea Res., Part II* 52: 529–543.

Haines K, Blower J, Drecourt JP, Liu C, Vidard A, Astin I, Zhou X. 2006. Salinity assimilation using S(T) relationships. *Mon. Wea. Rev.* 134: 759–771.

Ingleby B, Huddleston M. 2007. Quality control of ocean temperature and salinity profiles—Historical and real-time data. *J. Mar. Syst.* 65: 158–175.

Large WG, Yeager SG. 2004. Diurnal to decadal global forcing for ocean and sea-ice models: The data sets and flux climatologies. *Technical Report TN-460+STR*, NCAR, 105pp.

Madec G, Delecluse P, Imbard M, Levy C. 1998. OPA 8.1 general circulation model reference manual. Notes de l'IPSL, University P. et M. Curie, B102 T15-E5, Paris, No. 11, p91.

Madec G. 2008: NEMO reference manual, ocean dynamics component : NEMO-OPA. Preliminary version. Note du Pole de modélisation, Institut Pierre-Simon Laplace (IPSL), France, No 27 ISSN No 1288-1619.

Martin MJ, Hines A, Bell MJ. 2007. Data assimilation in the FOAM operational short-range ocean forecasting system: a description of the scheme and its impact. *Q. J. R. Meteorol. Soc.* 133: 981–995.

Mugford R, Haines K, Smith GC. 2010. Impact of data assimilation on heat and freshwater transports in the Arctic. *in preparation*.

Penduff T, Juza M, Brodeau L, Smith GC, Barnier B, Molines J-M, Treguier A-M. 2009. Impact of model resolution on sea-level variability characteristics at various space and time scales: insights from four DRAKKAR global simulations and the AVISO altimeter data. *Ocean Sci. Discuss.*, 6, 1513-1545.

Roullet G, Madec G. 2000. Salt conservation, free surface, and varying levels: a new formulation for ocean general circulation models. *J. Geophys. Res.* 105 (23): 23927-23942.

Smith GC, Haines K. 2009. Evaluation of the S(T) assimilation method with the Argo dataset. Q. J. R. Meteorol. Soc. 135: 739-756.

Smith GC, Haines K, Kanzow T, Cunningham S. 2009. *Ocean Sci. Discuss.* 6, 2667-2715.

Troccoli A, Haines K. 1999. Use of the temperature–salinity relation in a data assimilation context. *J. Atm. Oc. Tech.* 16: 2011–2025.

Southern Ocean Fronts in the Bluelink Reanalysis

By Clothilde Langlais[1,2], Andreas Schiller[2,3] and Peter R. Oke[2,3]
[1] *University of Tasmania, Sandy Bay TAS, Australia*
[2] *CSIRO Marine and Atmospheric Research, Castray Esplanade 7000 Hobart TAS, Australia*
[3] *CAWCR-CSIRO, Castray Esplanade 7000 Hobart TAS, Australia*

Introduction

The Southern Ocean (SO) has a central place in the global thermohaline circulation. Most of the major water masses of the global ocean cross each other around Antarctica, being upwelled, transformed, subducted or simply generated in the area. The meridional overturning circulation of the water masses induces a southward shoaling of the isotherms that is associated with the Antarctic Circumpolar Current (ACC). The ACC consists in several circumpolar jets or fronts that separate different geographic zones with distinct physical and bio-chemical properties.

A variety of definitions have been used to identify the fronts of the Southern Ocean. Arising from hydrographic cruises, the definitions are usually based on criteria related to the interior ocean structure: transport maxima, gradients along particular isopycnals, latitude where a property isoline crosses a particular isobar (Peterson and Stramma, 1991; Orsi et al. 1995; Belkin and Gordon, 1996; Sokolov and Rintoul, 2002). The same simple phenomenological criteria can be used to locate the fronts along their circumpolar extent. Those definitions underline the persistent and robust character of the fronts.

High resolution observations (satellite altimetry, high resolution hydrographic sections) and numerical models have revealed more complex structures than the climatological hydrographic data, with multiple branches that merge and diverge (Sinha and Richards, 1999; Hughes and Ash, 2001, Sokolov and Rintoul, 2008). From those observations, new frontal definitions appeared. As the ACC is associated with large geostrophic currents, the fronts can be associated with sea surface temperature (SST) and sea surface height (SSH) gradients (Gille, 1994; Hughes and Ash, 2001; Dong H et al. 2006; Sokolov and Rintoul, 2008).

More recently, Sokolov and Rintoul (2008) showed that each ACC branch remains mainly associated with a particular streamline. The association between jets and streamlines appears to be persistent along the circumpolar pathway despite the interactions with bathymetry and eddies. In equivalent barotropic flow like in the SO, the streamlines can be approximated by SSH contours (Killworth and Hughes, 2002). Particular values of SSH can then be used to define fronts in the SO: a maximum in SSH gradient (the core of a ACC jet) can be tracked with a particular SSH contour. By applying a nonlinear fitting procedure, Sokolov and Rintoul (2008) identified ten SSH values that describe the multi-branch structure of the ACC south of Australia (100 to 180 ºE) during a 12 year period.

In equivalent-barotropic flow, the streamlines correspond to a particular water column structure (Sun and Watts, 2001; Watts et al. 2001).This means that frontal definitions based on either SSH values or on water mass properties should give the same frontal positions in such a flow regime. This idea is confirmed in Sallee et al. (2008) where the frontal SSH contours are found by using subsurface hydrography.

In this paper, we combine hydrologic and dynamic criteria to identify the ACC fronts in the Bluelink ocean model, including a free run and an assimilating run. Our objective is to reveal the time and spatial variability of the fronts. We apply a SSH contour criteria to define the ACC fronts from Ocean General Circulation Model (OGCM) outputs. To identify the SSH contours, we use the SO thermodynamical structure, i.e. water masses and transport properties.

After a description of the model runs, the method used to identify the ACC fronts is described. The variability of the fronts in the SO is then presented, followed by our conclusions.

Ocean model and assimilation

The OGCM is based on version 4p1 of the Modular Ocean Model (Griffies, 2004) with a free surface formulation. No horizontal diffusion is applied and the horizontal viscosity is resolution and state-dependent based on the Smagorinsky scheme with a biharmonic operator (Griffies and Hallberg, 2000). For tracer advection, the model uses the third-order quicker scheme (Leonard, 1979). For vertical mixing, the hybrid mixed layer model described by Chen et al. (1994) is used: under a Niiler-Klaus bulk layer, the mixing is parametrized with a Richardson number dependent scheme.

The model configuration is called Ocean Forecasting Australia Model (OFAM) with a resolution of 1/10° in the Asian-Australian region (90-180°E, south of 17°). Outside this domai n, the horizontal resolution decreases to 1° across the Indian and Pacific Oceans and 2° in the Atlantic Ocean. OFAM has 47 ve rtical levels, with 10 m resolution to 200m depth and 35 levels in the top 1000m. Partial cells are used at the bottom.

The Bluelink ReANalysis (BRAN; Schiller et al. 2008) is a multiyear model run with data assimilation. Observations assimilated in BRAN includes sea-level anomaly (SLA) from satelllite altimetry and tide gauges, satellite-derived SST and in situ Temperature (T) and Salinity profiles (Argo floats, CTD, XBT, TAO array...). The Bluelink Ocean Data Assimilation System (BODAS) is an ensemble optimal interpolation system (Oke et al. 2008). In order to project the observations onto the full ocean model state, BODAS uses model-based, multivariate background error covariances. BODAS is used to sequentially assimilate observations once every 7 days.

BRAN is integrated from 1992 to 2006 and forced with interannual 6-hourly surface fluxes. From 1992 to mid-2002, wind stress, heat and freshwater fluxes are provided by the ERA40 reanalysis (Kallberg et al., 2004) and from mid-2002 until 2006 by the ECMWF forecast. The initial conditions come from a 13 years spin-up run, spanning 1994-2002, with no data assimilation. The spin-up run is initialized with a blend of CARS climatologies (CSIRO Atlas of Regional Seas; Ridgway et al., 2002) and Levitus (2001). During the first year of integration of the spin-up run, OFAM is forced with climatological surface fluxes (Southampton Oceanographic Centre, Josey et al., 1998). Forcing fields are provided by the ERA40 reanalysis for the period 1994-2006, with restoring surface salinity to Levitus (2001) over a 30 day period.

For this study, fields from BRAN and the spin-up run, hereafter referred to as the OFAM free run, are used as databases to identify the ACC fronts.

ACC fronts

Transport and temperature criteria as front indicators

A natural definition of a front in the SO is the maximum of gradients of SSH or SST. Since the OGCM provides a complete description of the ocean circulation, we can explore characteristics of fronts by examining many aspects of the time-evolving temperature, salinity, and density, as well as zonal total transport and geostrophic transport, for all meridional sections south of Australia. Figure 1 presents meridional sections of temperature and zonal transport at 135ºE for the two databases used here in January 1998. The model simulations reveal a complex structure of the SO with multiple ACC fronts, meanders and eddies.

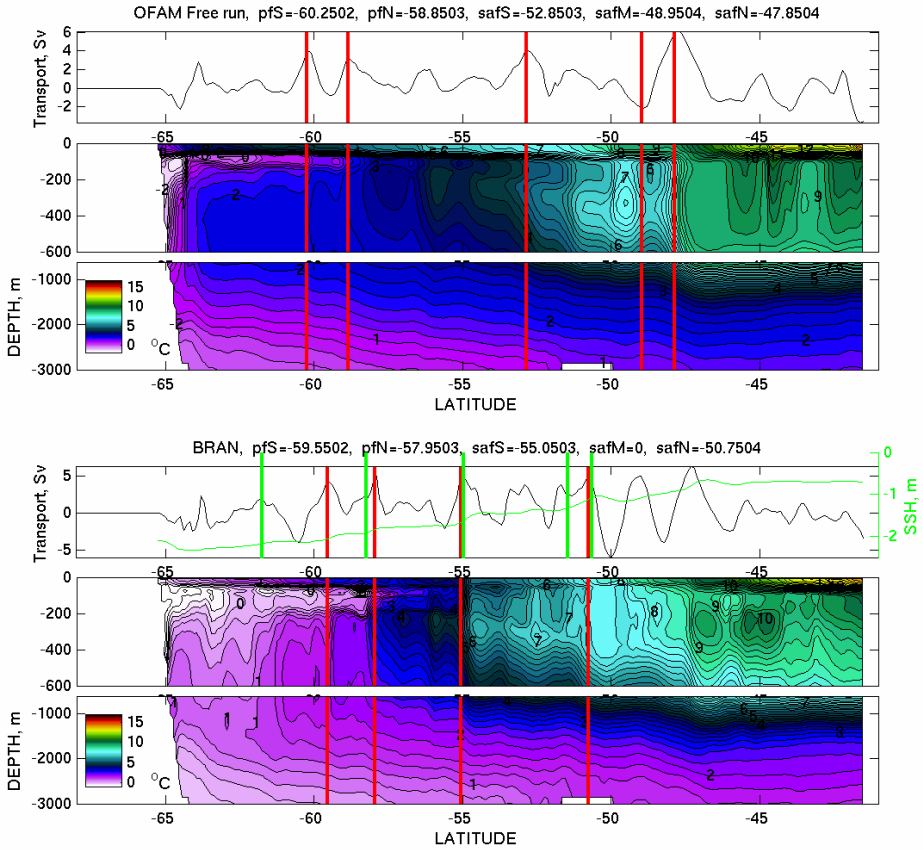

Figure 1

Transport (Sv) and temperature (℃) at 135ºE sectio n along with fronts positions using the transport and Temperature criteria in red and using the SSH criteria in green for January 1998. Upper panels: OFAM free run, lower panels: BRAN.

Consistent with previous findings (Belkin and Gordon, 1996; Sokolov and Rintoul, 2002), the Subantarctic Front (SAF) corresponds to maxima of transport and maxima of temperature gradient between 300 and 400 m. The northern Polar Front (PF-N) is the northern limit of the Antarctic zone and a traditional limit is the northern extent of the Antarctic Winter Water (AAWW) characterized by subsurface temperature minima. In the two simulations (OFAM and BRAN), the northern end of the subsurface temperature minimum layer (Tmin-layer) is associated with a maximum of transport and a maximum of gradient along the Tmin-layer. The southern Polar Front (PF-S) coincides with an increase in depth of the Tmin-layer (Gordon, 1967, 1971) and an enhanced temperature gradient along the Tmin-layer (Sokolov and Rintoul, 2002) which leads to a maximum of transport.

However the water masses do not have the same characteristics in the two simulations and the ACC jets are not associated with the same hydrographic limits. Table 1 regroups the temperature criteria used to identify the fronts and compares them with the criteria identified by Sokolov and Rintoul (2002) in the South Australia sector. To identify those limits, we studied the T gradients of interannual means in Tmin-layer and at around 380 m (see table 1 for the exact depth used for the two simulations) for different sections south of Australia (OFAM and BRAN) (see Figure 2 for BRAN). The maxima of the T gradients correspond to the position of the SAF and PF. The fronts are not located at the same latitude all around Antarctica (Figure 2a), but they always occur in particular temperature limits (Figure 2b). Depending on the longitude, we can identify two or three SAFs.

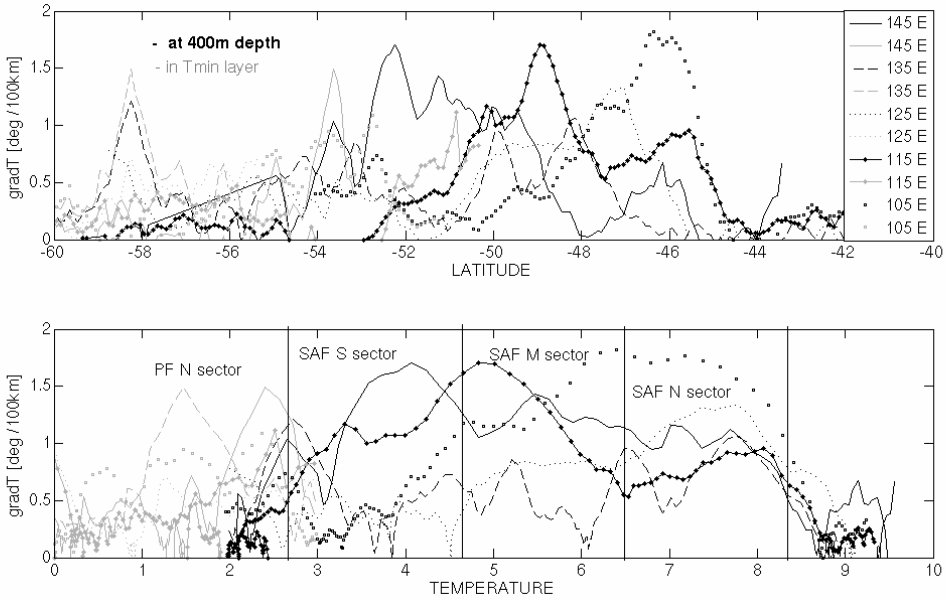

Figure 2

BRAN meridional temperature gradients (℃/100km) in the subsurface temperature minimum layer (grey lines) and at 372m depth (black lines) for different longitude south of Australia (top) as a function of latitude, and (bottom) as a function of temperature.

Fronts		OFAM	BRAN	Sokolov and Rintoul, 2002
SAFs	depth/level	372 m / level 28	372 m / level 28	400 dbar
SAFs	Transport maxima between	3ºC < T < 9ºC	3ºC < T < 8.5ºC	
SAF-N	T limits	7ºC < T < 8.75ºC	6.5ºC < T < 8.25ºC	6ºC < T < 8ºC
SAF-M	T limits	5ºC < T < 7ºC	4.7ºC < T < 6.5ºC	5ºC < T < 6ºC
SAF-S	T limits	3ºC < T < 5ºC	2.6ºC < T < 4.7ºC	4ºC < T < 5ºC
PF	T limit of AAWW	3.2ºC	2.8ºC	2ºC

Table 1

Front indicators for the two simulations, OFAM and BRAN, and comparison with the indicators for the Australian sector of the Southern Ocean from Sokolov and Rintoul (2002).

The identification of the three SAFs and two PFs is performed on weekly mean outputs for all the meridional sections south of Australia. To locate the SAF on meridional sections, we first identify the position of the transport maxima within an area delimited by T characteristics around 380 m depth. Each transport maxima is then associated with a particular front regarding the T characteristic around 380 m. For the PF-N, we monitor the AAWW, following the depth and temperature of the Tmin-layer. We use the T limit of table 1 to identify the northern limit of the AAWW. The PF-N is then defined as the maximum of transport south of this limit. For the PF-S, we locate the maximum of increase in depth of the Tmin-layer. The PF-S corresponds to the maximum of transport nearby this position. The results for the 135ºE section are shown on Figure 1.

Towards SSH contours

Using transport and temperature criteria has the advantage to reconcile two frontal views: the hydrographic and dynamical views. The traditional hydrographic indicators underline the persistence of the fronts that separate different bio-geo-hydrographic zones. The maximum of transport criteria ensures that our analysis also reflects the dynamical part of the fronts that are associated with large geostrophic currents, the ACC jets.

However the method has some limitations. Since we identify the fronts on weekly mean outputs, meanders and eddies perturb the transport and temperature fields, thereby complicating the identification of the fronts. The merging and splitting of the fronts can limit the number of fronts. Large meandering or deflection of the fronts can lead to two meridional positions for one single front.

The seasonal formation of a summer thermocline is also problematic for the study of the Tmin-layer. Since the AAWW are generated during the winter, the Tmin-layer is a subsurface layer in summer but reach the surface in winter. Our transport and temperature criteria for the southern front tend to identify the PF-S during the summer and the South ACC front (sACCf) in winter.

Another limitation comes from the temperature limits (table 1). Frequency distributions of temperature for the ACC fronts do not reveal a particular isotherm but exhibit broad Gaussian variations that overlap (figure not shown). As a result, a particular isotherm may correspond to two different fronts that our method cannot reliably distinguish between. Figure 3 underlines this tendency to jump from one front to another.

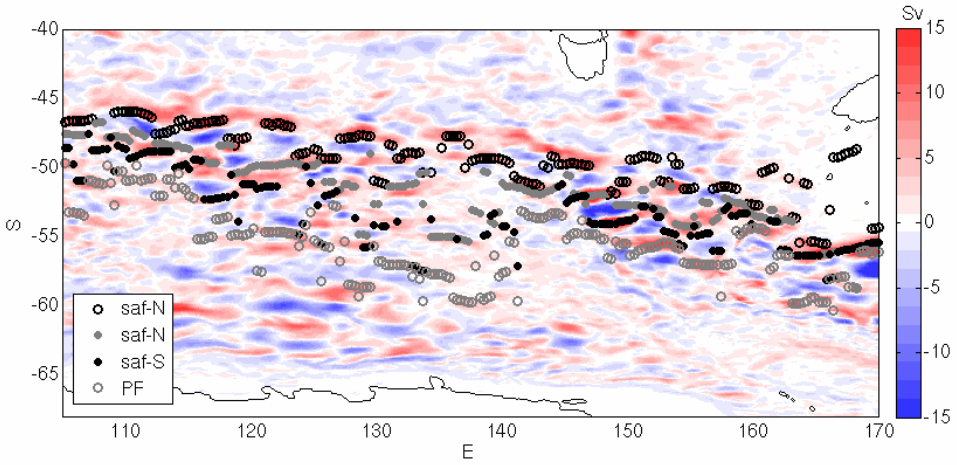

Figure 3

Transport field (Sv, red and blue colors) south of Australia (week 8 1998) overlaid with the position of the 4 ACC fronts (black and grey) identified with the transport and temperature criteria for BRAN.

The results obtained with the transport and temperature criteria are used as a first guess to locate five of the main ACC jets. Using frequency distribution of SSH for this frontal database, we then identify SSH contours that best fit each front. Figure 4 shows histograms of the SSH contours derived from this weekly database for BRAN. Because of uncertainty distinguishing different fronts using transport and temperature criteria, the Gaussian peaks of the histogram overlap. However, as mentioned by Sokolov and Rintoul (2008) and Sallee et al. (2008), each front is characterized by a particular SSH value.

Table 2 regroups the SSH contour values for BRAN. Unfortunately, the SSH contour definition can not be applied to OFAM because of long-term SSH trends that are present in the simulation.

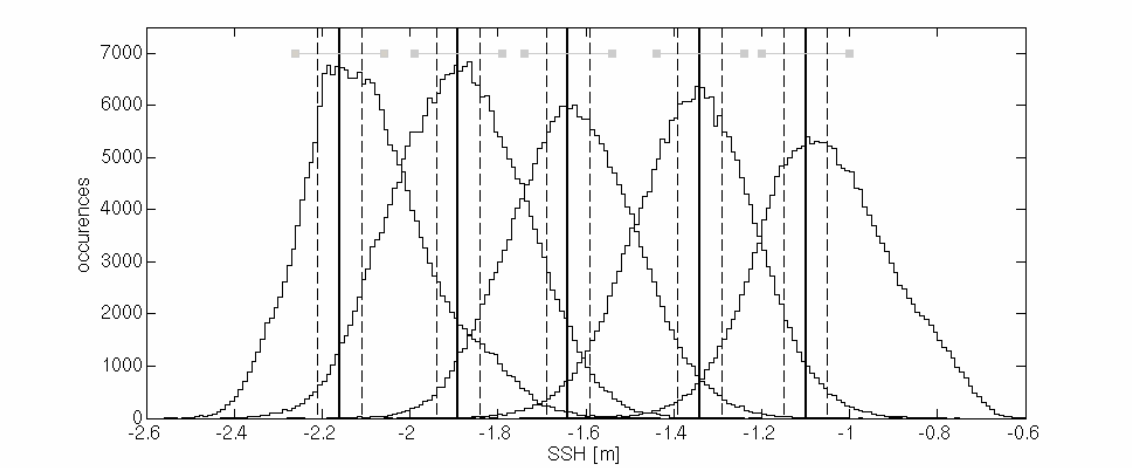

Figure 4

Frequency distribution of SSH contours (number of occurences) for the fronts identified with the transport and temperature criteria method for BRAN. The vertical lines identify some windows around the peak value for the SSH filtering.

Fronts	BRAN
SAF-N	-1.1
SAF-M	-1.34
SAF-S	-1.64
PF	-1.89
sACCf	-2.16

Table 2

SSH contour values (m) associated with the ACC fronts in the Southern Ocean for the BRAN reanalysis (South Australian sector).

Reanalysis (BRAN) versus Non-Assimilating Model (OFAM)

Because of assimilation, one can argue that the jets in BRAN are controlled by altimetry and do not represent hydro-geographic barriers that separate the water masses in the SO. A comparison between BRAN and OFAM is necessary to ensure that the fronts identified in BRAN are due to the model physics and not the assimilation step.

Our method based on transport and temperature criteria does not reliably distinguish the fronts (figure 3). To remove the uncertainty and identify a single front, the best-fit SSH contours are used as filter value. A window of +/- 0.1 m around the SSH peak values (figure 4) is applied to filter the database of frontal positions. Figure 5 shows the mean position of the ACC fronts in the Australian sector for the two simulations. The mean PF-S and SAF-N positions from Sallee et al. (2008) and the mean fronts from Sokolov and Rintoul (2008) are also superimposed. The fronts of the two model runs exhibit similar spatial patterns, with the same meandering tendency downstream of the main bathymetric features. Their positions agree quite well, especially when the fronts are steered by the fractures of the southeast Indian Ridge or by the Campbell Plateau, and when they cross the Macquarie Ridge. If our SAF agree globally with the mean SAF position of Sokolov and Rintoul (2008) and Sallee et al. (2008), our PF seems to differ as our PF-N seems to correspond to their PF-S and our PF-S more likely corresponds to a South ACC front (sACCf). The Tmin-layer approach is problematic in winter, when the surface mixed-layer is deep. By contrast, the SSH filtering approach can identify a single front in both winter and summer.

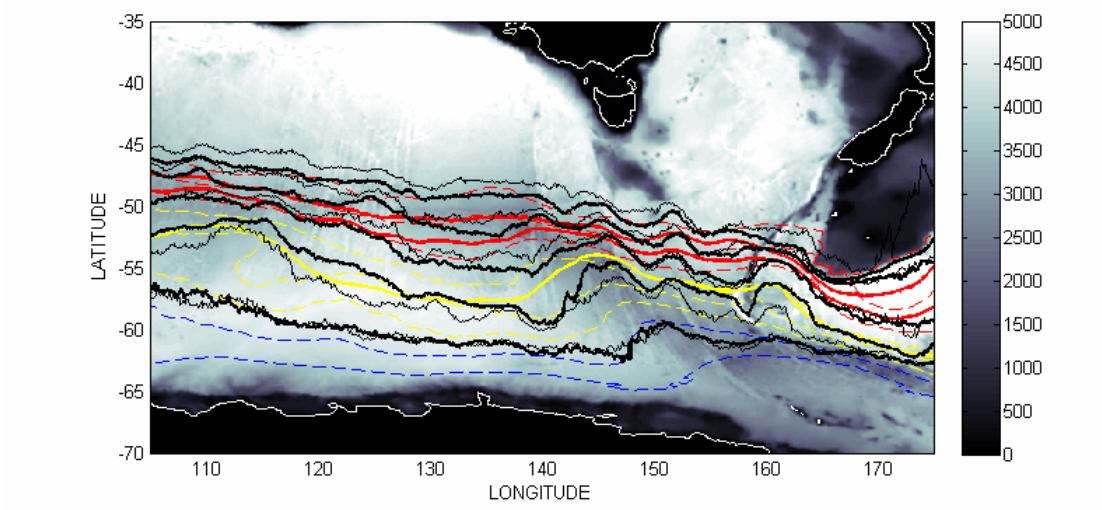

Figure 5

Mean ACC fronts position from the transport and temperature criteria with a SSH filtering for OFAM (black) and BRAN (thick black) superimposed with the bathymetry (m) in the south Australian sector. The ACC fronts from Sallee et al., (2008) (color dash lines) and from Sokolov and Rintoul (2008) (color lines) are also represented: SAF in red, PF in yellow and sACCf in blue.

SSH contours versus hydro-dynamic criteria

In figure 1, the frontal positions of the transport and temperature method and of the SSH contour method can be analyzed and compared for a section south of Australia. The sections and dates chosen for figure 1 underline the main agreements and discrepancies found all around Antarctica. For the SAF and PF, the two methods give similar positions which are superimposed most of the time, with discrepancies of no more than 0.5℃ (figure 1). For the position of the sACCf, the discrepancy between the two methods is more significant and can reach a few degrees. In summer, the southern front corresponds to the PF-N for the transport and temperature criteria and to the sACCf for the SSH contour definition. The SSH contours method has the advantage of revealing the five fronts systematically.

In figure 6, the SSH contours fronts follow and join the strongest simulated ACC jet. The SAF-N and M appear to be the most intense current jets south of Australia (figure 6).

Figures 1 and 6 confirm that SSH contours can be used to approximate streamlines (in particular the core of the ACC jets) and can be associated with subsurface hydrographic structure in the Southern Ocean.

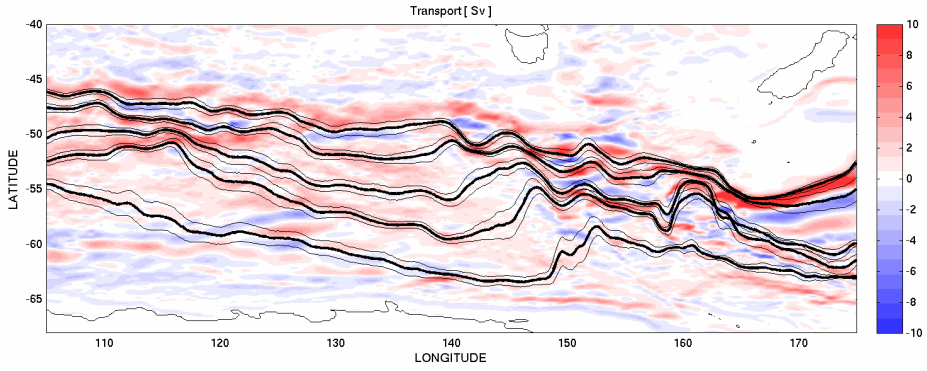

Figure 6

Mean SSH gradient (Sv, read and blue colors) superimposed with the mean positions of fronts for BRAN (bold black lines). The standard deviation envelope (meridional spatial variability) of the fronts position is represented by thin black lines.

Variability of the ACC fronts

ACC fronts mean positions

The mean frontal positions of BRAN agree quite well with the mean positions of Sallee et al., (2008) and Sokolov and Rintoul (2008) (figure 5). In both cases, mean pathways and meridional deflections of the fronts are controlled by topography. Along its circumpolar path, the ACC has a number of large topographic barriers that perturb the flow. South of Australia, the main obstacles are the South-eastern Indian Ridges, the South Tasmanian Ridge (SIR), the Macquarie Ridge and the Campbell Plateau. The ACC fronts are typically steered around these obstacles or over the shallow plateau. The topographic steering leads to sharp meridional deflection. When a jet is constrained to pass over a shallow plateau or ridge, all the fronts tend to move equatorward to compensate for loss of potential vorticity.

Downstream of topographic barriers, mesoscale activity tends to be developed. The frontal meandering is coherent and persistent enough to appear in the mean position of the fronts. Those coherent mesoscale meanders are less clear in the frontal database calculated from satellite altimetry products than in BRAN. South of the STR (downstream of the SIR), two meanders are very distinct. A weaker signature of those meanders can be observed in Sallee et al., (2008) but do not appear in Sokolov and Rintoul (2008). Downstream of the Macquarie Ridge, all the fronts deflect northward and are then constrain to deflect southward by the Campbell Plateau, generating sharp meanders with an amplitude of almost 4°. Once again this signature is not clearly revealed in Sallee et al., (2008) or Sokolov and Rintoul (2008).

Variability

The topography not only controls the pathways of the ACC fronts but also their variability (e.g., Gordon et al. 1978; Chelton et al. 1990; Gille 1994; Moore et al. 1999; Sokolov and Rintoul 2008; Dong et al. 2006). Steep bottom slopes are associated with very weak variations of the front position, whereas flat-bottom areas are subject to large movement of the fronts (Figure 6). When the jets are steered by topography, the meridional variability drops and the intensity of the flow increases. When the fronts cross a shallow plateau or ridge, a drop of variability is also observed and is associated with a decrease in the intensity of the jets. Over the abyssal plain, the intensity of the fronts stays quite strong with an increase in variability. With no bathymetric control, the fronts are predominantly forced by atmospheric forcing and the meridional movements of fronts can be correlated with climatic modes from ENSO (El Nino Southern Oscillation) and SAM (Southern Annular Mode) (Sallee et al, 2008).

Conclusion

A SSH contour definition is used to identify the position of ACC fronts in a 15-year ocean reanalysis. SSH contours are found by using subsurface hydrography combined with depth integrated properties. The results for the reanalysis and from a free model run are quite consistent, giving us confidence in BRAN fronts positions database. The positions of the fronts are controlled primarily by the model physics and not by the assimilation step.

The next step is to use this ACC fronts analysis as a tool to perform intercomparisons with the next generation of BRAN and OFAM runs, and also intercomparisons with other reanalysis (e.g., GLORYS) or OGCM (ORCA025, Langlais et al., 2010). This new metric will enhance our understanding of the differences between the hydrographic definitions of the fronts and the differences in the spatial position and variability of the ACC jets.

Acknowledgements

Financial support for this research is provided by the Quantitative Marine Science joint program between University of Tasmania and CSIRO and through the CSIRO Wealth from Ocean flagship program.

References

Belkin, I. M., and A. L. Gordon, 1996: Southern Ocean fronts from the Greenwich Meridian to Tasmania. J. Geophys. Res., 101, 3675–3696.

Chelton, D.B., M.G. Schlax, D.L. Witter, and J.G. Richman, 1990: Geosat Altimeter Observations of the Surface Circulation of the Southern Ocean, J. Geophys. Res., 95(C 10), 17877–17903.

Chen, D., L.Rothstein, and A.Busalacchi, 1994: A hybrid vertical mixing scheme and its application to tropical ocean models, Journal of Physical Oceanography, 24, 2156-2179.

Dong, S., J. Sprintall, and S. T. Gille, 2006: Location of the Antarctic polar front from AMSR-E satellite sea surface temperature measurements. J. Phys. Oceanogr., 36, 2075–2089.

Gille, S. T., 1994: Mean sea surface height of the Antarctic Circumpolar Current from Geosat data: Method and application. J. Geophys. Res., 99, 18 255–18 273.

Gordon, A.L., 1967. Structure of Antarctic waters between 20°W and 170°W. Am. Geogr. Soc. Antarct. Map Folio Ser., Folio 6 (10 pp.).

Gordon, A.L., 1971. The Antarctic Polar Front zone. In: Reid, 1096 J.L. (Ed.), Antarctic Oceanology I. Antarctic Research Series, 1097 vol. 15. American Geophysical Union, pp. 205–221.

Gordon, A. L., E. Molinelli, and T. Baker, 1978: Large-scale relative topography of the Southern Ocean. J. Geophys. Res., 83, 3023–3032.

Griffies, S.M., 2004: Fundamentals of ocean climate models, Princeton University Press, Princeton, USA,

Griffies, S.M., and R.W. Hallberg, 2000: Biharmonic friction with a Smagorinsky viscosity for use in large-scale eddypermitting ocean models, Monthly Weather Review, 128, 2935-2946.

Hughes, C. W., and E. Ash, 2001: Eddy forcing of the mean flow in the Southern Ocean. J. Geophys. Res., 106, 2713–2722.

Josey, S.A., Kent, E.C., Taylor, P.K., 1998. The Southsampton Pceanography Centre (SOC) ocen-atmosphere heat, momentum and freshwater flux atlas. Southampton Oceanography Centre, report No. 6, 30 pp.

Kallberg, P., A. Simmons, S. Uppala, M. Fuentes (2004), The ERA-40 Archive, ERA-40 Project Report Series No. 17, ECMWF.

Killworth, P. D., and C. W. Hughes, 2002: The Antarctic Circumpolar Current as a free equivalent-barotropic jet. J. Mar. Res., 60, 19–45.

Langlais C., Schiller A., Rintoul S., Coleman R. 2010 : Variability of the Southern Ocean fronts. In preparation.

Leonard, B. P., 1979: A stable and accurate convective modeling procedure based on quadratic upstream interpolation. Comput. Methods Appl. Mech. Eng., 19, 59–98

Levitus, S. , 1989: Interpentadal variability of temperature and salinity in the deep North Atlantic, 1970 – 74 versus 1955 – 59, J. Geophys. Res., 94, 16,125 – 16,131.

Levitus S., 2001. World Ocean Database, vol. 13. U.S. Department of Commerce. National Oceanic and Atmospheric Administration.

Moore, J., M. Abbott, and J. Richman, 1999: Location and dynamics of the Antarctic polar front from Satellite Sea surface temperature data. J. Geophys. Res., 104, 3059–3073.

Oke, P. R., G. B. Brassington, D. A. Griffin and A. Schiller, 2008: The Bluelink Ocean Data Assimilation System (BODAS), Ocean Modelling, 21, 46-70

Orsi, A., T. Whitworth III, and W. Nowlin Jr., 1995: On the meridional extent and fronts of the Antarctic Circumpolar Current. Deep-Sea Res. II, 42, 641–673.

Peterson, R. G., and L. Stramma, 1991: Upper-level circulation in the South Atlantic Ocean. Prog. Oceanogr., 26, 1–73.

Ridgway, K. R., J. R. Dunn, and J. L. Wilkin, 2002 : Ocean Interpolation by Four-Dimensional Weighted Least Squares Application to the Waters around Australasia, Journal of atmospheric and oceanic thechnology 19, 1357-1374

Sallee, J.B., K. Speer, and R. Morrow, 2008: Response of the Antarctic Circumpolar Current to Atmospheric Variability, Journal of Climate, 21, 3020-3039.

Schiller, A., P. R. Oke, G. B. Brassington, M. Entel, R. Fiedler, D. A. Griffin, and J. V. Mansbridge, 2008: Eddy-resolving ocean circulation in the Asian-Australian region inferred from an ocean reanalysis effort. Progress in Oceanography, 76, 334-365.

Sinha, B., and K. J. Richards, 1999: Jet structure and scaling in Southern Ocean models. J. Phys. Oceanogr., 29, 1143–1155.

Sokolov, S., and S. R. Rintoul, 2002: Structure of Southern Ocean fronts at 140°E. J. Mar. Syst., 37, 151–184.

Sokolov, S., and S. R. Rintoul 2008: Multiple jets of the Antarctic Circumpolar Current south of Australia. J. Phys. Oceanogr., 37, 1394–1412.

Sun, C., and D. R. Watts, 2001: A circumpolar gravest empirical mode for the Southern Ocean hydrography. J. Geophys. Res., 106, 2833–2856.

Watts, D. R., C. Sun, and S. R. Rintoul, 2001: A two-dimentional gravest empirical modes determined from hydrographic observations in the Subantarctic Front. J. Phys. Oceanogr., 31, 2186–2209.

Notebook

Editorial Board:

Laurence Crosnier

Secretary:

Fabrice Messal

Articles:

Contact :

Please send us your comments to the following e-mail address: webmaster@mercator-ocean.fr

Next issue: April 2010